Final Report to CNSC

R444.3

Project Title: Research on effects of non-linearity of soil and soil-structure interaction on the seismic response of nuclear facilities

Report submitted by:

Dr. Liang Cui

Dr. Mamadou Fall

University of Ottawa, Canada;

161 Colonel by, Ottawa (Ontario), K1N 6N5;

Phone: +1-613-562 5800 # 6558

mfall@uottawa.ca

March 15, 2019

Abstract

Nuclear facilities, such as nuclear power plants, must be seismically qualified, and shown to withstand the design basis earthquake without loss of containment. When the facilities are built on or are embedded in soil deposits, the soil can amplify the earthquake motion to the structure components. Additionally, in some types of soils such as loose sands, the earthquake can generate an increase in pore pressure in the groundwater, resulting in a decrease in effective stress and a loss in shear strength that might lead to foundation failure, and impact the structural integrity of the overlying or embedded structures. In order to assess the above phenomena and their implications on the structural integrity of nuclear facilties, a dynamic coupled elastoplastic-hydraulic model for soil behaviour under seismic loadings is developed. The governing equations of the model are based on conservation of momentum for the porous skeleton, and conservation of water mass. Pore water flow is assumed to follow Darcy's law while the solid skeleton is assumed to be elasto-plastic, with the adoption of the modified Cam Clay model to simulate its stress-strain behaviour. The model is tested against dynamic triaxial tests and a shaking table experiment. The results show that the model can capture (1) the development of permanent deformation in soil, (2) the shear induced volume change (including both contraction and expansion), (3) the generation and dissipation of excess pore water under the dynamic loading, and (4) the strain hardening and softening behaviour of soil under complex stress paths. Finally, the model is used for the scoping analyses of the seismic response of a hypothetical small modular reactor (SMR) on sandy soil. The obtained results indicate that the

developed model can be used as a useful tool to predict the non-linear behaviour of soil and its effect on nuclear facilities.

Table of Contents

List of Figures

List of Tables

CHAPTER 1

Literature Review

1.1 Introduction

The process in which soil response influences the motion of structures and vice versa is referred to as soil–structure interaction (SSI). As one of the most important topics in earthquake engineering, SSI analysis has received much attention in recent decades (e.g., Luco and Contesse 1973; Roesset and Tassoulas 1982; Zhang and Makris 2002; Lou et al. 2011; Cakir 2013; Khoshnoudian et al. 2017). Previous investigations (e.g., Bielak 1976; Rodriguez and Montes 2000; Stehmeyer and Rizos 2008; Lou et al. 2011; Van Nguyen et al. 2017) have elucidated that the dynamic response of a structure found on flexible soil may differ significantly from the counterpart supported on a rigid based.

To understand the SSI phenomenon, the wave propagations in a coupled system (i.e., soil-structure system (SSS)) must be realistically assessed. When an earthquake occurs, the dynamic excitation can affect the SSS. As a result, the response of a structure and its foundation to earthquakes can affect ground motion. Specifically, in the case of a flexible-base structure, the motion of the foundation of this structure is usually different from the free motion of the ground. Rocking caused by the flexibility of the support due to the horizontal motion of the foundation is incorporated into the dynamic response of the foundation of a structure. Moreover, vibrating energy can also be transferred to the soil layer and dissipated due to geometric damping (i.e., radiation damping) and material damping (i.e., damping of hysteresis caused by friction and/or plastic deformation). The characteristics of the dynamic response of soil strongly depend on its properties, the structure and the type of earthquake. Therefore, SSI can be broadly

viewed as two types of phenomena: (1) kinematic interaction and (2) inertial interaction. Ground motion caused by earthquakes leads to soil displacement which is known as free-field motion. However, the foundation which is embedded into the soil will not follow the free-field motion. This inability of the foundation to follow the free-field motion causes a kinematic interaction. There are three factors that contribute to kinematic interaction, which include incoherent ground motion, base slab averaging, and ground motion reduction with depth (Jones 2013). More coherent studies on kinematic interaction can be found in Gazetas (1991), Makris and Gazetas (1992), Lai and Martinelli (2013), and Hussien et al. (2015). On the other hand, the vibration of foundations can give rise to base shear and moment. As a result, the inertial force that develops in a structure can disturb the free-field motion of the foundation and cause further soil deformation, which is called inertial interaction.

SSI (i.e., kinematic and inertial interactions) can significantly change the system response from negligible to profound (Trifunac et al. 2001). For example, SSI systems have longer natural periods of vibration compared to fixed-base systems (Pitilakis et al. 2008). Previous studies on SSI issues (Luco et al. 1986; Trifunac and Todorovska 1998; M. Trifunac et al. 2001) have found that destructive shaking is often accompanied by the nonlinear response of the foundation soils. To accurately and efficiently assess the response of a structure-soil system, a nonlinear SSI analysis should be carried out. Hence, this aims to clarify the mechanisms that control SSI, associated factors and the resultant seismic response of the SSS. For this purpose, four components related to SSI research

are reviewed in this report: (1) the analysis methods (including both direct and substructure approaches) of SSI under dynamic loading; (2) the seismic response of the SSS at both the laboratory and field scales; (3) the dynamic behaviour of cohesionless and cohesive soils; and (4) the soil-structure interface. Due to the significant influence of excess pore-water pressure on SSI problems, the relevant research results are also reviewed and incorporated into the seismic response of soil, and the nonlinear behaviour of the soil-structure interface.

1.2 Methods of analysis of SSI under dynamic loading

The analysis of SSI under dynamic loading is an important means of predicting the overall structural response. The methods to solve the SSI problem can be classified into two approaches: direct and substructure approaches.

1.2.1 Direct approach

The direct approach (DA) is the most rigorous way of solving a dynamic SSI problem. The entire SSS is modeled in one single step which fully takes into consideration wave propagation, and the dynamic response and interaction of the soil-structure. Ground motion can be applied at the boundaries at the base and sides of the model, and then kinematicinteraction can be incorporated into the calculations. Several numerical discretization techniques are available to implement the DA, (e.g., finite element method (FEM), spectral element method, finite difference method, etc.) (Jones 2013; Lai and Martinelli 2013). For instance, the structure can be modeled as beam and/or frame elements, and soil can be

modeled with solid 3D elements with the FEM. The corresponding equation of motion (EOM) for an SSI/FEM model can be written as:

$$[M_{sss}]\{\ddot{u}_{sss}\}+[K_{sss}]\{u\}=-[M_{sss}]\{\ddot{u}_g\} \quad (1)$$

where $[M_{sss}]$ and $[K_{sss}]$ respectively represent the mass and stiffness matrices of the SSS, $\{\ddot{u}_{sss}\}$ and $\{u\}$ refer to the acceleration and displacement vectors of the system, and $\{\ddot{u}_g\}$ denotes the input displacement vector.

The DA can provide in detail the response of the structure, foundation and soil when subjected to dynamic loading (e.g., earthquakes) and the related damage (Li et al. 2014). Moreover, as superposition is not assumed in the DA, true nonlinear analyses can be applied to SSI problems. However, the great computational efforts mean that the DA is not easily implemented (Lu 2016). In practice, the DA is commonly performed through equivalent-linear methods to approximate the effects of soil nonlinearity (Sáez et al. 2013). In addition, when finite element mesh discretization is carried out, the soil will dominate the total number of nodes of the mesh of the SSS. Consequently, the DA is difficult to carry out and costly in terms of computation time (Jones 2013). Hence, the DA is usually applied to only two dimensional (2D) modeling.

1.2.2 Substructure approach

The substructure approach (SA) involves three steps in which the principle of superposition is used to isolate the two primary causes of SSI (i.e., kinematic and inertial interactions of soil-foundation systems) (Pitilakis and Clouteau 2010; Jones 2013). Then, the response of each component of the SSI system is individually solved and step-by-step successively. Detailed information on the decomposition of an SSI system by using the SA can be found for example in Endres et al. (1984); Mylonakis et al. (2006); and Lai and Martinelli (2013). A brief review of these three steps, which are evaluating the foundation input motion (FIM), obtaining the Impedance function, and analyzing a structure on a compliant base subjected to FIM, is provided in the following sections.

1.2.2.1 Evaluation of foundation input motion (FIM)

The FIM refers to the motion that occurs on the base-slab if the structure and foundation have no mass. The FIM is dependent on the soil and foundation properties (stiffness) and geometry. Moreover, the FIM only demonstrates the effects of kinematic interaction since inertial effects are neglected.

1.2.2.2 Obtaining impedance function

The impedance function is used to evaluate the stiffness and damping characteristics of soil-foundation interaction. Specifically, the stiffness and damping characteristics of soil are analyzed by either relatively simple impedance

function models for rigid foundations or the distribution of springs and dashpots in series around the foundation (Nasser 2009). The stiffness of soil is represented by springs whereas soil damping characteristics are described by the dashpots. The SSI effect is incorporated through the dynamic soil springs (i.e., dynamic impedance function). Then the FIM is applied to the dynamic impedance function.

1.2.2.3 Analyzing structure on compliant base subjected to FIM

Due to its flexibility (i.e., the independence of the involved three steps), an SA analysis can help to place resources on the most significant aspects of a problem. Moreover, compared to the DA, the SA can reduce the number of degrees of freedom by orders of magnitude. Through the decomposition of the soil–foundation–structure system into several subdomains, the solution of the SSI problem can be obtained very fast and easy to implement by using a substructuring technique (Pitilakis et al. 2008). However, the SA relies on the principle of superposition which has obvious significant limitations (Halabian and El Naggar 2002), especially for the analysis of the non-linear behaviour of structures (e.g., progressive degradation), foundations (e.g., uplifting and/or sliding) and soil (e.g., permanent deformation). Consequently, the SA is limited to either linear elastic or viscoelastic analyses.

1.3 Experimental data for the seismic response of soil-structure systems

During earthquakes, the soil that underlies the foundation of a building is subjected to a series of vibratory stress which can cause large deformations in the soil and thus its failure. However, during the dynamic loading of local soil deposits, the resultant earthquake damage may differ from one site to another. To evaluate the dynamic response characteristics of soil, extensive experiments have been conducted at both the laboratory and field scales. The following is primarily a review of the experimental results found in the literature. Moreover, the soil dynamic properties are summarized based on the obtained experimental results.

1.3.1 Laboratory tests and results

Due to the use of smaller-scale physical models, laboratory tests are not representative of the in-situ conditions of SSI. Nevertheless, the preliminary results are important as a benchmark or reference for further studies on SSI problems (Field et al. 1998; Chandra 2014). Moreover, compared with field investigations on SSI problems, smaller-scale laboratory investigations provide an alternative means of examining the issues in terms of reducing cost and time. With improvements in lab apparatuses, a significant amount of experimental work can now be conducted on scaled SSSs, either on a shaking table (e.g., Chau et al. 2009; Anastasopoulos et al. 2013; Massimino and Maugeri 2013; Tabatabaiefar 2017) or a centrifuge (e.g., Trombetta et al. 2013; Bryden et al. 2014; Hussien et al. 2016).

To investigate the seismic response characteristics of buildings with surface and embedded foundations, Hosseinzadeh et al. (2012) conducted a series of experimental tests on a shaking table. A scaled model building was constructed on two different types of soft soil (Types II and III as defined in the Iranian seismic code (Iranian standard (IS)2800)). The dynamic characteristics of tested soil are listed in Table 1.1. The results indicated the important effects of SSI on reducing the frequencies of motion in soil deposit and increasing the damping ratios of structural models as compared to fixed base models.

Table 1.1. Experimental frequency and damping ratio for different types of structural models and foundations (Data from Hosseinzadeh et al. (2012)).

Structural model	Fixed		with SSI (surface)		with SSI (embedded)	
	Frequency	Damping ratio	Frequency	Damping ratio	Frequency	Damping ratio
5 stories	1.55	0.43	1.54	0.93	-	-
10 stories	0.8	7.03	0.68	2.9	-	-
15 stories	0.54	1.45	0.50	2.26	0.518	1.47
20 stories	0.374	1.57	0.355	2.58	0.363	2.42

de Barros and Luco (1995) examined the results from forced vibration tests through instrumented seismic tests with a quarter-scale concrete containment structure in Hualien, Taiwan. The stiffness and damping functions were found to be dependent on the frequency of forced vibration (see Figure 1.1.1).

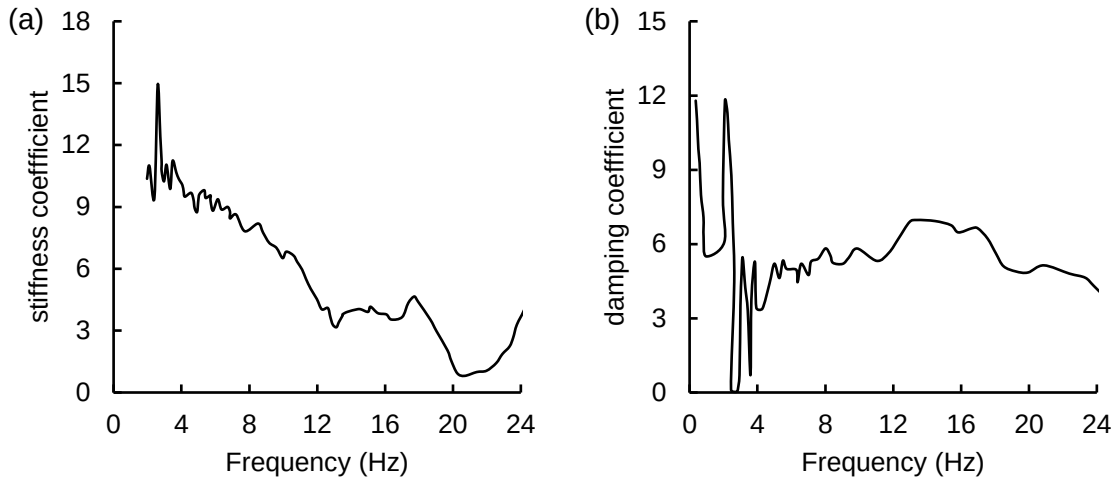

Figure 1.1. Dependence of (a) stiffness function, and (b) damping function on frequency (Data from (de Barros and Luco 1995))

1.3.2 Field tests and measurements

Although laboratory tests can be very useful for improving the current understanding of the controlling mechanisms of SSI problems, a full-scale experimental investigation of SSI on an actual building with the most comprehensive testing methods would be more optimal.

To assess the dynamic characteristics of actual buildings under the effect of SSI, Ellis (1996) conducted four groups of forced vibration tests on four different buildings. Then, after the decay of vibration was analyzed, damping and the associated properties were obtained. A representative decay curve of the recorded acceleration at the corner of the uppermost story of a building is plotted in Figure 1.2. From this figure, it can be clearly observed that the recorded amplitude of acceleration gradually decreases and the associated frequency increases with time.

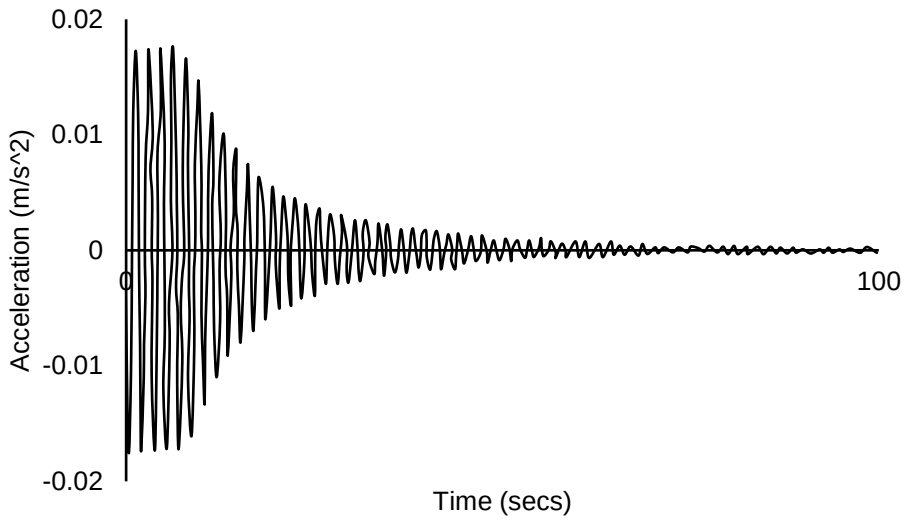

Figure 1.2. Decay of vibration from forced vibration test on actual building (data from (Ellis 1996))

The obtained measurements from the four groups of actual buildings are listed in Table 1.2. The reduction in frequency was determined by calculating the base stiffness and the comparing the building with an equivalent building on a fixed based. The measured data indicate that the SSI can contribute to energy dissipation and increase of damping. Moreover, the SSI can also reduce the natural frequencies of building.

Table 1.2. The effects of SSI on the dynamic characteristics of actual buildings (data from(Ellis 1996))

Building	Forcing frequency (Hz)	Damping (% crit)	Reduction in frequency (%)	Energy lost in foundation (%)
Dunstan Mill	1.49	2.29	8.6	17.0
	2.22	2.94	21.5	31.3
	3.90	3.07	4.03	11.9
Stoneham	1.33	2.51	35.6	60.2
	1.35	2.40	48.1	59.5
Roman Point	0.84	1.10	11.0	22.1
Hume Point	0.90	0.98	21.0	39.3
	1.10	1.20	23.3	42.8
	1.26	1.60	0.64	2.9

1.4 Dynamic behaviour of cohesionless and cohesive soils, including the influence of pore pressure generation

Under dynamic loading, soil materials can exhibit strongly non-linear behaviour such as nonlinear volumetric response, and pressure-sensitive and rate-sensitive shear behaviour (Ishihara 1996; Boulanger and Idriss 2004; Thirugnanasampanther 2016), which is often accompanied with the rapid generation of excess pore pressure (Mitchell and King 1977; Zergoun and Vaid 1994; Hsu and Vucetic 2006; Lo et al. 2016). A significant amount of research has been conducted to improve current understanding on the dynamic behaviour of both cohesionless (granular) and cohesive soils by using a variety of laboratory techniques such as the cyclic torsional shear, cyclic direct simple shear, cyclic triaxial and resonant column tests.

1.4.1 Nonlinear volumetric response

When subjected to dynamic loading, the soil may exhibit non-linear volumetric response. There are two types of irreversible volume changes: isotropic pressure induced permanent and shear-induced volume changes. Extensive studies have been carried out to examine the nonlinear volumetric behaviour of soil.

Volume changes induced by isotropic pressure can be observed in consolidation tests, while irrecoverable volume change induced by shear can be obtained during shear tests (e.g., direct shear tests or cyclic torsional tests). For example, Pradhan et al. (1989) found that the number of cycles and stress ratios can affect the volume change of sand under cyclic loading conditions. Similar

results were obtained from the cyclic simple shear tests on clay samples prepared in a slurry consolidometer (Yildirim and Erşan 2007) (see Figure 1.3).

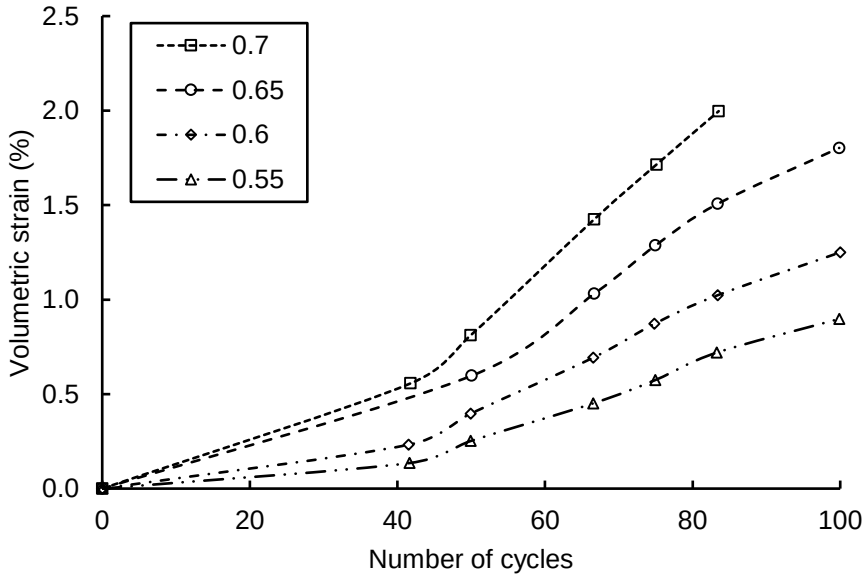

Figure 1.3. Variation of volumetric strain with the number of cycles for different stress ratios (data from (Yildirim and Erşan 2007))

When subjected to shearing, soil particles slide over each other and rearrange themselves, which may cause soil volume changes (de Silva et al. 2014). Extensive experimental studies have been conducted to evaluate the shear-induced volumetric behaviour of soil. For instance, Yasuhara et al. (1982) found that the dilatancy effect exerted during repeated loading is governed by both the effective stress ratio and the frequency of repeated loading (see Figure 1.4). Through the obtained results from strain-controlled tests on sand, Silver and Seed (1971) conclude that the soil volume changes during cyclic loading are sensitive to cyclic shear strain rather than shear stress amplitude.

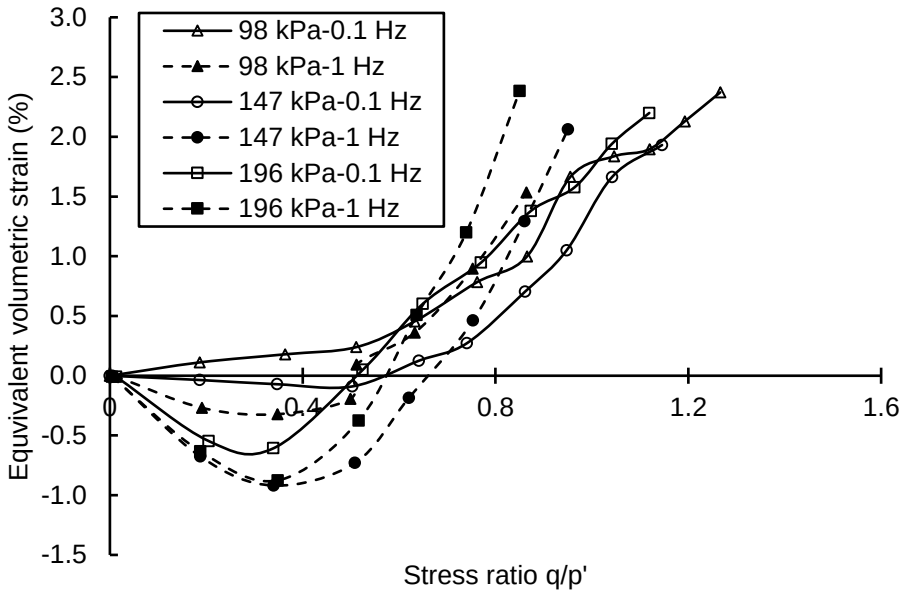

Figure 1.4. Dilatancy of isotropically consolidated clay under repeated loading (data from (Yasuhara et al. 1982)).

1.4.2 Pressure-sensitive behaviour

The behaviour of a material is pressure-sensitive when irreversible deformation depends on the first stress invariant (i.e., the sum of the three principle stresses), which can result in pressure-sensitive yielding and plastic dilatation. Previous studies have found that: (1) the effective mean principal stress affects the degradation of sand (e.g., Hardin and Drnevich 1972; Augustesen et al. 2004; Ma et al. 2017); (2) the dynamic shear modulus explicitly depends on the mean principal stress (e.g., Ling and Liu 2003; Altun and Goktepe 2006); and (3) the damping ratio is also directly affected by the confining pressure - the damping ratio is smaller with a high confining pressure (e.g., Assimaki et al. 2000; Elgamal et al. 2005; Fei and Xu 2017). To demonstrate the pressure sensitive behaviour of soil,

the results from two reported experimental tests for both cohesionless and cohesive soils are provided as examples.

To study the effect of confining pressure on the dynamic shear modulus and pore pressure, El Mohtar et al. (2013) conducted a series of undrained resonant column tests on clean sand. The obtained results are presented in Figure 1.5, where there is to a large extent, a normalized shear modulus (ratio of the measured shear modulus and maximum shear modulus) reduction with reduced confining pressure. Moreover, at higher confining pressure, the pore water pressure (PWP) is decreased for a given shear strain.

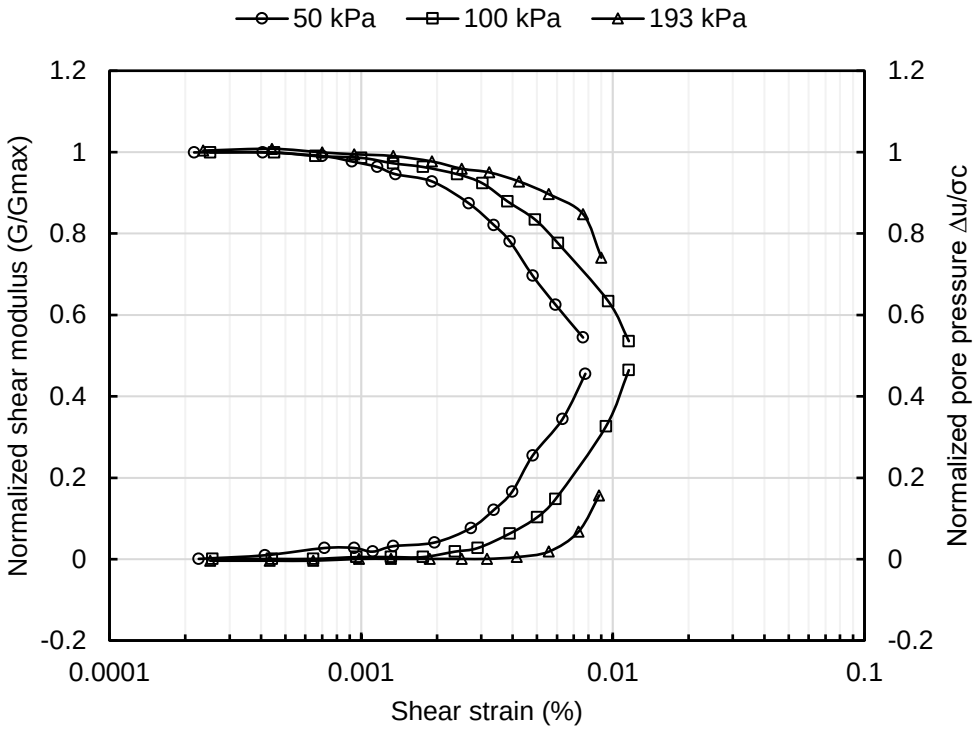

Figure 1.5. Effect of confining pressure on normalized shear modulus and pore pressure from undrained resonant column tests on clean sand (data from (El Mohtar et al. 2013))

Ma et al. (2017) conducted a series of static triaxial tests with split Hopkinson pressure bars (TSCP-SHPB) under confining pressure to study the effects of confining pressure on the dynamic behaviour of sandy clay. Figure 1.6 presents the dynamic stress-strain curves with different confining pressures. It is evident that the dynamic behaviour (shown by stiffness and peak stress) is dependent on confining pressure values.

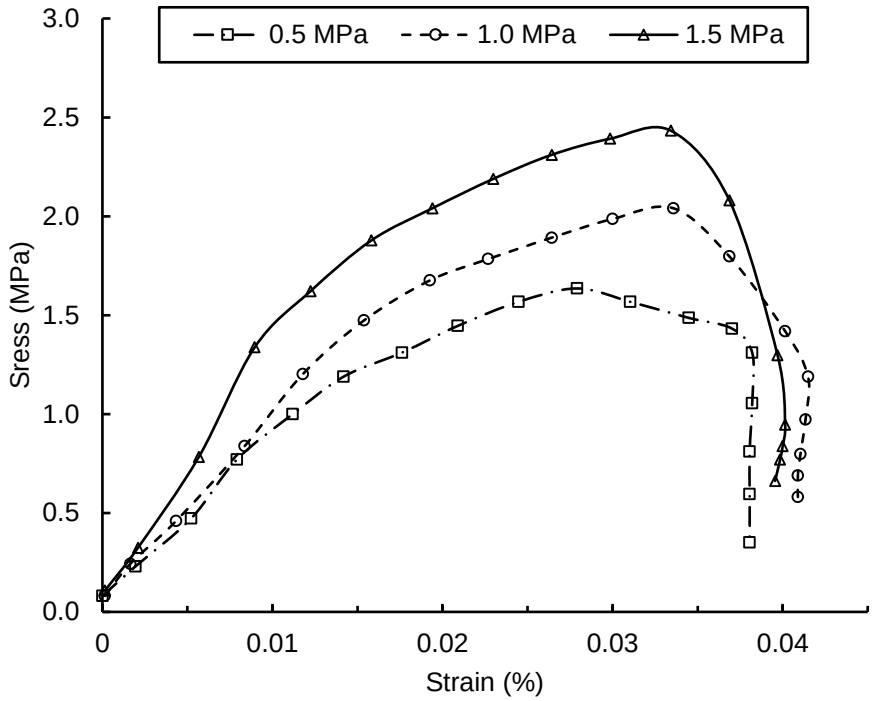

Figure 1.6. Dynamic strain-stress curves of sandy clay at different confining pressure (data from TSCP-SHPB tests conducted by Ma et al. (2017))

1.4.3 Rate-sensitive shear behaviour

Based on the experimental results from cyclic triaxial tests on cohesionless (Carroll 1963) and cohesive (Lefebvre and Leboeuf 1987; Teachavorasinskun et

al. 2002; Moses et al. 2003) soils, it has been found that the soil behaviour is dependent on the shear strain rate. For example, drained triaxial compression tests on crushed coral sand carried out by Yamamuro et al. (2011) showed that with increasing strain rates, (1) the elastoplastic stiffness significantly increases; (2) the failure shear strength moderately increases; (3) the axial strain at the peak stress significantly decreases; and (4) and volumetric strains become more dilatant.

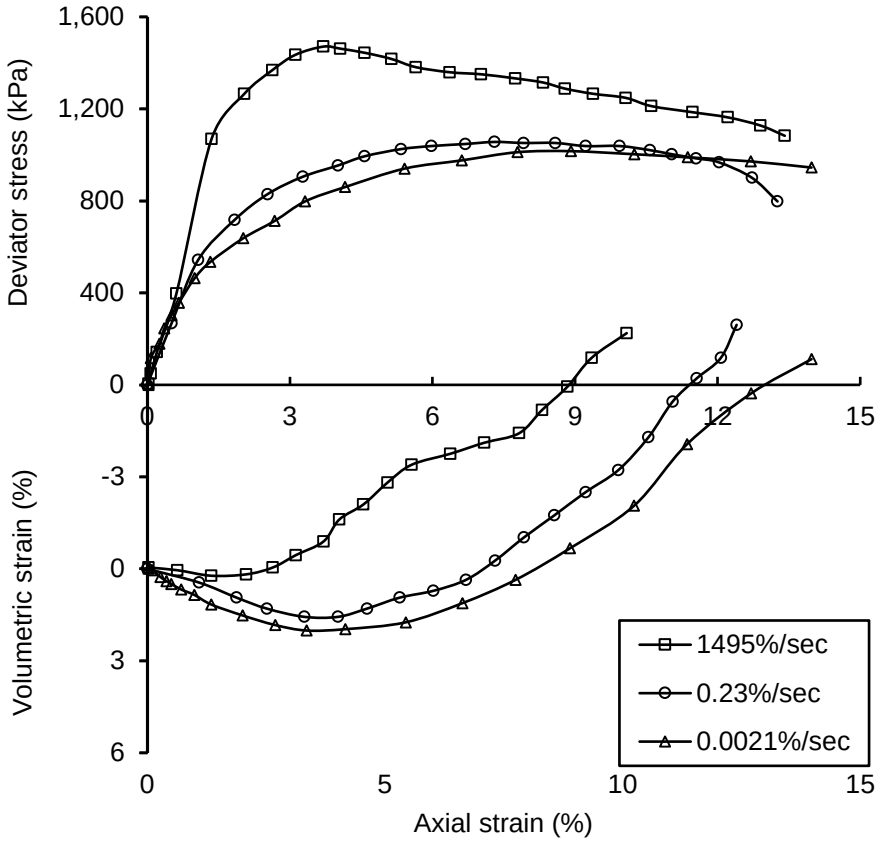

Figure 1.7. Effect of strain rate on stress-strain curve (including the stiffness, volumetric strain, peak stress value and associated axis strain) (Data from (Yamamuro et al. 2011))

1.4.4 Pore water pressure generation under dynamic loading

To assess the rate and magnitude of PWP generation under dynamic loading, two experimental testing methods are available at the laboratory scale: (1) evaluating the PWP generated in relation to the ratio of the number of cycles of loading applied to the number of cycles required to cause liquefaction by using a stress-controlled method (Lee and Albaisa 1974), and (2) using a strain-controlled method demonstrated in Dobry et al. (1982). However, previous studies (Silver and Seed 1971; Matasovic and Vucetic 1992; Sitharam and Govindaraju 2007) on PWP generation under cyclic loading showed that, compared to stress-controlled tests, strain-controlled tests can cause less water content redistribution in soil samples before the initial liquefaction occurs and thus provide more realistic predictions of in situ pore pressure with more pressure-sensitive behaviour than those obtained from stress-controlled tests. Hence, the shear strain is a more fundamental parameter for studying PWP generation. As a result, the strain-controlled approach has been preferred over the stress-controlled approach for cyclic loading tests. In this regard, extensive experimental studies have been carried out to investigate the PWP generation and related influential factors. Figure 1.8 presents the experimental data from strain-controlled cyclic triaxial tests on Bhui soil reported by Sitharam and Govindaraju (2007). It can be clearly observed that the pore pressure is sensitive to the changes of cyclic shear strain amplitude and number of cycles. For a given relative density and loading cycle, the rate of PWP build-up in Bhui soil increases with increases in the amplitudes of the cyclic shear strain.

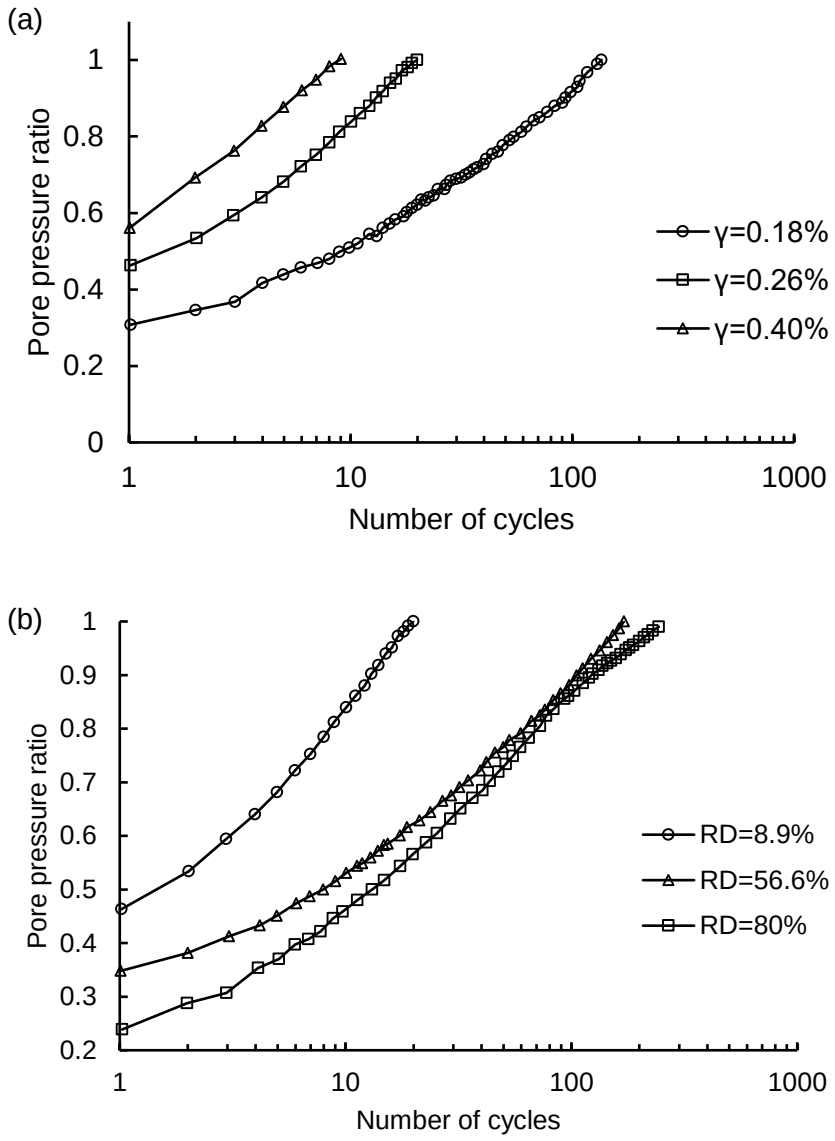

Figure 1.8. Pore water pressure generation with the change of (a) sing-amplitude shear strain (γ), and (b) relative density (RD) in Bhui soil subjected to effective confining pressure of 100 kPa and frequency of 1 Hz during cyclic triaxial tests (data from (Sitharam and Govindaraju 2007))

Moreover, Dash and Sitharam (2009) found that the silt content, confining pressure and loading frequency can also affect PWP generation in soil under cyclic loading. The results obtained from their study are plotted in Figure 1.9. From this figure, it can be observed that (1) the rate of PWP generation relative to loading cycles decreases with increases in confining pressure (see Figure 1.91.9a); (2) in

terms of the influence of silt content (see Figure 1.9b), the rate of the generation of PWP substantially increases with increases in silt content until a silt content of 20%. Then, the opposite trend is observed with further increases of silt.

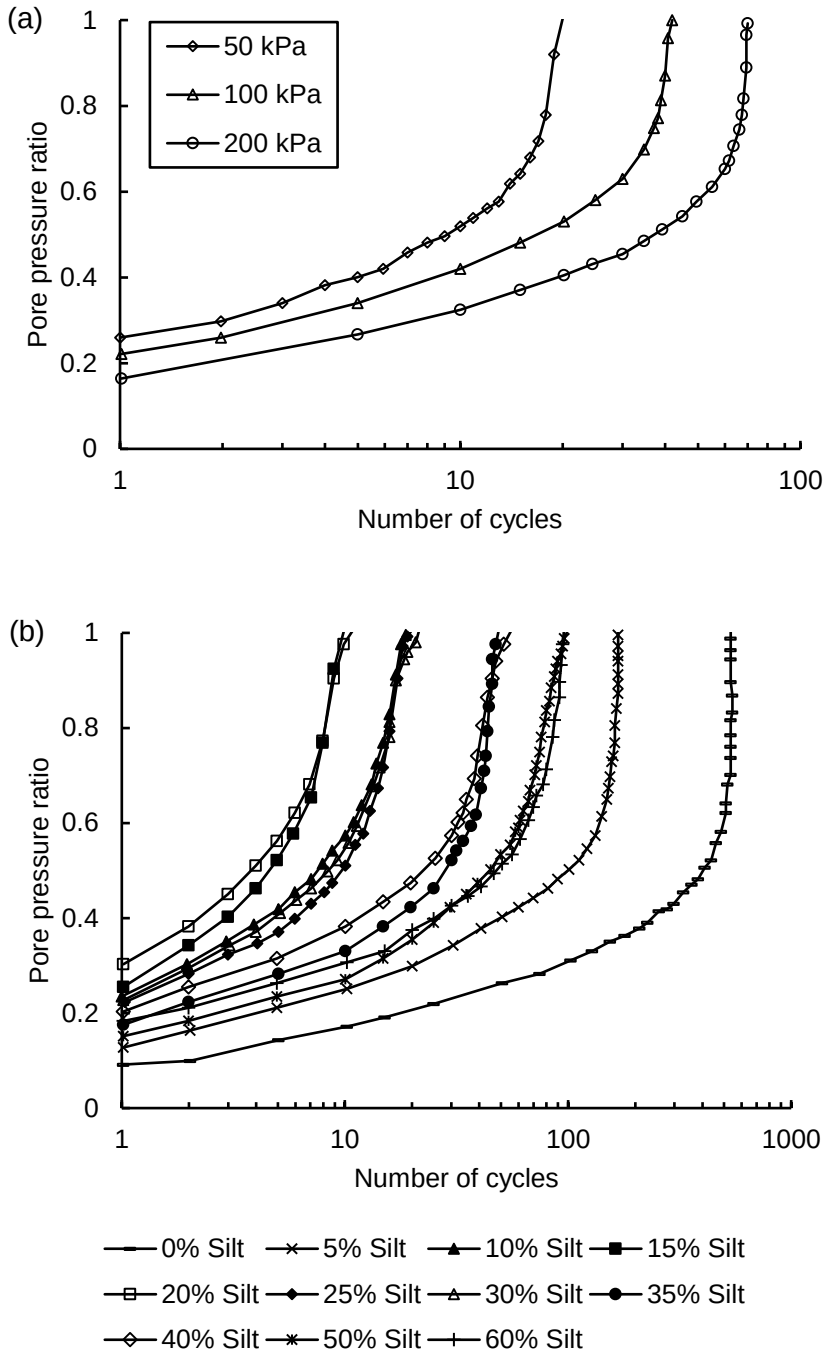

Figure 1.9. Pore water pressure generation with the change of (a) confining pressure, and (b) silt content in soil during cyclic triaxial tests (data from (Dash and Sitharam 2009))

The cyclic shear strain amplitude γ_c which differentiates no PWP accumulation vs. significant accumulation is called the cyclic threshold shear strain γ_t (Dobry et al. 1982). Therefore, if $\gamma_c > \gamma_t$, permanent volume changes (i.e., shear induced volume changes) will occur in soil and thus result in permanent residual excess PWP under undrained conditions. However, if $\gamma_c < \gamma_t$, no permanent volume changes or excess PWP develops in soil. To study the threshold shear strain γ_t of both cohesive and cohesionless soils, Hsu and Vucetic (2006) conducted a series of direct simple shear tests. The test results confirmed that γ_t in cohesive soils is greater than in cohesionless soils and increases with the plasticity index (PI) of the soil.

Table 1.3. Characteristics of Soil Samples Tested and Cyclic Threshold Shear Strains Obtained

Soil type	Plasticity index (PI) (%)	Cyclic threshold shear strain range γ_t (%)
Nevada sand	Non plastic soil	0.012-0.016
Irvine silt	14	0.040-0.060
Commercial kaolinite	20	0.024–0.033
Southern California clay	30	0.030–0.060

Zhang et al. (2009) conducted a series of shaking table tests to study the behaviour of excess PWP in different soft soil-foundations of SSI systems. The soil used in this physical model consisted of clayey silt (top layer) and silty clay (bottom layer). Under the loading process of two cycles, the excess PWP variations were

monitored in this study. The obtained results (Figure 1.10) showed that (1) the excess PWP increases with increases in dynamic loading; (2) after each dynamic excitation, the dissipation of excess PWP immediately takes place in the soil, and the dissipation of excess PWP is even greater in clayey silt (with less clay content) compared to silty clay; and (3) a relatively small excess PWP is obtained during repeated loading processes. Therefore, the obtained results indicate that excess PWP depends on the soil type (i.e., clay content) and dynamic loading conditions (i.e., intensity and number of cycles).

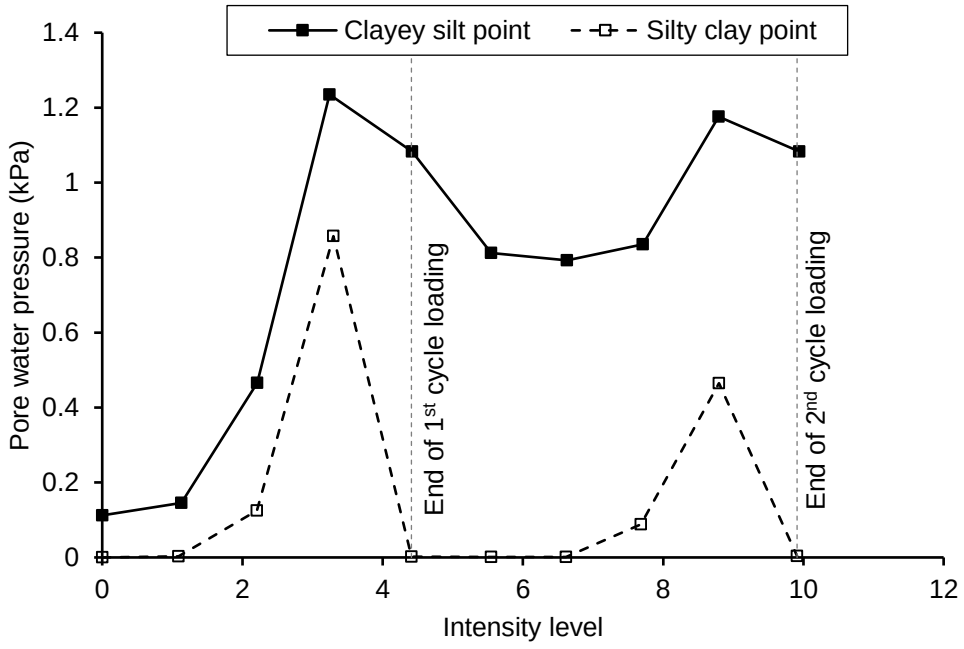

Figure 1.10. Comparison of excess pore water pressure in silty clay and clayey silt

Therefore, the previous studies have indicated that the soil properties (e.g., clay and silt contents, relative density and plasticity index), confining pressure, and dynamic loading conditions (e.g., number of cycles, loading amplitude and single-

amplitude strain) can significantly affect PWP generation under the effects of SSI. Moreover, pore pressure buildup near the foundation of structures may eventually cause soil liquefaction and severely affect the stability of the structures (Liang et al. 2017). Therefore, the effects of PWP generation should be incorporated into analyses of SSI problems.

1.5 Nonlinear behaviour of the soil-structure interface

The monotonic and cyclic behaviours of the soil-structure interface can significantly affect the mechanical response of an SSI system (Zhang and Zhang 2009). Therefore, the behaviour of the soil-structure interface has been one of the main focuses of SSI systems (e.g., embankments, nuclear power plants, earth reinforcements and underground structures) (Zhang et al. 2011). Systemic studies have been carried out to evaluate the behaviour of the soil-structure interface, including simple shear (Desai et al. 1985; Uesugi and Kishida 1986), triaxial shear (Coyle and Sulaiman 1967), direct shear (Potyondy 1961; Clough and Duncan 1973; Zhang et al. 2011), annular shear (Brumund and Leonards 1973), and ring torsion (Yoshimi and Kishida 1981) tests. Based on these studies, the nonlinear behaviour (including the nonlinear tangential stress-displacement and dilatancy behaviour) of the soil-structure interface and related factors (including the roughness of the structure, behaviour of the soil and normal stress) are comprehensively reviewed. Moreover, a comparison of existing interface models is conducted in this section as well.

1.5.1 Nonlinear stress-displacement relationship of interface

The interface shear tests showed that the failure of a rough soil-structure interface is accompanied with strongly nonlinear stress-displacement behaviour including strain hardening/softening behaviour (Hu and Pu 2003), and degradation of the shear stress due to repeated loading (Mortara et al. 2007). Moreover, it has been found that nonlinear stress-displacement behaviour is affected by normal stress (see Figure 1.11a), relative density (see Figure 1.11b), surface roughness (see **Error! Reference source not found.**), and cyclic loading (see Figure 1.12). Therefore, to accurately predict SSI problems, the nonlinear stress-displacement relationship of the soil-structure interface must be fully considered.

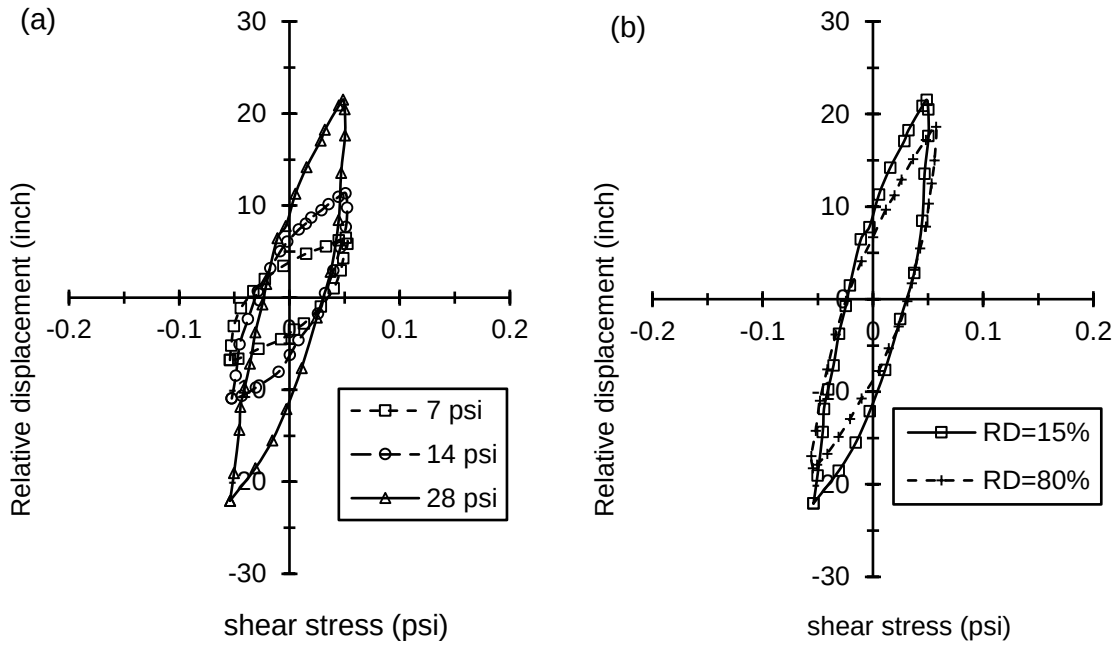

Figure 1.11. Effect of (a) normal stress and (b) relative density (RD) on the stress-relative displacement of Ottawa sand-concrete interface from cyclic shear tests conducted by Desai et al. (1985)

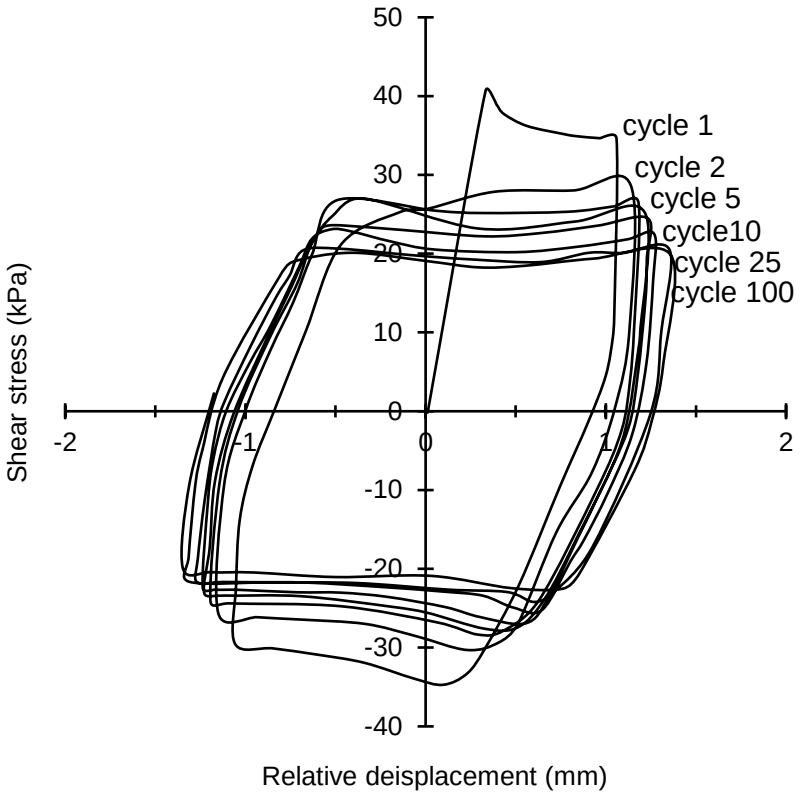

Figure 1.12. Effect of cyclic loading on the stress-displacement curves from a cyclic multi-degree-of-freedom testing device on clay (data from (Desai and Rigby 1997))

1.5.2 Dilatancy behaviour of interface

As one of key characteristics of soil, the dilatancy behaviour of interfaces (i.e., the volumetric change induced by shear) has been investigated by many researchers (for example Uesugi and Kishida 1986; Reddy et al. 2000; Dove and Jarrett 2002). In this regard, direct and simple shear tests have been widely used to characterize the dilatancy behaviour of interfaces (see Figure 1.13), although these types of tests may cause a non-uniform distribution of stress or strain along the interface (Zhang et al. 2011). Previous studies have found that the factors that affect the dilatancy behaviour of interfaces include surface roughness (Nakamura

et al. 1999; Dove and Jarrett 2002), normal stress (Zhang and Zhang 2009) number of cyclic loadings (Mortara et al. 2007) and soil type (Zhang et al. 2011).

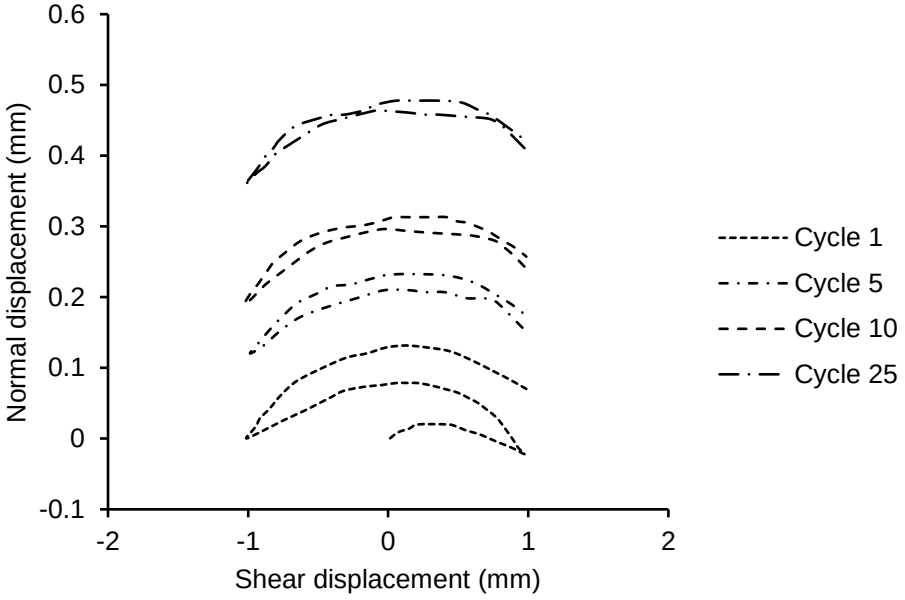

Figure 1.13. The normal displacement versus shear displacement from cyclic direct shear tests (data from (Mortara et al. 2007))

1.5.3 Effect of pore water pressure on interface behaviour

During the development of shear displacement that takes place between a saturated soil-structure interface, the narrow shear zone of soil near the interface may first experience compaction (i.e., volume contraction), then dilation (i.e., volume expansion), and finally deform at constant volume in a typical test (see Figure 1.14). Correspondingly, the changes in the PWP will be accompanied with volume changes of the narrow shear zone. Specifically, shear-induced compaction will cause the development of excess pore water, especially for the saturated soil case, which can reduce the effective shear strength of the interface. Then, with

further development of shear displacement along the interface, shear-induced dilation may occur, which results in the dissipation of the PWP in the shear zone. As a result, the shear strength of the interface will increase briefly (i.e., the dilation hardening (Davis 1995)). This is followed by volume dilation, in which the constant volume stage gradually appears. The redistribution of the PWP from the soil to the narrow shear zone may allow the recovery of PWP to some extent. Consequently, the increase in interface shear strength is only temporary.

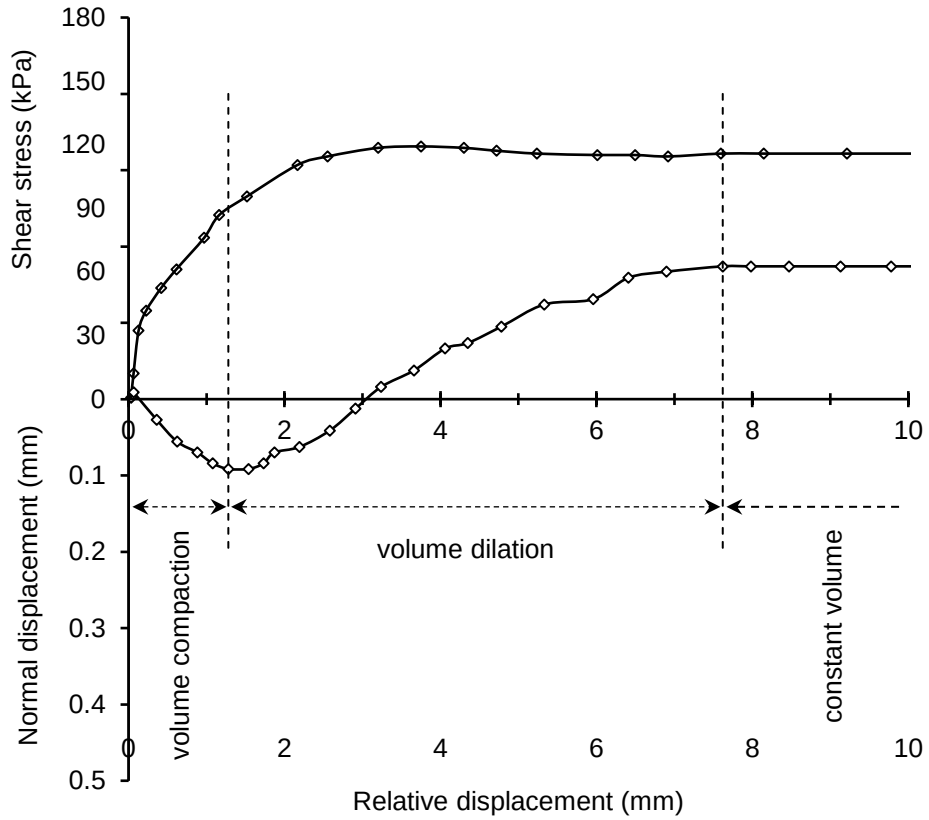

Figure 1.14. The typical three-stage volume change obtained from direct shear test on interface (data from (Hossain and Yin 2014))

1.6 Modeling approaches of interface

Many interface models have been proposed to analyze the behaviour of the soil-structure interface under both monotonic and cyclic loadings (Hu and Pu 2004; Romero et al. 2017; Stutz and Mašín 2017). The relevant constitutive models can be further divided into two categories: (1) elasticity-based models, (2) plasticity-based models. The former are fairly simple to use and widely accepted by engineers. However, plastic deformation and volumetric changes cannot be easily analyzed. Hence, elasticity-based models can be used for a limited range of different SSI analyses (Zhang and Zhang 2009). In contrast, both elastic and plastic components are incorporated into plasticity-based models. Thus, the interface behaviour and the resultant SSI problems can be analyzed in a more applicable manner. A detailed comparison between the two different interface modeling approaches is provided in Table 1.4.

Table 1.4. Comparison of elasticity-based models and plasticity-based models of interface

Model type	Representative models	Comments
Elasticity model	Modified Romberg-Osgood model (Desai et al. 1985)	The interface behaviour is simulated by a hyperbolic elastic model; The loading and unloading processes are described by piecewise elastic model; Effects of normal stress and surface roughness are considered; Plastic displacement is not considered; Stress path effects during debonding and rebonding are not considered.
	Shakir and Zhu (2009) model	Effects of water content and normal stress are considered; Shear failure and deformation are considered respectively; Unable to predict the effect of surface roughness; Unable to predict Dilatancy behaviour.

Elastoplasticity model	Mohr-Coulomb isochoric interface model (Zeghal and Edil 2002)	Nonassociative flow rule is adopted; Able to predict the work hardening/softening behaviour; Able to predict the dilatancy behaviour The effect of grain crushing is considered; Unable to characterize the effect of cyclic loading.
	Hypoplastic Cam-clay interface model (Stutz and Mašín 2017)	Able to describe the strain hardening/softening behaviour; Effects of surface roughness and normal stress are considered. Same parameters of modified Cam-clay model are adopted; Unable to characterize the effect of cyclic loading.
	Viscoplastic interface model (Samtani et al. 1996)	Able to characterize the effect of cyclic loading; Able to predict the time-dependent behaviour of interface; Able to predict the dilatancy and strain hardening behaviour; Non-associated flow rule is adopted; Unable to predict the strain-softening behaviour.
	Elastoplasticity damage interface model (Hu and Pu 2003)	Able to describe the strain hardening/softening behaviour; Able to describe the dilative response of interface; Non-associated flow rule is adopted; Able to predict the effect of normal stress, relative density and surface roughness; Unable to describe the effect of cyclic loading.

1.7 Conclusions

The following conclusions are drawn based on the review in this report.

1. The effects of SSI need to be obtained for accurate and reliable assessments of the seismic response of SSSs;
2. The DA and SA can be adopted to analyze SSI problems. True nonlinear analyses can be conducted by using the former but with great computational effort. The latter can substantially reduce the number of degrees of freedom by orders of magnitude through linear superposition;

3. The SSI (i.e., kinematic and inertial interactions) can greatly change the system response. As a result, the SSSs have longer natural periods of vibration and larger damping ratios compared with their counterparts in a fixed-base system;
4. Under dynamic loading, soil (both cohesionless and cohesive soils) materials can strongly exhibit non-linear behaviour, such as nonlinear volumetric response, and pressure-sensitive and rate-sensitive shear behaviour. In addition, the generation of excess pore water can affect the effective stress that is acting on the soil particles and thus the response of SSSs.
5. The soil-structure interface demonstrates strong nonlinear behaviour under dynamic loading, including nonlinear stress-displacement relations, shear-induced dilation behaviour and the generation of PWP.

   In this study we focused on point 4, the influence of the soil behaviour and the generation and dissipation of PWP on the seismic response of structures built on or embedded in soil deposits.

1.8 References

Altun, S., and Goktepe, A. (2006). "Dependence of dynamic shear modulus of uniform sands on stress level and density." *Civil Engineering and Environmental Systems*, 23(2), 101-116.

Anastasopoulos, I., Loli, M., Georgarakos, T., and Drosos, V. (2013). "Shaking Table Testing of Rocking—Isolated Bridge Pier on Sand." *Journal of Earthquake Engineering*, 17(1), 1-32.

Assimaki, D., Kausel, E., and Whittle, A. (2000). "Model for dynamic shear modulus and damping for granular soils." *Journal of Geotechnical and Geoenvironmental Engineering*, 126(10), 859-869.

Augustesen, A., Liingaard, M., and Lade, P. V. (2004). "Evaluation of time-dependent behavior of soils." *International Journal of Geomechanics*, 4(3), 137-156.

Bielak, J. (1976). "Modal analysis for building-soil interaction." *Journal of the Engineering Mechanics Division*, 102(5), 771-786.

Boulanger, R. W., and Idriss, I. M. (2004). "Evaluating the potential for liquefaction or cyclic failure of silts and clays." Citeseer.

Brumund, W., and Leonards, G. (1973). "Experimental study of static and dynamic friction between sand and typical constuction materials." *Journal of Testing and Evaluation*, 1(2), 162-165.

Bryden, P., El Naggar, H., and Valsangkar, A. (2014). "Soil-structure interaction of very flexible pipes: centrifuge and numerical investigations." *International Journal of Geomechanics*, 15(6), 04014091.

Carroll, W. F. (1963). "Dynamic Bearing Capacity of Soils: Vertical Displacements of Spread Footings on Clay: Static and Impulsive Loadings." US Army Engineer Waterways Experiment Station, Corps of Engineers.

Chandra, J. (2014). "Nonlinear seismic response of the soil-structure system: experimental analyses." Ph.D. thesis, Université Grenoble Alpes, France.

Chau, K., Shen, C., and Guo, X. (2009). "Nonlinear seismic soil–pile–structure interactions: shaking table tests and FEM analyses." *Soil Dynamics and Earthquake Engineering*, 29(2), 300-310.

Clough, G. W., and Duncan, J. M. (1973). "Finite element analysis of retaining wall behavior." *Journal of Soil Mechanics & Foundations Div*, 99(sm 4).

Coyle, H. M., and Sulaiman, I. H. (1967). "Skin friction for steel piles in sand." *Journal of Soil Mechanics and Foundations Division*, 92(SM6), 261-277.

Dash, H., and Sitharam, T. (2009). "Undrained cyclic pore pressure response of sand–silt mixtures: effect of nonplastic fines and other parameters." *Geotechnical and Geological Engineering*, 27(4), 501-517.

Davis, R. (1995). "Pore pressure effects on interface behavior." *Studies in Applied Mechanics*, 42, 449-461.

de Barros, F. C., and Luco, J. E. (1995). "Identification of foundation impedance functions and soil properties from vibration tests of the Hualien containment model." *Soil Dynamics and Earthquake Engineering*, 14(4), 229-248.

De Silva, L. I. N., Koseki, J., Wahyudi, S., and Sato, T. (2014). "Stress–dilatancy relationships of sand in the simulation of volumetric behavior during cyclic torsional shear loadings." *Soils and Foundations*, 54(4), 845-858.

Desai, C., Drumm, E., and Zaman, M. (1985). "Cyclic testing and modeling of interfaces." *Journal of Geotechnical Engineering*, 111(6), 793-815.

Desai, C. S., and Rigby, D. B. (1997). "Cyclic interface and joint shear device including pore pressure effects." *Journal of geotechnical and geoenvironmental engineering*, 123(6), 568-579.

Dobry, R., Ladd, R., Yokel, F. Y., Chung, R. M., and Powell, D. (1982). *Prediction of pore water pressure buildup and liquefaction of sands during earthquakes by the cyclic strain method*, National Bureau of Standards Gaithersburg, MD.

Dove, J. E., and Jarrett, J. B. (2002). "Behavior of dilative sand interfaces in a geotribology framework." *Journal of geotechnical and geoenvironmental engineering*, 128(1), 25-37.

El Mohtar, C. S., Drnevich, V. P., Santagata, M., and Bobet, A. (2013). "Combined resonant column and cyclic triaxial tests for measuring undrained shear modulus reduction of sand with plastic fines." *Geotechnical Testing Journal*, 36(4), 484-492.

Elgamal, A., Yang, Z., Lai, T., Kutter, B. L., and Wilson, D. W. (2005). "Dynamic response of saturated dense sand in laminated centrifuge container." *Journal of Geotechnical and Geoenvironmental Engineering*, 131(5), 598-609.

Ellis, B. (1996). "Full-scale measurements of the dynamic characteristics of buildings in the UK." *Journal of wind engineering and industrial aerodynamics*, 59(2-3), 365-382.

Endres, A., Arnold, J., and Roesset, J. (1984). "Soil-structure response using fixed base structural modes." *Proc., 8th World Conference on Earthquake Engineering, California*, 937-944.

Fei, K., and Xu, J. (2017). "Dynamic behavior of clay–aggregate mixtures." *Advances in Materials Science and Engineering*, 2017, 1-10.

Field, E., Kramer, S., Elgamal, A.-W., Bray, J., Matasovic, N., Johnson, P., Cramer, C., Roblee, C., Wald, D., and Bonilla, L. (1998). "Nonlinear site response: where we're at (a report from a SCEC/PEER seminar and workshop)." *Seismological Research Letters*, 69(3), 230-234.

Gazetas, G. (1991). "Formulas and charts for impedances of surface and embedded foundations." *Journal of geotechnical engineering*, 117(9), 1363-1381.

Halabian, A. M., and El Naggar, M. H. (2002). "Effect of non-linear soil–structure interaction on seismic response of tall slender structures." *Soil Dynamics and Earthquake Engineering*, 22(8), 639-658.

Hardin, B. O., and Drnevich, V. P. (1972). "Shear modulus and damping in soils: measurement and parameters effects." *Journal of the soil mechanics and foundations division*, 98(7), 667-692.

Hossain, M. A., and Yin, J.-H. (2014). "Dilatancy and strength of an unsaturated soil-cement interface in direct shear tests." *International Journal of Geomechanics*, 15(5), 04014081.

Hosseinzadeh, N., Davoodi, M., and Roknabadi, E. R. (2012). "Shake Table Study of Soil Structure Interaction Effects in Surface and Embedded Foundations." *Proc., the 15th World Conference on Earthquake Engineering*, 1-10.

Hsu, C.-C., and Vucetic, M. (2006). "Threshold shear strain for cyclic pore-water pressure in cohesive soils." *Journal of geotechnical and geoenvironmental engineering*, 132(10), 1325-1335.

Hu, L., and Pu, J. (2004). "Testing and modeling of soil-structure interface." *Journal of Geotechnical and Geoenvironmental Engineering*, 130(8), 851-860.

Hu, L., and Pu, J. L. (2003). "Application of damage model for soil–structure interface." *Computers and Geotechnics*, 30(2), 165-183.

Hussien, M. N., Karray, M., Tobita, T., and Iai, S. (2015). "Kinematic and inertial forces in pile foundations under seismic loading." *Computers and Geotechnics*, 69, 166-181.

Hussien, M. N., Tobita, T., Iai, S., and Karray, M. (2016). "Soil-pile-structure kinematic and inertial interaction observed in geotechnical centrifuge experiments." *Soil Dynamics and Earthquake Engineering*, 89, 75-84.

Ishihara, K. (1996). *Soil behaviour in earthquake geotechnics*, Clarendon Press.

Jones, K. C. (2013). "Dynamic Soil-Structure-Soil-Interaction Analysis of Structures in Dense Urban Environments." Ph.D. Thesis, University of California, Berkeley, USA.

Lai, C. G., and Martinelli, M. (2013). "Soil-Structure Interaction Under Earth-quake Loading: Theoretical Framework." *Proc., ALERT Doctoral School*, Technische Universitat Dresden, Germany, 3-44.

Lee, K. L., and Albaisa, A. (1974). "Earthquake induced settlements in saturated sands: 9F, 2T, 29R. J. GEOTECH. ENGNG. DIV. V100, N. GT4, APR. 1974, P387–406." *Proc., International Journal of Rock Mechanics and Mining Sciences & Geomechanics Abstracts*, A164.

Lefebvre, G., and Leboeuf, D. (1987). "Rate effects and cyclic loading of sensitive clays." *Journal of Geotechnical Engineering*, 113(5), 476-489.

Li, M., Lu, X., Lu, X., and Ye, L. (2014). "Influence of soil–structure interaction on seismic collapse resistance of super-tall buildings." *Journal of Rock Mechanics and Geotechnical Engineering*, 6(5), 477-485.

Liang, J., Fu, J., Todorovska, M. I., and Trifunac, M. D. (2017). "In-plane soil-structure interaction in layered, fluid-saturated, poroelastic half-space II: Pore

pressure and volumetric strain." *Soil Dynamics and Earthquake Engineering*, 92, 585-595.

Ling, H. I., and Liu, H. (2003). "Pressure-level dependency and densification behavior of sand through generalized plasticity model." *Journal of Engineering Mechanics*, 129(8), 851-860.

Lo, W.-C., Sposito, G., Lee, J.-W., and Chu, H. (2016). "One-dimensional consolidation in unsaturated soils under cyclic loading." *Advances in Water Resources*, 91, 122-137.

Lou, M., Wang, H., Chen, X., and Zhai, Y. (2011). "Structure–soil–structure interaction: literature review." *Soil Dynamics and Earthquake Engineering*, 31(12), 1724-1731.

Lu, Y. (2016). "Seismic soil-structure interaction in performance-based design." Ph.D. Thesis, University of Nottingham, England.

Luco, J., Wong, H., and Trifunac, M. D. (1986). "Soil-structure interaction effects on forced vibration tests." University of Southern California.

Ma, D., Ma, Q., and Yuan, P. (2017). "SHPB tests and dynamic constitutive model of artificial frozen sandy clay under confining pressure and temperature state." *Cold Regions Science and Technology*, 136, 37-43.

Makris, N., and Gazetas, G. (1992). "Dynamic pile ‐ soil ‐ pile interaction. Part II: Lateral and seismic response." *Earthquake engineering & structural dynamics*, 21(2), 145-162.

Massimino, M. R., and Maugeri, M. (2013). "Physical modelling of shaking table tests on dynamic soil–foundation interaction and numerical and analytical simulation." *Soil Dynamics and Earthquake Engineering*, 49, 1-18.

Matasovic, N., and Vucetic, M. (1992). "A pore pressure model for cyclic straining of clay." *Soils and Foundations*, 32(3), 156-173.

Mitchell, R., and King, R. D. (1977). "Cyclic loading of an Ottawa area Champlain Sea clay." *Canadian Geotechnical Journal*, 14(1), 52-63.

Mortara, G., Mangiola, A., and Ghionna, V. N. (2007). "Cyclic shear stress degradation and post-cyclic behaviour from sand–steel interface direct shear tests." *Canadian Geotechnical Journal*, 44(7), 739-752.

Moses, G., Rao, S., and Rao, P. (2003). "Undrained strength behaviour of a cemented marine clay under monotonic and cyclic loading." *Ocean engineering*, 30(14), 1765-1789.

Mylonakis, G., Nikolaou, S., and Gazetas, G. (2006). "Footings under seismic loading: Analysis and design issues with emphasis on bridge foundations." *Soil Dynamics and Earthquake Engineering*, 26(9), 824-853.

Nakamura, T., Mitachi, T., and Ikeura, I. (1999). "Direct shear testing method as a means for estimating geogrid-sand interface shear-displacement behavior." *Soils and Foundations*, 39(4), 1-8.

Nasser, M. (2009). "Seismic response of R/C frames considering dynamic soil-structure interaction." *Proc., the 18th International Conference on the Application of Computer Science and Mathematics in Architecture and Civil Engineering*, Weimar, Germany.

Pitilakis, D., and Clouteau, D. (2010). "Equivalent linear substructure approximation of soil–foundation–structure interaction: model presentation and validation." *Bulletin of Earthquake Engineering*, 8(2), 257-282.

Pitilakis, D., Dietz, M., Wood, D. M., Clouteau, D., and Modaressi, A. (2008). "Numerical simulation of dynamic soil–structure interaction in shaking table testing." *Soil dynamics and earthquake Engineering*, 28(6), 453-467.

Potyondy, J. G. (1961). "Skin friction between various soils and construction materials." *Geotechnique*, 11(4), 339-353.

Pradhan, T. B., Tatsuoka, F., and Sato, Y. (1989). "Experimental stress-dilatancy relations of sand subjected to cyclic loading." *Soils and Foundations*, 29(1), 45-64.

Reddy, E. S., Chapman, D., and Sastry, V. (2000). "Direct shear interface test for shaft capacity of piles in sand."

Rodriguez, M. E., and Montes, R. (2000). "Seismic response and damage analysis of buildings supported on flexible soils." *Earthquake engineering & structural dynamics*, 29(5), 647-665.

Romero, A., Galvín, P., António, J., Domínguez, J., and Tadeu, A. (2017). "Modelling of acoustic and elastic wave propagation from underground

structures using a 2.5 D BEM-FEM approach." *Engineering Analysis with Boundary Elements*, 76, 26-39.

Sáez, E., Lopez-Caballero, F., and Modaressi-Farahmand-Razavi, A. (2013). "Inelastic dynamic soil–structure interaction effects on moment-resisting frame buildings." *Engineering structures*, 51, 166-177.

Samtani, N. C., Desai, C. S., and Vulliet, L. (1996). "An interface model to describe viscoplastic behavior." *International journal for numerical and analytical methods in geomechanics*, 20(4), 231-252.

Shakir, R., and Zhu, J. (2009). "Nonlinear elastic model for compacted clay concrete interface." *Frontiers of Architecture and Civil Engineering in China*, 3(2), 187-194.

Silver, M. L., and Seed, H. B. (1971). "Volume changes in sands during cyclic loading." *Journal of Soil Mechanics & Foundations Div*.

Sitharam, T., and Govindaraju, L. (2007). "Pore pressure generation in silty sands during cyclic loading." *Geomechanics and Geoengineering: An International Journal*, 2(4), 295-306.

Stehmeyer, E. H., and Rizos, D. C. (2008). "Considering dynamic soil structure interaction (SSI) effects on seismic isolation retrofit efficiency and the importance of natural frequency ratio." *Soil Dynamics and Earthquake Engineering*, 28(6), 468-479.

Stutz, H., and Mašín, D. (2017). "Hypoplastic interface models for fine‐grained soils." *International Journal for Numerical and Analytical Methods in Geomechanics*, 41(2), 284-303.

Tabatabaiefar, H. R. (2017). "Development of synthetic soil mixture for experimental shaking table tests on building frames resting on soft soils." *Geomechanics and Geoengineering*, 12(1), 28-35.

Teachavorasinskun, S., Thongchim, P., and Lukkunaprasit, P. (2002). "Stress rate effect on the stiffness of a soft clay from cyclic, compression and extension triaxial tests." *Géotechnique*, 52(1), 51-54.

Thirugnanasampanther, S. (2016). "Cyclic behaviour and dynamic properties of soils under simple shear loading." Master thesis, Carleton University Ottawa, Ottawa, ON, Canada.

Trifunac, M., Ivanović, S., and Todorovska, M. (2001). "Apparent periods of a building. II: Time-frequency analysis." *Journal of Structural Engineering*, 127(5), 527-537.

Trifunac, M., and Todorovska, M. (1998). "Nonlinear soil response as a natural passive isolation mechanism—the 1994 Northridge, California, earthquake." *Soil Dynamics and Earthquake Engineering*, 17(1), 41-51.

Trifunac, M. D., Todorovska, M., and Hao, T. (2001). "Full-scale experimental studies of soil-structure interaction—a review." *Proc., Proc. of the Second US—Japan Workshop on Soil-Structure Interaction, Tsukuba City, Japan*.

Trombetta, N. W., Mason, H. B., Hutchinson, T. C., Zupan, J. D., Bray, J. D., and Kutter, B. L. (2013). "Nonlinear soil–foundation–structure and structure–soil–structure interaction: centrifuge test observations." *Journal of Geotechnical and Geoenvironmental Engineering*, 140(5), 04013057.

Uesugi, M., and Kishida, H. (1986). "Frictional resistance at yield between dry sand and mild steel." *Soils and foundations*, 26(4), 139-149.

Van Nguyen, Q., Fatahi, B., and Hokmabadi, A. S. (2017). "Influence of Size and Load-Bearing Mechanism of Piles on Seismic Performance of Buildings Considering Soil–Pile–Structure Interaction." *International Journal of Geomechanics*, 04017007.

Yamamuro, J. A., Abrantes, A. E., and Lade, P. V. (2011). "Effect of strain rate on the stress-strain behavior of sand." *Journal of Geotechnical and Geoenvironmental Engineering*, 137(12), 1169-1178.

Yasuhara, K., Yamanouchi, T., and Hirao, K. (1982). "Cyclic strength and deformation of normally consolidated clay." *Soils and Foundations*, 22(3), 77-91.

Yildirim, H., and Erşan, H. (2007). "Settlements under consecutive series of cyclic loading." *Soil Dynamics and Earthquake Engineering*, 27(6), 577-585.

Yoshimi, Y., and Kishida, T. (1981). "A ring torsion apparatus for evaluating friction between soil and metal surfaces."

Zeghal, M., and Edil, T. B. (2002). "Soil structure interaction analysis: modeling the interface." *Canadian Geotechnical Journal*, 39(3), 620-628.

Zergoun, M., and Vaid, Y. (1994). "Effective stress response of clay to undrained cyclic loading." *Canadian Geotechnical Journal*, 31(5), 714-727.

Zhang, G., Wang, L. p., and Zhang, J. M. (2011). "Dilatancy of the interface between a structure and gravelly soil." *Géotechnique*, 61(1), 75-84.

Zhang, G., and Zhang, J. (2009). "State of the art: mechanical behavior of soil–structure interface." *Progress in Natural Science*, 19(10), 1187-1196.

Zhang, Z., Cho, C., Pan, Q., and Lu, X. (2009). "Experimental Investigation on Excess Pore Water Pressure in Soft Soil-Foundations under Minor Shocks." *International Journal of Civil, Environmental, Structural, Construction and Architectural Engineering*, 3(2), 88-92.

CHAPTER 2

Formulation of a Dynamic Coupled Elastoplastic-Hydraulic Model for Soils

2.1 Introduction

Previous investigations (e.g., Bielak 1976; Rodriguez and Montes 2000; Stehmeyer and Rizos 2008; Lou et al. 2011; Van Nguyen et al. 2017) have found that the dynamic response of a structure supported on soil may differ significantly from that of a structure on a more rigid base, such as rock. Therefore, the characterization of the soil behaviour under earthquake shaking is necessary for the analysis of SSI.

In most cases, the soil foundation which is composed of saturated silt, fine sand or clay has been the focus of earthquake engineering since the potential energy during liquefaction can be easily accumulated during seismic action (Polito and Martin II 2001; Zhang et al. 2009). During dynamic loading, volumetric deformation can cause the generation of excess pore water pressure. Correspondingly, the effective stress and thus the soil strength will be affected. Therefore, an analysis of pore water pressure and its influence on soil stress under dynamic loadings is necessary for the assessment of SSI. As seismic waves (including both p-wave and s-wave propagate through soil), permanent deformation can develop in soil and thus affect the excess pore-water pressure.

To characterize soil behaviour, including the development of excess pore water pressure, and changes in effective stress, a dynamic coupled soil-pore water model is proposed in this study. The model is implemented into a commercial FEM software—COMSOL Multiphysics. For the stress-strain response of the soil skeleton, an elastic-viscous constitutive model is first incorporated, followed by an elasto-viscoplastic model.

2.2 Theoretical formulations of dynamic coupled soil-pore water model

To analytically examine the dynamic characteristics of coupled soil-pore water interaction, the following assumptions are made.

i. Soil is considered to be a two-phase (solid and liquid) porous medium. The constituents (soil particles and pore water) are considered to be two independent overlapping continua in the context of the theory of mixtures. Pore water and the solid skeleton are compressible.
ii. The voids in a soil skeleton are fully saturated with pore water. Moreover, it is assumed that the pore water does not undergo a phase transition (evaporation or freezing).
iii. It is assumed that the solid skeleton has small deformations with respect to its mechanical response, and only elastic deformation is considered in the present study.
iv. The effects of temperature changes and chemical reactions are not taken into consideration in this study.
v. The compressive stress is considered to be negative.

2.2.1 Continuity equations

In order to describe the transport of conserved quantities, such as mass and momentum in saturated soil under dynamic loading, the continuity equations need to be satisfied. Then, the dynamic coupled soil-pore water model (governing

equations) can be formulated when the constitutive equations (e.g., stress and strain relationships and Darcy's law) are substituted into the continuity equations viz. mass, energy and momentum (mechanical equilibrium) equations. In this study, three balance equations: (i) water mass, (ii) solid phase mass, and (iii) momentum (mechanical equilibrium) are considered.

2.2.2 Mass conservation equation

Based on the volume-averaging method, the mass balance equations can be derived in a Lagrangian framework (i.e. variation of the state variables with respect to the moving coordinate system) in terms of a material derivative, viz., $D(\cdot)/Dt = \partial(\cdot)/\partial t + \mathbf{v}_s \cdot \nabla(\cdot)$ with respect to the velocity of the solid phase $\mathbf{v}_s$.

$$(1-\phi)\frac{D\rho_s}{Dt} - \rho_s \frac{D\phi}{Dt} + \rho_s (1-\phi)\nabla \cdot \mathbf{v}_s = 0 \tag{2.1}$$

$$\rho_w \frac{D\phi}{Dt} + \phi \frac{D\rho_w}{Dt} + \nabla \cdot \left(\phi \rho_w \mathbf{v}^{rw}\right) + \phi \rho_w \nabla \cdot \mathbf{v}_s = 0 \tag{2.2}$$

where ρ_i denotes the density (*i* refers to the solid phase and pore water), ϕ is the porosity, $\mathbf{v}_s$ and $\mathbf{v}^{rw}$ denote the phase velocity with respect to the fixed spatial axes (Eulerian coordinates), and the corresponding relative apparent velocity of the fluids in the porous medium, respectively, which can be written as:

$$\mathbf{v}_w = \mathbf{v}_{rw} + \mathbf{v}_s \tag{2.3}$$

$$\mathbf{v}^{rw} = \phi \mathbf{v}_{rw} \tag{2.4}$$

It is assumed that the solid phase displacement is $\mathbf{u}$ (a vector field). With respect to the Eulerian coordinate system $\mathbf{x}(x_1, x_2, x_3)$, the volumetric strain of the solid phase can be expressed as:

$$\varepsilon_v = \frac{\partial u_i}{\partial x_i} = \nabla \cdot \mathbf{u} \tag{2.5}$$

Based on the definition of the volumetric strain of the solid phase, the divergence of the solid phase velocity can be rewritten in terms of the volumetric strain of the soil skeleton ε_v (Bear and Buchlin 1991):

$$\nabla \cdot \mathbf{v}_s = \nabla \cdot \dot{\mathbf{u}} = \frac{D\varepsilon_v}{Dt} = \frac{\partial \varepsilon_v}{\partial t} + \mathbf{v}_s \cdot \nabla \varepsilon_v \approx \frac{\partial \varepsilon_v}{\partial t} \quad \left(\partial \varepsilon_v / \partial t >> \nabla \varepsilon_v\right) \tag{2.6}$$

By rearranging the mass balance equation of the solid phase, the time rate of the change of the porosity can be derived as:

$$\frac{D\phi}{Dt} = \frac{(1-\phi)}{\rho_s} \frac{D\rho_s}{Dt} + (1-\phi) \nabla \cdot \mathbf{v}_s \tag{2.7}$$

Due to the assumption of a small strain of the porous medium, the second term that is found in the material derivative of the fluid quantity, i.e. $\mathbf{v}_s \cdot \nabla(\cdot)$, is negligible. Therefore, by substituting Eqs. (2.6) and (2.7) into Eq.(2.2), the fluid mass conservation equations that involve a solid phase mass balance equation can be rewritten as:

$$\phi \frac{\partial \rho_w}{\partial t} + (1-\phi) \frac{\rho_w}{\rho_s} \frac{\partial \rho_s}{\partial t} + \nabla \cdot \left(\phi \rho_w \mathbf{v}^{rw}\right) = -\rho_w \frac{\partial \varepsilon_v}{\partial t} \tag{2.8}$$

As indicated in Eq. (2.8), the time rate change of the volumetric strain that occurs in soil can affect the pore-water mass balance equation. Consequently, excess pore-water pressure is incorporated into the analysis.

2.2.3 Momentum conservation equation

The momentum conservation (i.e. mechanical equilibrium) equation can be written as:

$$\nabla \cdot \boldsymbol{\sigma} + \left[\left(1-\phi\right)\rho_s + \phi\rho_w \right]\mathbf{g} = \left[\left(1-\phi\right)\rho_s + \phi\rho_w \right]\ddot{\mathbf{u}} \tag{2.9}$$

where $\boldsymbol{\sigma}$ is the (macroscopic) total stress tensor, and $\mathbf{g}$ is the acceleration of gravity.

2.3 Constitutive relations

2.3.1 Mechanical model

The soil is fully saturated with pore water. In considering the effects of the pore water, the total stress vector $\boldsymbol{\sigma}$ is decomposed into effective stress $\boldsymbol{\sigma}'$ and average pore pressure P under static loading. When dynamic loading is applied onto a two-phase porous medium, the additional stress which is proportional to the strain rate will become another component of the total stress, which represents energy that is dissipated by viscous damping in soil under dynamic loading. Correspondingly, the effective stress $\boldsymbol{\sigma}'$ can be defined as:

$$\boldsymbol{\sigma}' = \boldsymbol{\sigma} + \mathbf{I}p_w - \boldsymbol{\sigma}_{vs} \tag{2.10}$$

where $\mathbf{I}$ is the identity matrix (i.e., the 6×6 square matrix with ones on the main diagonal and zeros elsewhere). It should be noted that the compressive stress is considered to be negative in this study. However, the pore water pressure in the saturated soil is considered to be positive in compression per soil mechanic conventions.

Since effective stress is responsible for the deformation of the solid skeleton, the deformation model can be written in the following general form:

$$\boldsymbol{\sigma}' = \mathbf{D}^{e}\left(\boldsymbol{\varepsilon} - \boldsymbol{\varepsilon}_{p} - \boldsymbol{\varepsilon}_{vs}\right) \tag{2.11}$$

where $\boldsymbol{\varepsilon}$ is the total strain that has occurred in the soil, ε_p is the plastic strain , ε_{vs} is the viscous strain and $\mathbf{D}^{e}$ is a fourth-order tensor of material stiffness, and can be defined for an isotropic material as:

$$\mathbf{D}^{e} = \begin{bmatrix} 2\mu+\lambda & \lambda & \lambda & 0 & 0 & 0 \\ & 2\mu+\lambda & \lambda & 0 & 0 & 0 \\ & & 2\mu+\lambda & 0 & 0 & 0 \\ & & & \mu & 0 & 0 \\ & sym. & & & \mu & 0 \\ & & & & & \mu \end{bmatrix} \tag{2.12}$$

with μ and λ as the Lame's parameters:

$$\lambda = \frac{E\upsilon}{(1+\upsilon)(1-2\upsilon)} \qquad \upsilon = \frac{E}{2(1+\upsilon)} \tag{2.13}$$

where E and υ are the elastic modulus and Poisson's ratio respectively.

Based on the assumption of infinitesimal elastic deformation, the strain in the soil can be defined with a displacement gradient:

$$\boldsymbol{\varepsilon}_{\mathbf{e}} = \frac{1}{2}\left[\nabla\mathbf{u} + (\nabla\mathbf{u})^{T}\right] \tag{2.14}$$

where $\mathbf{u}$ is the displacement (a vector quantity defined with respect to the material coordinates).

2.3.1.1 Elastoviscous model

To characterize the energy dissipation induced by the rate of change of the soil volumetric and shear strain, viscous damping is incorporated into the stress analysis of saturated soil under dynamic loading.

$$\boldsymbol{\sigma}_{vs} = \eta_b \frac{\partial \boldsymbol{\varepsilon}_v}{\partial t} + 2\eta_s \frac{\partial \boldsymbol{\varepsilon}_{dev}}{\partial t} \tag{2.15}$$

where η_b and η_s respectively denote the bulk viscosity and shear viscosity, and $\boldsymbol{\varepsilon}_v$ and $\boldsymbol{\varepsilon}_{dev}$ represent the volumetric strain and deviatoric strain that have occurred in the soil. Based on the definition of strain (i.e., Eq.(2.14)), $\boldsymbol{\varepsilon}_v$ and $\boldsymbol{\varepsilon}_{dev}$ can be respectively defined as:

$$\boldsymbol{\varepsilon}_v = (\nabla \cdot \mathbf{u})\mathbf{I} \tag{2.16}$$

$$\boldsymbol{\varepsilon}_{dev} = \boldsymbol{\varepsilon}_{\mathbf{e}} - \frac{1}{3}\boldsymbol{\varepsilon}_v = \frac{1}{2}\left[\nabla \mathbf{u} + (\nabla \mathbf{u})^T\right] - (\nabla \cdot \mathbf{u})\mathbf{I} \tag{2.17}$$

As indicated in Eq. (2.15), both rate of compression (or expansion) and shear deformation can resist further stress development in the soil. The advantages of the viscous stress model (i.e., Eq. (2.15)) are that: (1) compared with other damping models (e.g., Rayleigh damping), the parameters (i.e., η_b and η_s) of the viscous stress model have direct physical meaning, and (2) due to the incorporation of both the rate of change of volumetric and shear strain, the effect of energy dissipation on both the compressional and shear waves can be captured by the developed model.

In determining the bulk and shear viscosities, η_b and η_s, Karato (2012) found that the former is in fact dependent on the latter as well as porosity ϕ (i.e., $\eta_b \sim$

η_s/ϕ). Therefore, the following predictive functions are adopted in this study based on the bulk and shear viscosities in Schmeling et al. (2012).

$$\eta_s = \eta_{s0}\left(1-\phi\right) \tag{2.18}$$

$$\eta_b = \eta_s \frac{1-\phi}{\phi} \tag{2.19}$$

where η_{s0} represents the initial shear viscosity of soil in the static state. An experimental study (Mahajan and Budhu 2008) on the initial shear viscosity confirmed that η_{s0} highly depends on the liquidity index (LI):

$$\eta_{s0} = a_1 \exp\left(a_2 LI\right) \tag{2.20}$$

where a_1 and a_2 are the fitting parameters for the initial shear viscosity of the soil, and LI is the liquidity index and $LI = \left(w_w - PL\right)/\left(LL - PL\right)$ with w_w as the natural water content, LL as the liquid limit, and PL as the plastic limit. Moreover, also based on the study by (Mahajan and Budhu 2008), a_1=5e6 Pa·s, and a_2 =-1.43.

It should be pointed out the viscoelastic model will be used as a reference to demonstrate the necessity of development of elasto-viscoplastic model. The detailed information about the elasto-viscoplastic model is presented in Subsection 2.3.1.2 and 2.3.1.3.

2.3.1.2 Elastoplastic model

During the propagation of seismic waves, both P-wave and S-wave can cause volume changes in soils, and thus affect the pore water and effective stress. However, based on the elasticity theory, no volumetric strain occurs when S-wave appears in soils. Therefore, the viscoelastic model cannot capture the behaviour

of soil during the period of earthquake. To describe the development of permanent deformation that occurrs in soil due the propagation of seismic waves, the Modified Cam-Clay (MCC) Model is incorporated into the coupled soil-pore water model.

The yield function F of the MCC model can be expressed by the following equation:

$$F = \frac{q^2}{p'^2} + M^2\left(1 - \frac{p'_{c0}}{p'}\right) = 0 \tag{2.21}$$

with

$$p' = \frac{I_1}{3} = \frac{\sigma'_1 + \sigma'_2 + \sigma'_3}{3}$$

$$q = \sqrt{3J_2} = \sqrt{\frac{1}{2}\left[\left(\sigma'_1 - \sigma'_2\right)^2 + \left(\sigma'_2 - \sigma'_3\right)^2 + \left(\sigma'_3 - \sigma'_1\right)^2\right]}$$

where q is the deviatoric stress, p' is the mean effective stress, p'_{c0} is the initial preconsolidation pressure, M is the slope of critical state line (CSL) which refers to a state in which further distortion can occur with no changes in volume and stress in soil, I_1 and J_2 respectively denote the first stress invariant and second invariant of deviatoric stress, and σ'_i stands for the principal stress (i=1, 2, and 3).

Moreover, to describe the development of plastic strain, the flow rule is needed. In this study, the associated flow rule is incorporated into the analysis (i.e., the yield function is identical to the potential function).

$$\dot{\varepsilon}_p = \dot{\lambda}_p \frac{\partial F}{\partial \sigma} = \dot{\lambda}_p \left[\frac{1}{3}\left(2p' - p_c\right)I + \frac{3}{M^2} dev\left(\sigma\right)\right] \tag{2.22}$$

where λ_p is the plastic consistency parameter, I is the identity tensor.

With the development of volumetric plastic strain, the initial yield surface may change if the critical state is not reached. As shown in Figure 2.1, the hardening behaviour (i.e., the expansion of yield surface) will take place if the stress points (represented by p' and q) reach the yield curve and below the CSL. If stress points reach the yield surface, the stress will stay on the yield curve and its direction will be perpendicular to the tangent line of the yield surface (Hashiguchi and Tsutsumi 2003). Correspondingly, on the right side of CSL, the mean effective stress component has a positive value, and thus causes volume reduction in soils (i.e., shear induced contraction). However, on the left side of CSL, the component of mean effective stress has a negative value, and thus increases the soil volume (i.e., shear induced expansion). Therefore, to capture the volume change in soil, the hardening and softening behavior of soil must be fully considered.

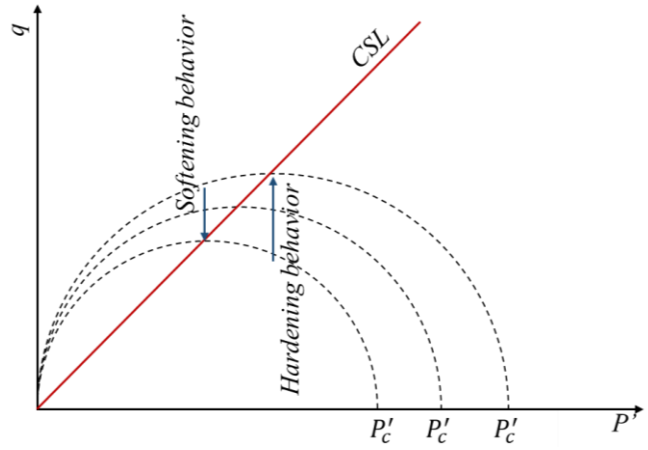

Figure 2.1. Evolution of yield surface (hardening and softening behaviors) of Modified Cam-Clay model

The right endpoint of the yield surface of MCC model is defined by the preconsolidation pressure p_c', which can be determined by the volumetric plastic strain (Yu 2006):

$$p_c' = p_{c0}' \exp\left(-\frac{1+e_0}{\lambda-\kappa}\varepsilon_v^p\right) \tag{2.23}$$

where e_0 is the initial void ratio of soil and ε_v^p is the volumetric plastic strain developed in soil.

To implement the MCC model, several model parameters, including the Poisson's ratio μ, the compression index λ, the swelling index κ, the slope of CSL M, and the bulk modulus K are needed.

To capture the dynamic nonlinear behaviour of soil (e.g., the strain-rate-dependence in soil), the Perzyna type of viscoplastic formulation is adopted in the current study. The latter has been proven valid in representing the rate effect in various geomaterials (e.g. Katona, 1985; Simo et al., 1986; Tong and Tuan, 2007; Aráoz and Luccioni, 2015; Lu and Fall, 2015).

In Perzyna's model, the total strain rate vector $\dot{\boldsymbol{\varepsilon}}$ consists of an elastic component $\dot{\boldsymbol{\varepsilon}}^e$ and a viscoplastic (inelastic) component $\dot{\boldsymbol{\varepsilon}}^{vp}$

$$\dot{\boldsymbol{\varepsilon}} = \dot{\boldsymbol{\varepsilon}}^e + \dot{\boldsymbol{\varepsilon}}^{vp} \tag{2.24}$$

The elastic strain rate independently of the viscosity is expressed as

$$\dot{\boldsymbol{\varepsilon}}^e = \mathbf{D}^{-1}\dot{\boldsymbol{\sigma}} \tag{2.25}$$

where $\dot{\boldsymbol{\sigma}}$ is the stress-rate tensor, and **D** is the stiffness matrix.

The viscoplastic strain rate in Perzyna's model is generally defined by the following viscoplastic flow rule:

$$\dot{\boldsymbol{\varepsilon}}^{vp} = \eta \left\langle \phi(F) \right\rangle \frac{\partial F}{\partial \boldsymbol{\sigma}} \tag{2.26}$$

where η is evolutive fluidity parameter for soil; $\langle\ \rangle$ is the Macaulay bracket defined as $\left\langle x \right\rangle = (x + |x|)/2$, *F* is the yield function defined by equation (2.21), and $\phi(F)$ is a dimensionless scaling function which is expressed as

$$\phi(F) = \frac{F}{F_0} \tag{2.27}$$

where *N* is the exponent and F_0 is the normalizing constant with the same unit as *F*. The associated flow rule is generally used in this type of model, and the direction of $\dot{\boldsymbol{\varepsilon}}^{vp}$ is given by *F* and in the outward normal direction of the yield surface.

2.3.2 Fluid flow model

As demonstrated in the pore water mass balance equation (i.e., Eq. (2.8)), there is a transport term (i.e., $\nabla \cdot \left(\phi \rho_w \mathbf{v}^{rw} \right)$) which is required to determine the pore water pressure in the soil. By incorporating the gravity effect, Darcy's law is used to calculate the pore water flow in the saturated soil:

$$\mathbf{v}^{rw} = -\frac{K}{\rho_w g} \nabla \left(p_w - \rho_w g D \right) \tag{2.28}$$

where K is a coefficient of permeability (i.e., the saturated hydraulic conductivity), and D represents the elevation head for the point of interest.

2.3.3 Storage term model

There are two time-derivative terms (i.e., the time rate of the change of storage of the pore water and solid phase) on the left side of Eq. (2.8). Applying the chain rule, Eq. (2.8) can be written as:

$$\phi\left(\frac{\partial \rho_w}{\partial p_w}\right)\frac{\partial p_w}{\partial t}+(1-\phi)\rho_w\left(\frac{\partial \rho_s}{\partial p_w}\Big/\rho_s\right)\frac{\partial p_w}{\partial t}+\nabla\cdot\left(\phi\rho_w\mathbf{v}^{rw}\right)=-\rho_w\frac{\partial \varepsilon_v}{\partial t} \tag{2.29}$$

The terms $\frac{\partial \rho_w}{\partial p_w}$ and $\frac{\partial \rho_s}{\partial p_w}\Big/\rho_s$ in Eq. (2.8) represent the compressibility of the pore water, β_w, and soil skeleton, α_s, respectively.

$$\alpha_s=\frac{\partial \rho_s}{\partial p_w}\Big/\rho_s \tag{2.30}$$

$$\beta_w=\frac{\partial \rho_w}{\partial p_w} \tag{2.31}$$

Through the storage term model, the influence of mechanical process (e.g., volumetric strain) on the pore water pressure (PWP) can be captured. In addition, through the definition of effective stress in the mechanical model, the effect of hydraulic process on the mechanical behaviour of soil can be quantitatively assessed. Therefore, the coupling between mechanical and hydraulic processes can be captured by the developed model. The characteristics of the developed dynamic elastoplastic-hydraulic model are as follows.

1. The time rate of the change of volumetric strain is considered in the pore water mass balance equation. Hence, the developed model can be used to assess the development of excess pore water pressure under dynamic loadings.

2. In this study, the deformation of the soil skeleton is caused by the effective stress rather than the total stress. Therefore, the effect of the pore water pressure on deformation can be captured by the developed model.
3. Ground input motion can be incorporated into the developed model by using an inertial term in the momentum conservation equation (i.e., $\left[(1-\phi)\rho_s + \phi\rho_w\right]\ddot{\mathbf{u}}$). Therefore, dynamical loadings (e.g., seismic or blast loadings) can be integrated into the analysis.
4. Viscous damping is incorporated into the model in order to assess the effect of the time rate of change of both the volumetric and shear strains on the energy dissipation during wave propagations through soil. Moreover, the parameters of the viscous damping function have direct physical meaning, which can provide in-depth insight into the effect of damping on soil behavior under dynamic loadings.

2.4 References

Bear, J., and Buchlin, J. M. (1991). Modelling and applications of transport phenomena in porous media, Kluwer Academic Publishers, Dordrecht, The Netherlands.

Bielak, J. (1976). "Modal analysis for building-soil interaction." *Journal of the Engineering Mechanics Division*, 102(5), 771-786.

Hashiguchi, K., and Tsutsumi, S. (2003). "Shear band formation analysis in soils by the subloading surface model with tangential stress rate effect." *International Journal of Plasticity*, 19(10), 1651-1677.

Lou, M., Wang, H., Chen, X., and Zhai, Y. (2011). "Structure–soil–structure interaction: literature review." *Soil Dynamics and Earthquake Engineering*, 31(12), 1724-1731.

Lu, G., L, M. (2015). "A coupled chemo-viscoplastic model for cemented tailings backfill under blast loading". *International Journal of Numerical and Analytical Methods in Geomechanics* 40:1123-1149.

Mahajan, S., and Budhu, M. (2008). "Shear viscosity of clays to compute viscous resistance." *Proc., Proceedings of the 12th International Conference of International Association for Computer Methods and Advances in Geomechanics (IACMAG), Goa, India*.

Polito, C. P., and Martin II, J. R. (2001). "Effects of nonplastic fines on the liquefaction resistance of sands." *Journal of Geotechnical and Geoenvironmental Engineering*, 127(5), 408-415.

Rodriguez, M. E., and Montes, R. (2000). "Seismic response and damage analysis of buildings supported on flexible soils." *Earthquake engineering & structural dynamics*, 29(5), 647-665.

Stehmeyer, E. H., and Rizos, D. C. (2008). "Considering dynamic soil structure interaction (SSI) effects on seismic isolation retrofit efficiency and the importance of natural frequency ratio." *Soil Dynamics and Earthquake Engineering*, 28(6), 468-479.

Van Nguyen, Q., Fatahi, B., and Hokmabadi, A. S. (2017). "Influence of Size and Load-Bearing Mechanism of Piles on Seismic Performance of Buildings

Considering Soil–Pile–Structure Interaction." *International Journal of Geomechanics*, 04017007.

Yu, H.-S. (2006). "Isotropic Hardening and Critical State Theory." *Plasticity and Geotechnics*, 86-152.

Zhang, Z., Cho, C., Pan, Q., and Lu, X. (2009). "Experimental Investigation on Excess Pore Water Pressure in Soft Soil-Foundations under Minor Shocks." *World Academy of Science, Engineering and Technology, International Journal of Civil, Environmental, Structural, Construction and Architectural Engineering*, 3(2), 88-92.

CHAPTER 3

Verification and Validation of the Coupled Elastoplastic-Hydraulic Model for Soils and its Engineering Application

3.1 Introduction

To assess the predictability of the coupled elasto-viscoplastic-hydraulic model developed in Chapter two, two case studies are performed to compare the predicted results and measured data collected from previous studies. In addition, to demonstrate the features of the developed model, the predicted results from the coupled viscoelastic-hydraulic model are presented in this chapter as well. From the results obtained with the viscoelastic-hydraulic model, it can be found that the nonlinear behaviour (i.e., the permanent deformation and the associated excess pore water) of soil cannot be captured. Therefore, it is necessary to incorporate plasticity into the quantitative assessment of soil behaviour under dynamic loadings conditions. This chapter will include the following topics. First, the verification of the elastoviscous-hydraulic model will be presented in section 3.2. Through this model, the soil dynamic behaviour will be investigated, and the limitations of the viscoelastic-hydraulic model will be discussed. Then, the coupled visco-elastoplastic-hydraulic model will be validated against the measured data collected from previous studies (including data from cyclic triaxial tests and shaking table tests) on soil in section 3.3. Moreover, the validated model will be adopted to simulatet the soil-structure interaction for a hypothetical small modular reactor in section 3.4.

3.2 Verification of the viscoelastic-hydraulic model

By using the developed viscoelastic-hydraulic model, the dynamic behavior of soil is examined in this study. A two-dimensional (2D) soil column submitted to an

input motion is analyzed. Various assumptions are made in the soil modeling in terms of the total stress, effective stress, and effective stress with damping.

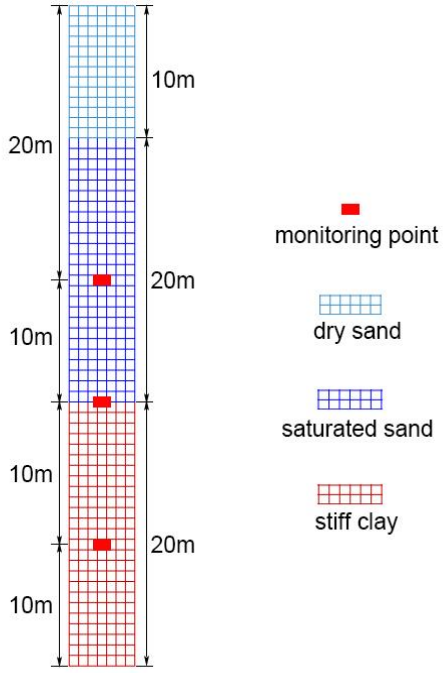

Figure 3.1. Geometry and mesh of the simulated soil column with three layers of different soils

As shown in Figure 3.1, the simulated soil column consists of three different layers: dry sand (thickness: 10 m), saturated sand (thickness: 20 m), and saturated stiff clay (thickness: 20 m). The material properties of the different types of soils and pore water are listed in Table 3.1, and the adopted boundary conditions are presented in Table 3.1.

Table 3.1. Properties of the soils used in the field investigation

Parameter	Density (kg/m^3)	Elasticity (MPa)	Poisson's ratio (-)	Porosity (-)	Compressibility (1/Pa)
Dry sand	1300	20	0.35	0.4	N/A
Saturated sand	1850	30	0.35	0.35	2.6e-8
Stiff clay	1400	50	0.30	0.5	2.6e-7
Parameter	LL (%)	PL (%)	Water content (%)	Coefficient of permeability (m/s)	
Dry sand	20	0	0	N/A	
Saturated sand	20	0	22.6	5.77e-5	
Stiff clay	100	25	27.8	4.21e-6	

* -: dimensionless unit.

Table 3.2. Specified boundary conditions of the soil column

Type of B.C.[a]	Specified B.C.
Mechanical process	
Top side	Free
Vertical sides	Spring Foundation B.C.
Bottom side	Fixed B.C.
Hydraulic process	
Surrounding sides	No flow
Input motion	
Bottom layer of soil column	Prescribed acceleration B.C.

[a] B.C.: boundary condition.

For the pore water, the required material properties include water density and water compressibility. In this study, ρ_i = 1000 kg/m^3 and β_w = 4.6e-10 Pa^{-1}. For the loading conditions, an input acceleration in the vertical direction (re: Figure 3.2) is applied at the bottom of the soil column, which can induce compressive strain in the soil column and thus generate excess pore water pressure.

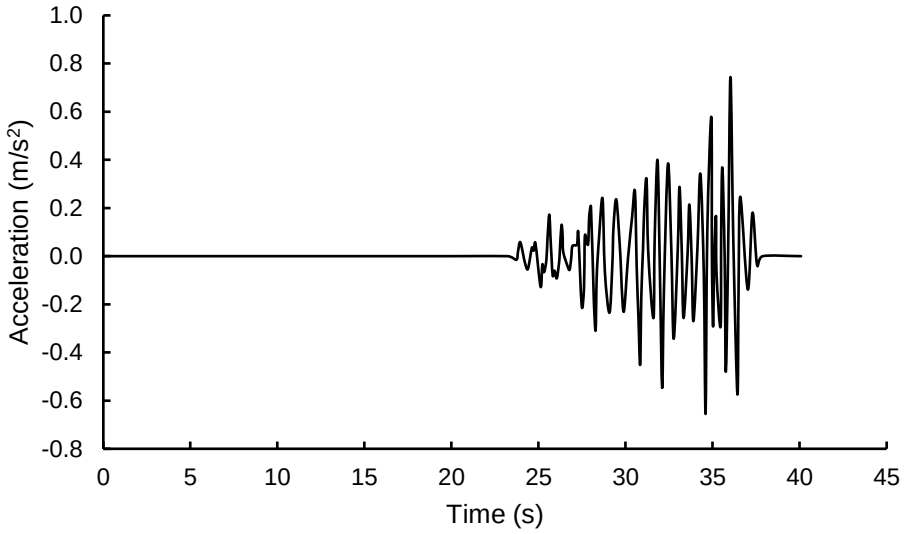

Figure 3.2. Inputted acceleration used in the investigation on soil column

To provide an in-depth insight into the soil behaviour, the predicted results obtained by using the developed effective stress model with damping are respectively compared with the counterparts obtained from total stress model and effective stress model without damping. In addition, the lowest monitoring point (10m from the base of soil column) is chosen to study the soil behaviour.

3.2.1 Discussion on the grid spacing and time-step size

Based on the previous studies (Lysmer and Kuhlemeyer 1969; Watanabe et al. 2017) on grid spacing and time-step size, it has been believed that approximately ten nodes per wavelength are appropriate in most cases to ensure accuracy and stability. Therefore, the requirements on the grid spacing Δx can be expressed as:

$$\Delta x \leq \frac{\lambda_{\min}}{10} = \frac{V_s T_{\min}}{10} \tag{3.1}$$

where $\lambda_{\min}$ denotes the minimum wavelength which can be calculated by product of shear wave velocity V_s and minimum period of the system $T_{\min}$.

As for the time-step size, the smallest fundamental period of the system should be represented with approximately ten time-steps.

$$\Delta t \leq \frac{\Delta x}{V_s} \tag{3.2}$$

Substituting the Eq. (3.1) into Equ. (3.2), the time-step size can be determined by the period of the system directly:

$$\Delta t \leq \frac{T_{\min}}{10} \tag{3.3}$$

3.2.2 Development of excess pore pressure under dynamic loading

The time rate of the change of volumetric strain can contribute to the development of excess pore pressure. Therefore, the changes in pore water pressure under seismic loading are assessed by using the developed model. Moreover, to further demonstrate the effect of viscous damping on the soil behavior, additional simulations without damping are performed as well. Figure 3.3 presents a comparison of the pore water pressure in soil under various damping conditions. The obtained results show that the effective stress model overestimates the generation of excess pore water if viscous damping is ignored, because energy dissipation by viscous damping is not taken into account. Hence, the rate of the change of volumetric strain will be reduced as well. However, it should be noted that because irreversible deformation is not considered in this study, the obtained

pore water pressure will gradually approach the hydrostatic pressure after seismic loading. Therefore, it is necessary to incorporate viscoplasticity into an analysis of the soil response to dynamic loading.

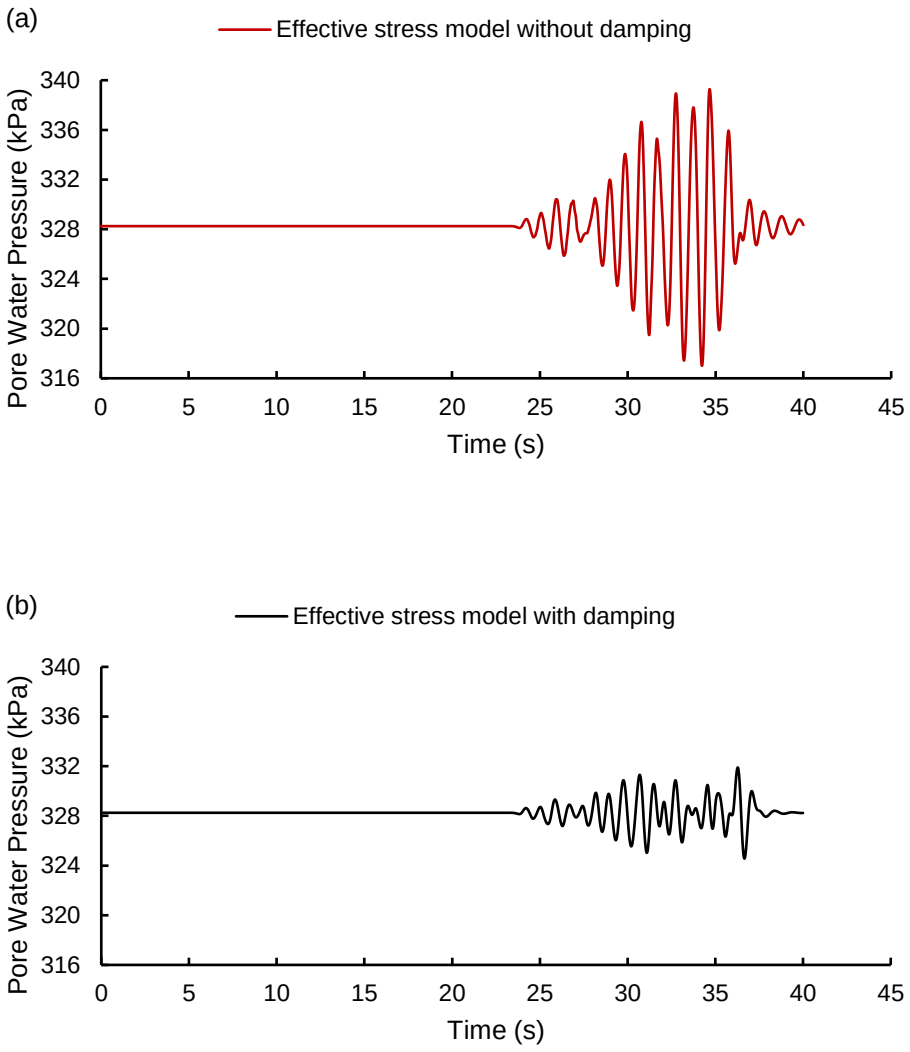

Figure 3.3. Development of pore water pressure in soil under seismic loading predicted by (a) effective stress model without damping, and (b) effective stress model with damping.

3.2.3 Development of volumetric strain under dynamic loading

An analysis of the volumetric strain in soil is conducted in this study. To do so, three cases are considered: i) with the total stress model, ii) effective stress model without damping, and iii) effective stress model with damping. The obtained results are plotted in Figure 3.4. From this figure it can be observed that: (1) the resultant volumetric strain in the soil predicted by the total stress model and effective stress model without damping is greater than that obtained by the effective stress model with viscous damping. The obtained results further confirm that the generation of excess pore water pressure and energy loss due to viscous damping have a significant influence on the soil deformation under seismic loading. Therefore, the effective stress model with viscous damping is strongly recommended for the analysis of soil behaviour under dynamic loadings; (2) similar to the development of pore water pressure (re: Figure 3.3), the change in volumetric strain gradually approaches zero with reduced input motion. This is due to the plasticity which is not considered in the current study. Therefore, to accurately assess soil deformation under dynamic and repeated loadings, viscoplasticity needs to be examined, and will be subsequently considered.

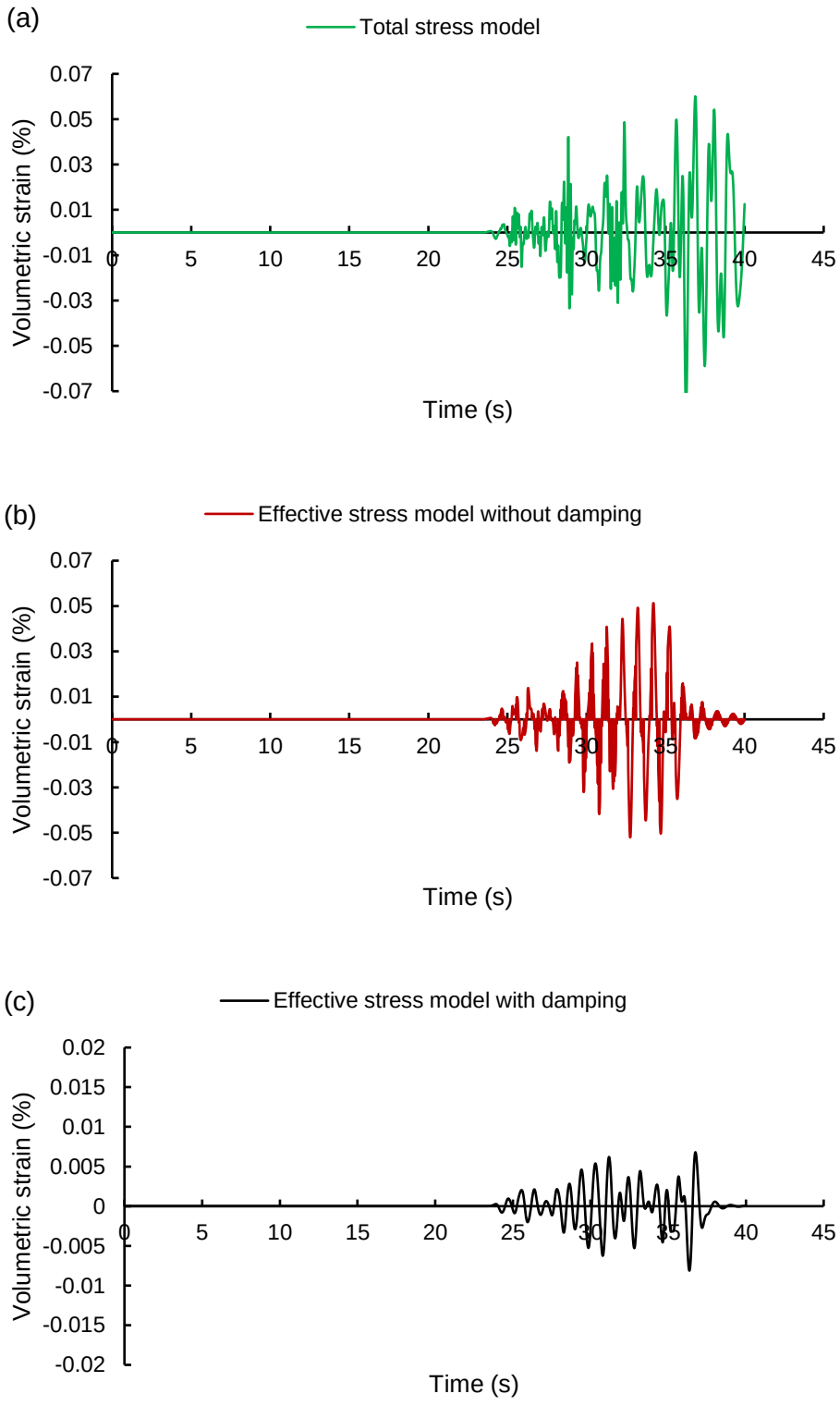

Figure 3.4. Development of volumetric strain simulated by using (a) total stress model, (b) effective stress model without damping, and (c) effective stress model with damping.

3.2.4 Development of vertical stress in soil under dynamic loading

Substantial changes in soil stress can take place under seismic loading. Input motion is applied on the bottom of the soil column which propagates through the soil in the vertical direction. Hence, the resultant vertical stress is analyzed in this study. To demonstrate the soil behaviour under dynamic loading, the vertical stress in soil is simulated by using the total stress model, effective stress model without damping, and effective stress model with viscous damping. The obtained results are presented in Figure 3.5. It can be observed that both the total stress model and the effective stress model without damping significantly overestimate the stress level. The relatively high vertical stress predicted by these two models can result in a larger strain (re: Figure 3.4), and excess pore water pressure in soil. Therefore, an effective stress model with viscous damping is necessary to obtain a reliable assessment of soil behaviour under dynamic loading.

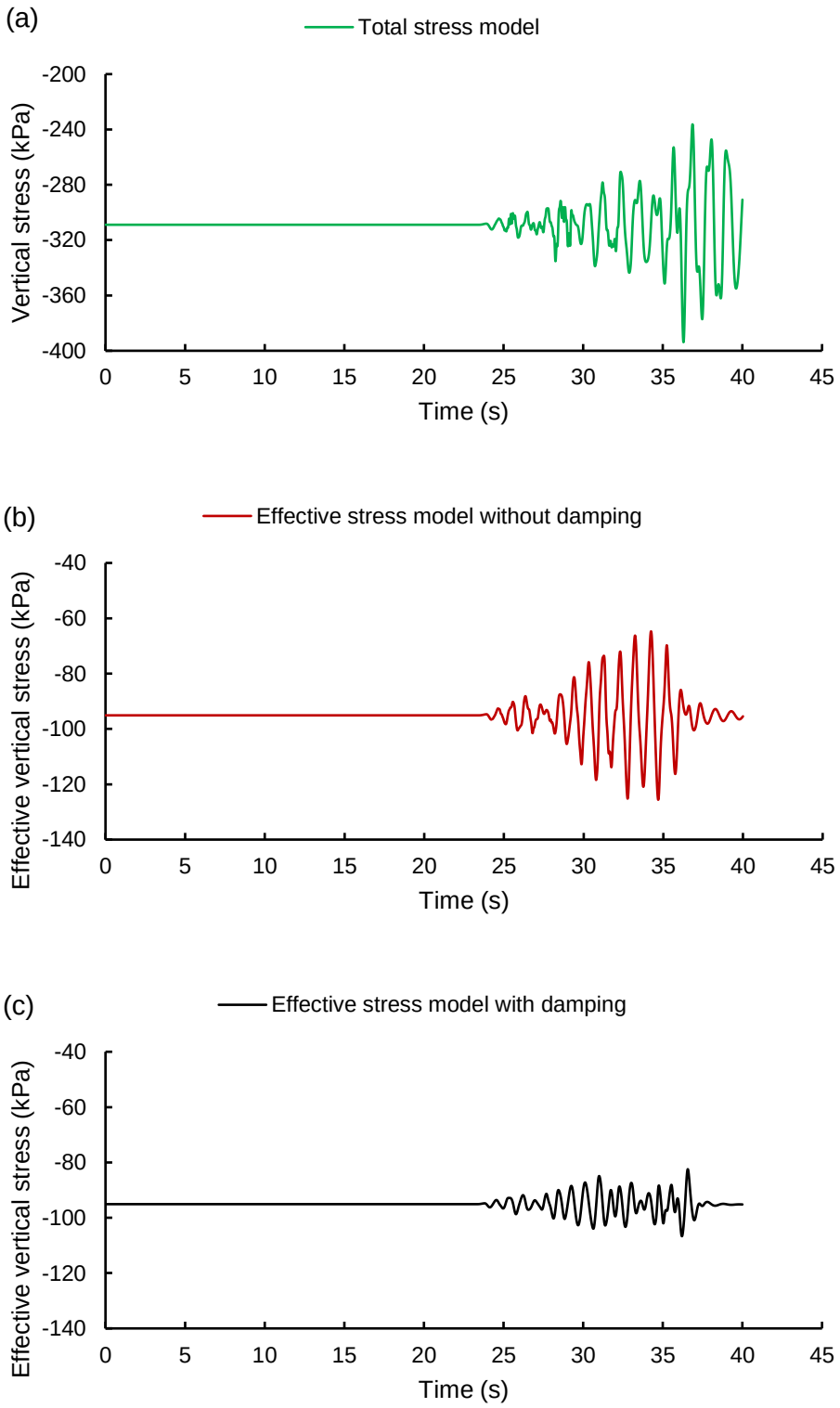

Figure 3.5. Comparison of vertical stress in soil simulated by using (a) total stress model, (b) effective stress model without damping, and (c) effective stress model with damping.

3.2.5 Effect of pure shear deformation on pore water pressure

For a viscoelastic material, the volumetric strain is only induced by the compressive (or tensile) strain rather than the shear strain. Therefore, to further verify the developed model, the simulation of pore water pressure under pure shear strain is carried out in this study. To generate pure shear strain, the selected acceleration (re: Figure 3.6) is applied at the base of soil in the horizontal direction. The obtained horizontal acceleration and pore water pressure at the monitoring point (30m from the base of soil column) is plotted in Figure 3.6. From this figure, it can be observed that there is no change in pore water pressure in soil under pure shear strain in soil, which can verify the developed model. Moreover, it is further demonstrated that an elastoplastic model should be developed to capture shear-induced volume change and associated generation of pore water pressure, which will be carried out at next stage of study for this project.

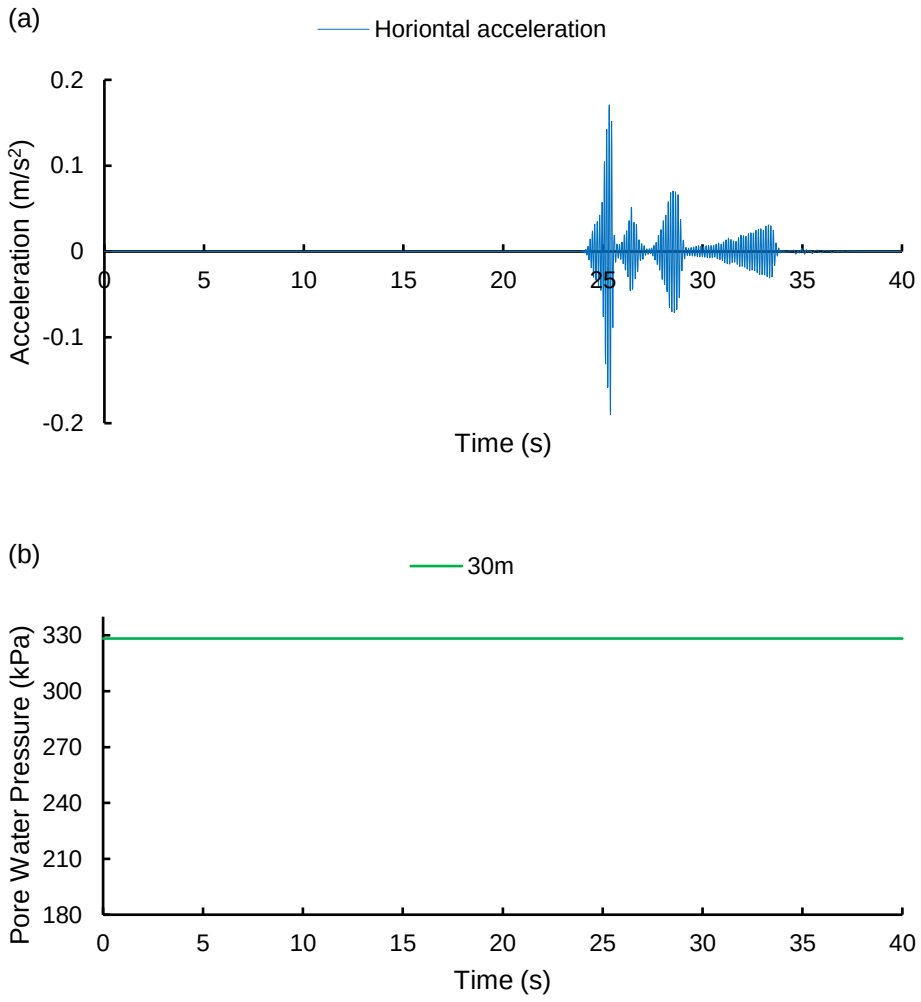

Figure 3.6. Effect of pure shear strain on pore water pressure in soil: (a) horizontal acceleration, and (b) pore water pressure at the monitoring point (30m from the base of soil column)

3.2.6 Variation of soil behaviour with the change of monitoring points

As shown in Figure 3.1, the saturated soil column consists of two different layers: saturated sand (thickness: 20 m), and saturated stiff clay (thickness: 20 m). Consequently, the material properties (density and elastic modulus) of each soil layer are different from each other. Hence, it is necessary to investigate the variation of soil behavior (pore water pressure, and deformation) in the different

soil layers. With the aid of the developed model, the predicted results are plotted in

Figure 3.7. From this figure, it can be observed that (1) the excess pore water pressure can develop to a higher value in the saturated sand (re:

Figure 3.7a). This is because the saturated sand has a lower elasticity (see Table 3.1) than the stiff clay; (2) correspondingly, larger volumetric strain in saturated sand is obtained in this study (re:

Figure 3.7b), namely, softer soil can amplify ground motion (site effect). Hence, the developed model can capture the effect of site effect occurred in soil.

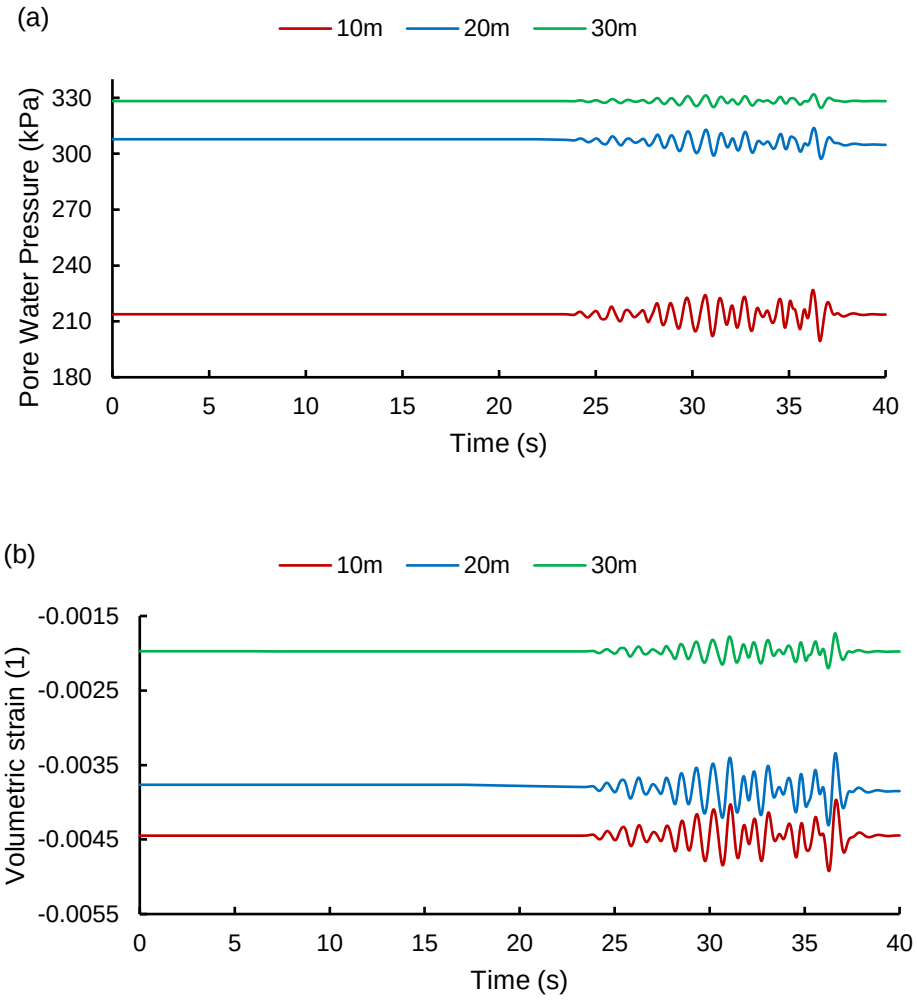

Figure 3.7. Time histories of (a) pore water pressure, and (b) volumetric strain at three monitoring points in soil column

3.3 Verification of coupled elastoplastic-hydraulic model

The limitations of the viscoelastic model are discussed in the preceding sections, namely, no volumetric shear-induced plastic strain could be simulated. A MCC-based model will be incorporated into the analysis in this study, in order to be able to simulate that fundamental behaviour of soils.

3.3.1 Case study 1: numerical investigation on soil column

3.3.1.1 Determination of model parameters

To implement the coupled elastoplastic-hydraulic model, several model parameters, including the Poisson's ratio μ , the compression index λ ,the swelling index κ , the slope of CSL M , and the bulk modulus K are needed. The detailed information on the determination of these model parameters are discussed in this section.

For the bulk modulus, the effects of volume change should be considered. In the MCC model, it was assumed that the bulk modulus is related to the mean effective stress p' and void ratio e (Vrakas 2017):

$$K = \frac{1+e}{\kappa} p' \tag{3.4}$$

The Poisson's ratio μ is assumed constant and thus the shear modulus G may therefore be assumed to vary with the stress level in soil ($G = \frac{3(1-2\mu)}{2(1+\mu)} K$).

The slope of critical state line can be related to the angle of internal friction ϕ of soil (Santamarina and Cho 2001):

$$M = \frac{6\sin\phi}{3-\sin\phi} \tag{3.5}$$

The consolidation indices (i.e., λ and κ) can be determined through oedometer tests on the target soils. In this study, the adopted model parameters are tabulated in Table 3.3.

Table 3.3. Properties of the soils used in the field investigation

Soil Density (kg/m^3)	Poisson's ratio (-)	Porosity (-)	Compressibility (1/Pa)	Poisson's ratio (-)
2000	0.33	0.36	2.6e-6	0.33
Swelling Index (-)	Compression Index (-)	Reference pressure (kPa)	Void ratio at reference pressure	
0.013	0.032	100	0.7	

* -: dimensionless unit.

By using the developed model, the field behaviour of soil under seismic loadings are examined in this study. A two-dimensional (2D) soil column is analyzed for the input motion (see Figure 3.8). The adopted boundary conditions are listed in Table 3.3. Properties of the soils used in the field investigation. The input motion is shown in Figure 3.8.

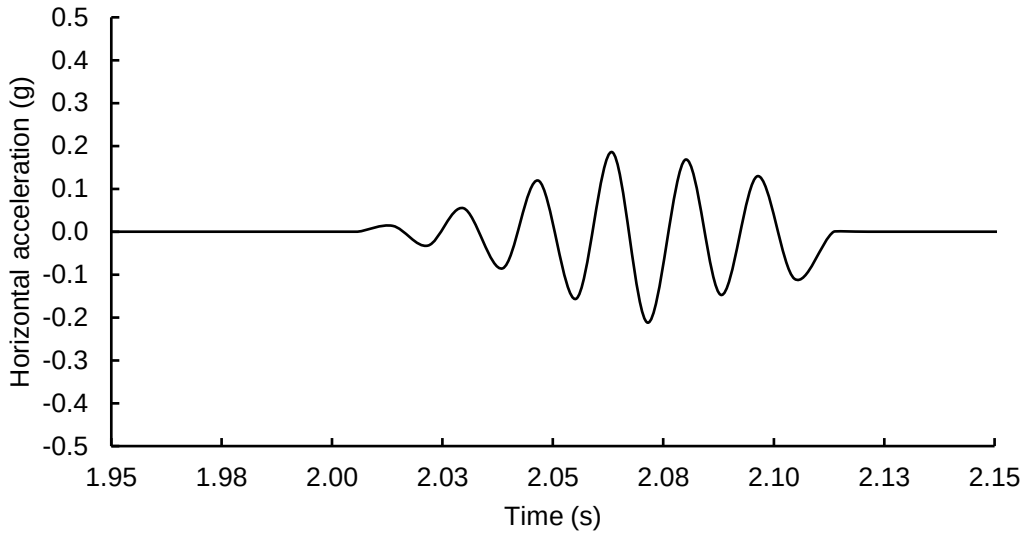

Figure 3.8. Input horizontal motion at the base of soil column

Based on the adopted input motion (see Figure 3.8), the minimum period is approximately equal to 0.02s. Therefore, the time-step size adopted in this study should satisfy the following relationship:

$$\Delta t \le \frac{0.02s}{10} = 0.002s \tag{3.6}$$

In addition, according to Eq. (3.2), the shear wave velocity V_s is needed to determine the mesh size. The shear wave velocity can be determined by shear modulus G and soil density ρ. The shear modulus can be further expressed by the Poisson's ratio and bulk modulus

$$V_s = \sqrt{\frac{G}{\rho}} = \sqrt{\frac{3(1-2\mu)}{2(1+\mu)\rho}K} \tag{3.7}$$

The bulk modulus will vary with mean effective stress and void ratio of the soil. Hence, the shear velocity of the soil is not constant as well. The shear wave velocity can be expressed as:

$$V_s = \sqrt{\frac{3(1-2\mu)}{2(1+\mu)\rho}\frac{(1+e)}{\kappa}p'} \tag{3.8}$$

To obtain approximately an shear wave velocity, the adopted values of material properties in Table 3.3 can be used. Hence, μ ,= 0.33, ρ = 2000 kg/m^3, e = 0.7, κ = 0.013 and p' =100kPa are adopted to calculate the shear wave velocity. Thus, a reference value (V_s =50 m/s) of shear wave velocity is obtained. Therefore, the grid spacing can be calculated:

$$\Delta x \le \frac{\lambda_{\min}}{10} = \frac{V_s T_{\min}}{10} = \frac{50 \times 0.02}{10} = 0.1m \tag{3.9}$$

3.3.1.2 Geometry, mesh and boundary conditions

Based on the discussion on the grid spacing and time-step size, the field behaviors of soil under horizontal motion acting at the base of soil column are examined in this study. As shown in Figure 3.9, the input motion (see Figure 3.8) is applied on the base of soil column. The detailed information on the boundary conditions are listed in Table 3.4.

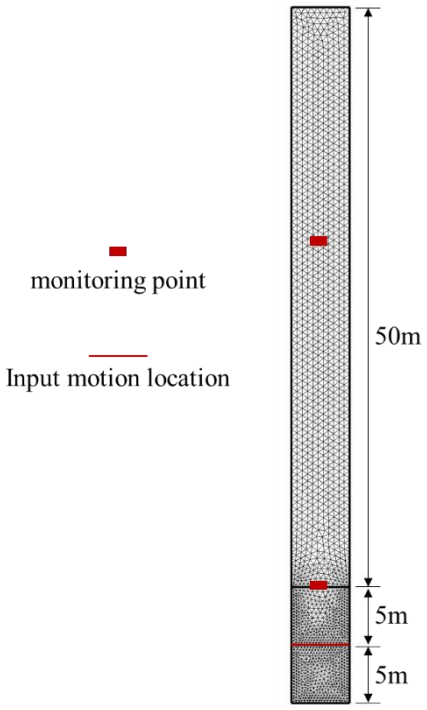

Figure 3.9. Geometry and mesh of the simulated soil column

Table 3.4. Specified boundary conditions of the soil column

Type of B.C.[a]	Specified B.C.
Mechanical process	
Top side	Free
Vertical sides	Spring Foundation B.C.
Bottom side	Roller B.C.
Hydraulic process	
Surrounding sides	No flow
Input motion	
Bottom layer of soil column	Prescribed acceleration B.C.

[a] B.C.: boundary condition.

3.3.1.3 Effect of horizontal motion on the behaviors of soil

As shown in Figure 3.10, the stress variation takes place with the application of input motion at the base of soil column. The expected wave propagation is

obtained in soil column, which indicates the specified mesh size and time-step size are appropriate in this study.

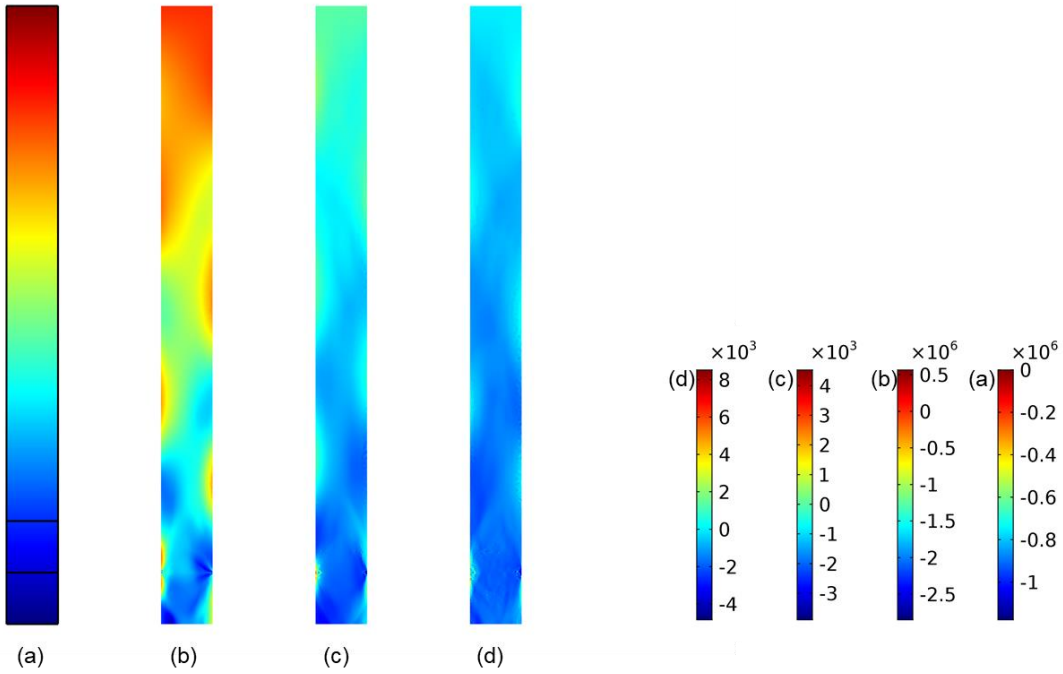

Figure 3.10. Variation of vertical stress with the horizontal motion at the base of soil column (a) t=0 s; (b) t=2.046s; (c) t=2.074s; (d) t=2.114s

As discussed previously, the major limitation of viscoelastic model is that the permanent deformation cannot be captured. Therefore, it is necessary to demonstrate the development of plastic strain in soil with S-wave propagation. As shown in Figure 3.11, the plastic strain zone (i.e., effective plastic strain greater than zero) gradually expands with the time (i.e., with the S-wave propagation). Hence, the developed model can capture the development of permanent deformation in soil under dynamic loadings.

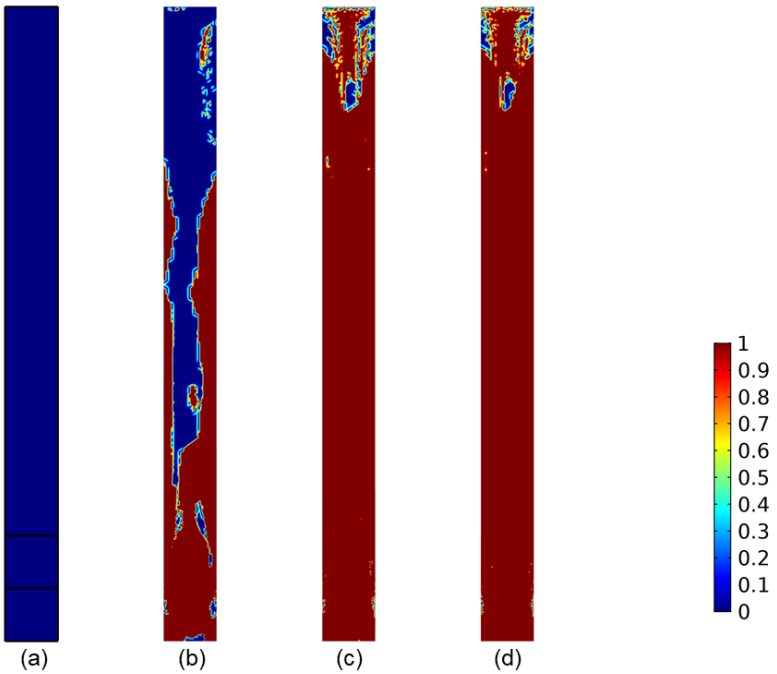

Figure 3.11. Development of plastic zone with the horizontal motion at the base of soil column (a) t=0 s; (b) t=2.046s; (c) t=2.074s; (d) t=2.114s

To show the spatial distribution of volumetric strain in the soil column the vertical line at the center of the soil column is selected. The variation of volumetric strain along the central cut line is shown in Figure 3.12. From this figure, it can be clearly seen that both volume contraction and expansion occurred in the soil during the S-wave propagation.

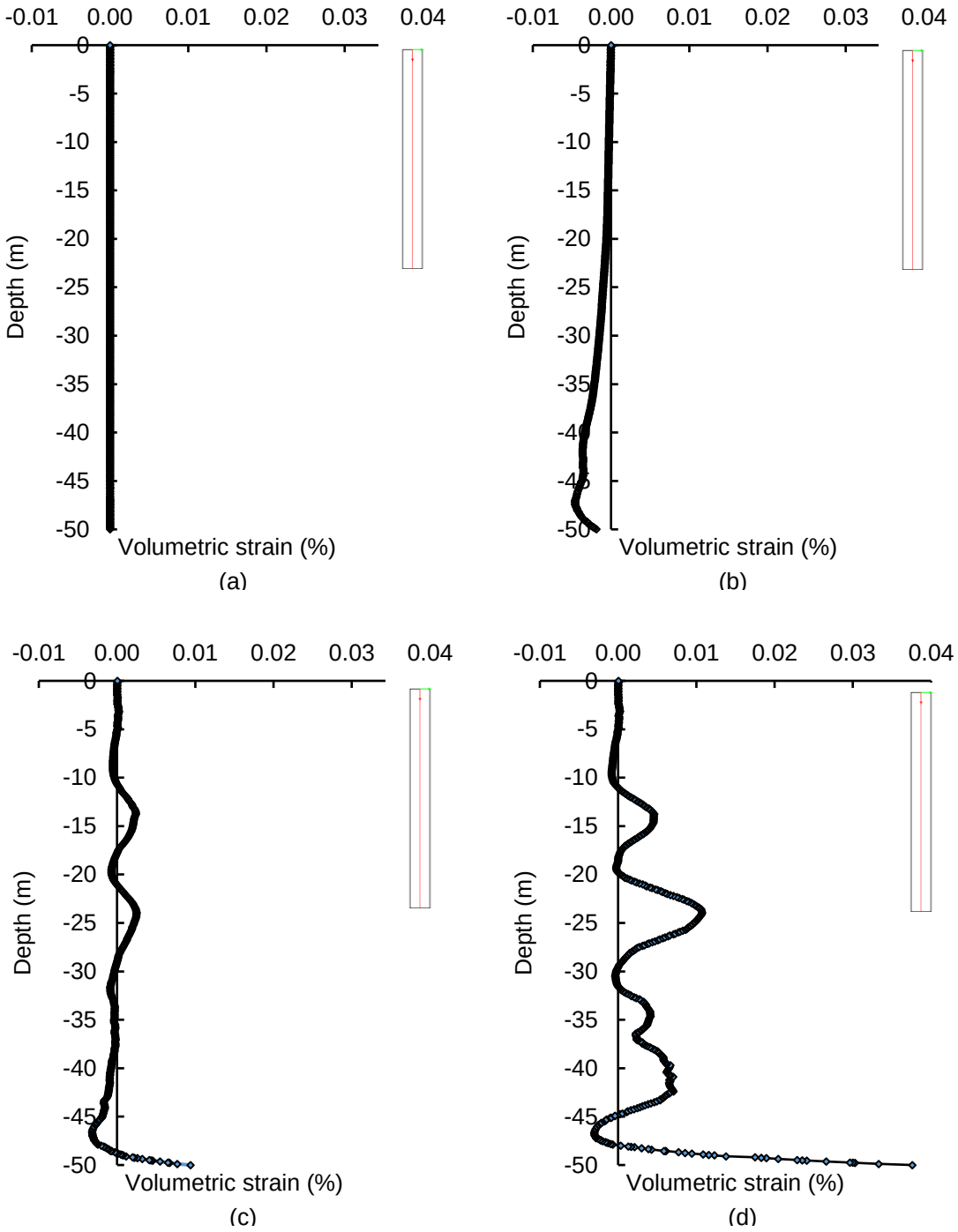

Figure 3.12. Development of volumetric strain along the central line of soil column (a) t=0 s; (b) t=2.046s; (c) t=2.074s; (d) t=2.114s

With the development of volumetric strain in soil, the pore-water pressure (PWP) will be affected and thus excess pore-water pressure will be generated. The

evolution of excess pore water pressure (i.e., the difference between PWP and hydrostatic pressure) is plotted in Figure 3.13. From this figure, it can be found that both positive and negative excess PWP are developed in the soil. This is induced by the shear-induced expansion and contraction (re: Figure 3.12). Therefore, the obtained results indicate that the developed model can capture the change in PWP due to the S-wave propagation.

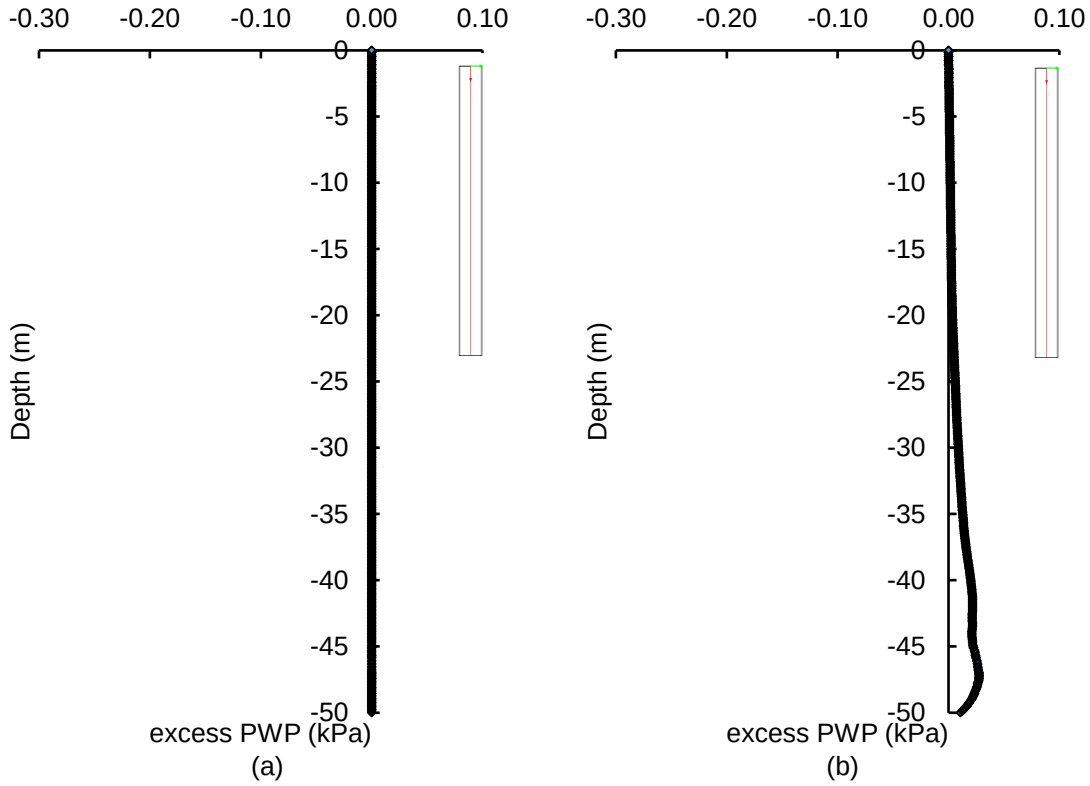

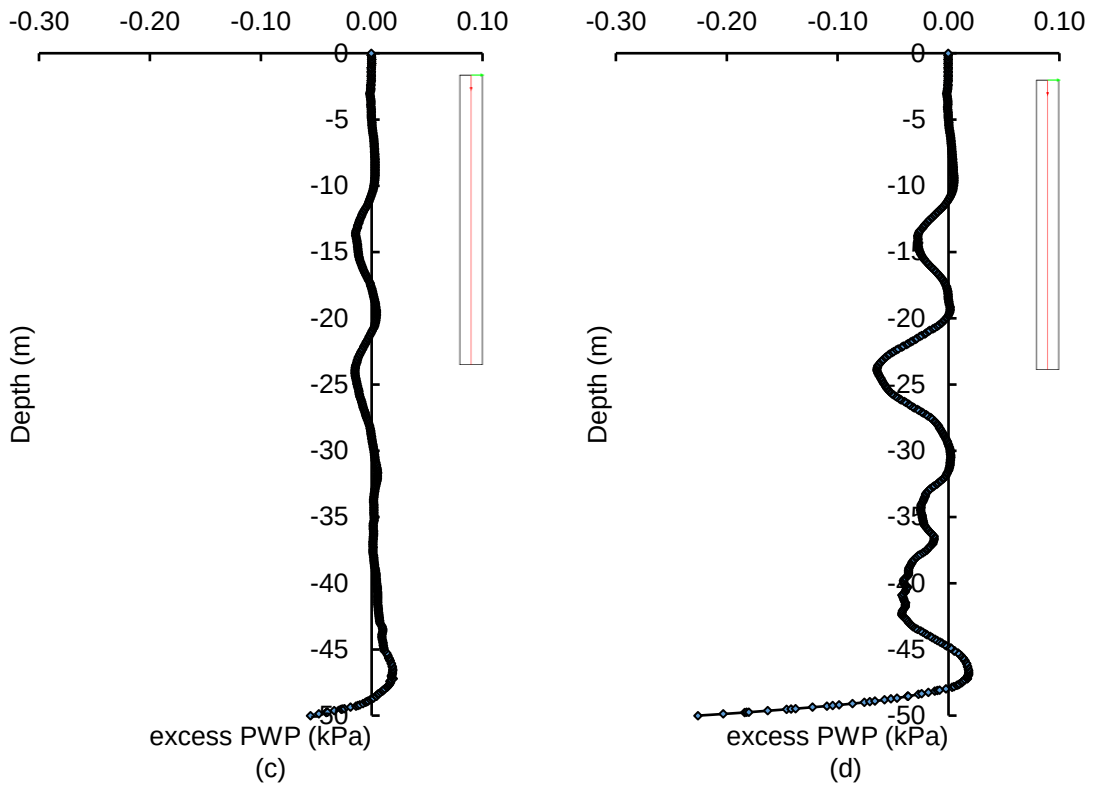

Figure 3.13. Development of excess PWP along the central line of soil column (a) t=0 s; (b) t=2.046s; (c) t=2.074s; (d) t=2.114s

3.3.2 Case study 2: Triaxial shear test

3.3.2.1 Determination of model parameters and Geometry, mesh and boundary conditions

The yield surface of MCC model is an ellipse. Accordingly, the yield surface can be divided into two parts with respect to the top vertex. When the stress reaches the left part of the yield surface, the stress state retains the yield surface. In addition, due to the normality rule (i.e., plastic strain increment is identical to the normal to the yield surface), the plastic strain can be decomposed into two parts relative to the deviatoric stress and mean effective stress. As a result, if the stress state

reaches the left side (a.k.a. wet side) of the yield surface, the component of plastic strain parallel to mean effective stress is in the negative direction. Hence, dilation takes place in soil. On the other hand, if the stress reaches the right side of the yield surface, a positive plastic strain increment can be expected. As a result, the soil contraction can occur. The stress states in soil are extremely complex, both dilation and contraction may take place in soil. Hence, it is necessary to further assess the predictability of the MCC model with respect to the volume change in soil.

To study the volume change in soil, the simulation of a standard soil sample (100mm(H)*50mm(D)) under triaxial shear test is performed in this study. Due to the cylindrical shape of the soil sample, an axisymmetric model is adopted in this study. The geometry and mesh are shown in Figure 3.14. The detailed information on the input value and boundary conditions are listed in Table 3.5.

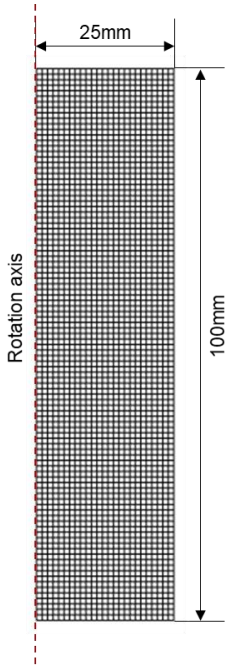

Figure 3.14. Geometry and mesh of the soil sample under triaxial shear test

Table 3.5. Values of the input parameters for the simulation of the triaxial shear test

Soil Density (kg/m^3)	Poisson's ratio (-)	Porosity (-)	Compressibility (1/Pa)	Initial consolidation pressure (kPa)
2400	0.2	0.36	2.6e-6	400
Swelling Index (-)	Compression Index (-)	Reference pressure (kPa)	Void ratio at reference pressure	
0.013	0.032	100	0.7	

3.3.2.2 Stress path control in triaxial shear test

As previously discussed, the soil may exhibit different volumetric changes under different stress paths. To fully show the volumetric change, including both soil expansion and contraction, two types of stress paths are adopted in this study. The first type of stress path aims to ensure the stress reaches the left part of the yield surface (i.e., the wet side of yield surface). Then, the obtained results can be used to verify the volume contraction that occurs in the soil sample. Correspondingly, the second type of stress path is to obtain a stress level which reaches the dry side of the yield surface.

To implement the stress path control, the minor principal stress is kept constant, and the major principal stress gradually increases during the test. The initial value of minor principal stress is 50 kPa and 350 kPa for the first type of stress path, and the second type of stress path. The obtained stress paths for these two cases are shown in Figure 3.15 and Figure 3.16.

The first type of stress path control is shown in Figure 3.15. From this figure, it can be found that the strain softening behaviour takes place when the stress reaches the initial yield surface. Then, the stress will gradually decrease with further shearing (i.e., the softening behaviour occurred in soil). However, when the stress reaches the critical state line (CSL), no further change in stress takes place.

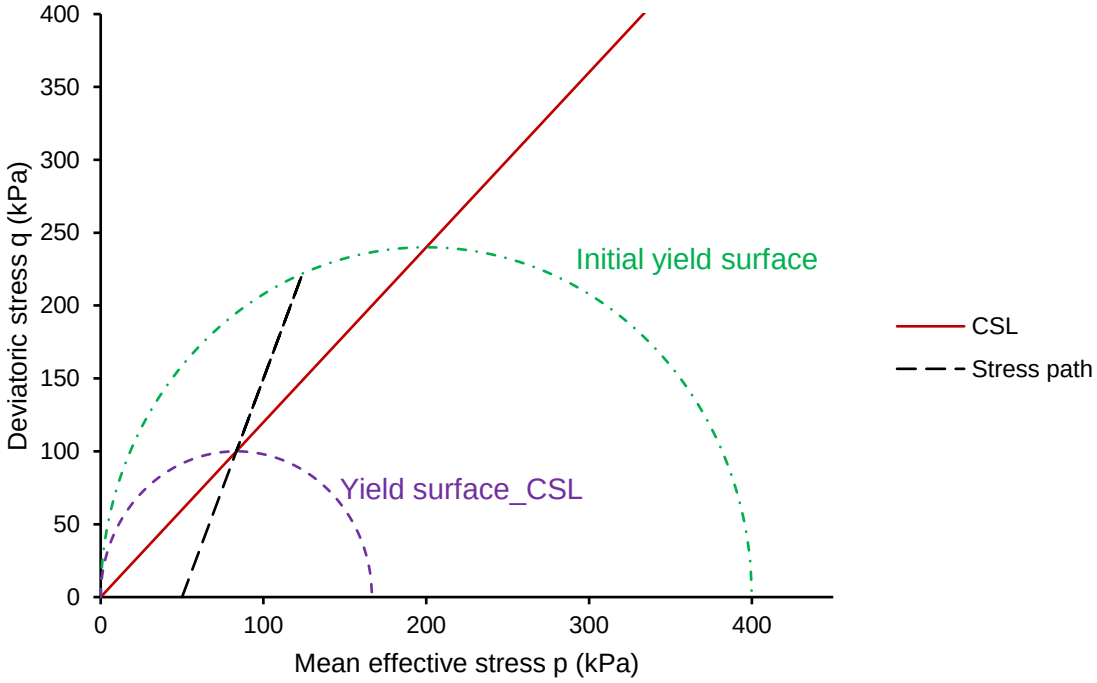

Figure 3.15. Stress path on the wet side of the yield surface

Similarly, as shown Figure 3.16, the strain hardening takes place when the stress state reaches the dry side of yield surface. Thus, the expansion of yield surface occurs. With further increase of the deviatoric stress, the stress state gradually approaches the critical state line (CSL). After the stress reaches the CSL, there is no further change in the stress and volumetric strain in the soil sample.

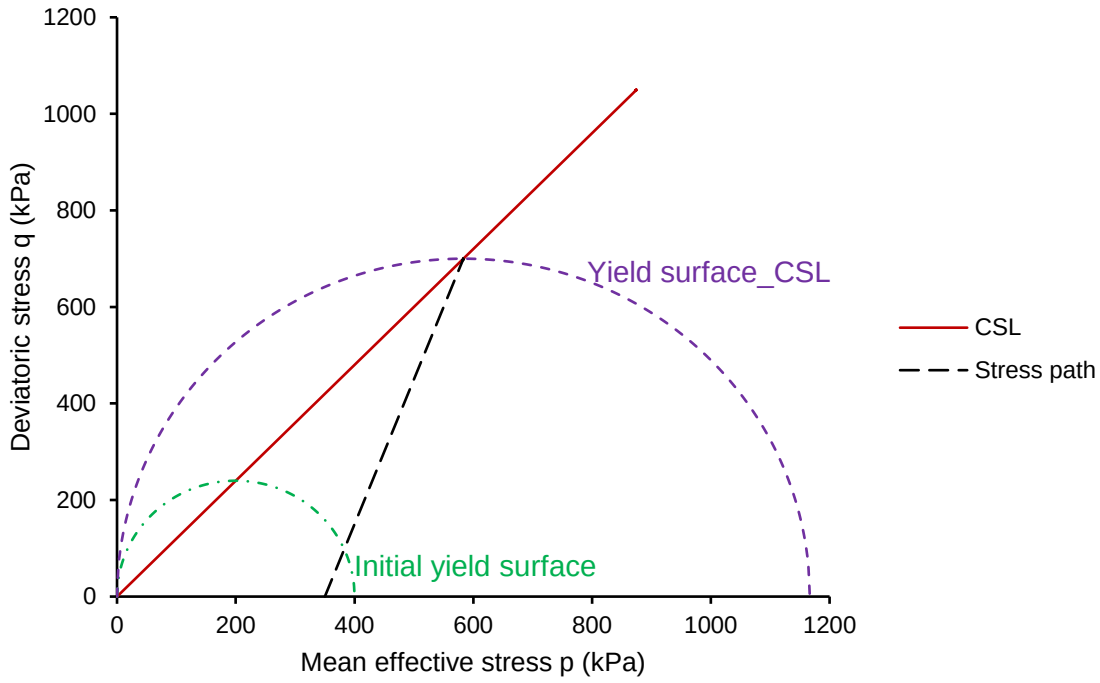

Figure 3.16. Stress path on the dry side of the yield surface

3.3.2.3 Stress-strain relationship from triaxial shear test

To demonstrate the strain hardening and softening behaviour in soil under different stress paths, the stress-strain relationship is analyzed in this study. The obtained stress-strain curves from the specified stress paths are plotted in Figure 3.17 and Figure 3.18. As shown in Figure 3.17, strain softening behavior takes place after the stress reaches the elastic limit. Then, the deviatoric stress gradually decreases with the further shearing in the soil sample. As mentioned above, this is due to the soil expansion that took place on the wet side of the yield surface. With the development of soil swelling, the strength of the soil will dramatically decrease, namely, the resistance to the shearing becomes weaker with the

accumulation of plastic strain. However, when the stress reaches the CLS (see Figure 3.15), there is no further change in stress in the soil.

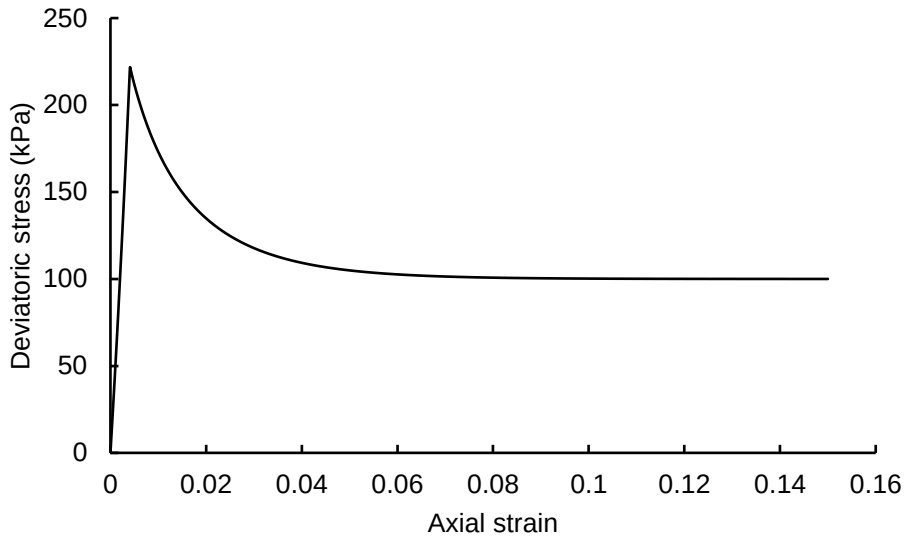

Figure 3.17. Strain softening behavior of the soil corresponding to the stress on the wet side of the yield surface

The strain hardening behaviour of the soil corresponding to the stress on the dry side of yield surface is depicted in Figure 3.18. Compared with the strain hardening behavior (see Figure 3.17), the stress on the dry side of the yield surface shows a different evolutionary trend. Specifically, the stress gradually increases after the stress exceeds the elastic limit, and then gradually reaches a stable state (i.e., CSL). This is because the stress on the dry side of yield surface can cause soil contraction, and the accumulation of compressive plastic strain can increase the strength of soil sample. As a result, the strain-hardening behaviour appears in soil when the change of yield stress takes place on the dry side of yield surface.

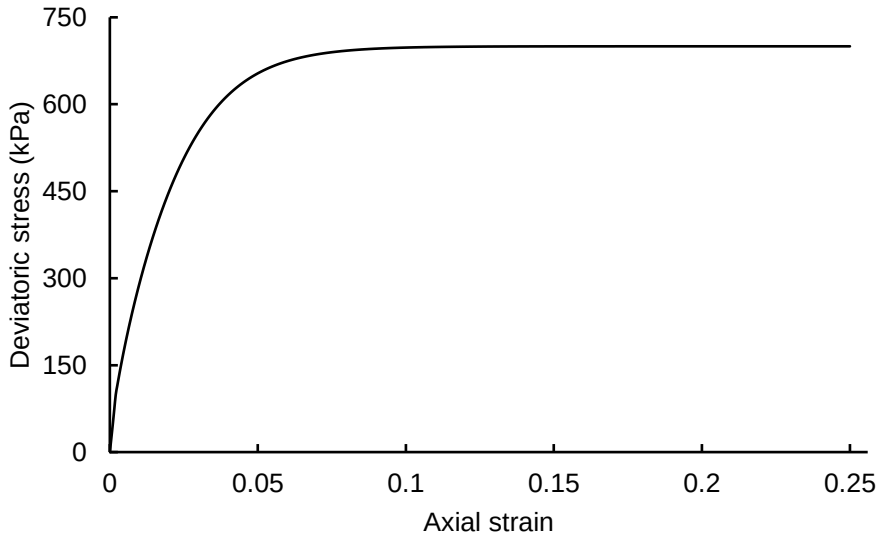

Figure 3.18. Strain hardening behavior of the soil corresponding to the stress on dry side of yield surface

3.3.2.4 Development of volumetric strain under different stress paths

As previously discussed, the hardening and softening behaviors are associated with the development of volumetric strain in the soil sample. Therefore, it is necessary to investigate the change of volumetric strain under different stress paths. The change of volumetric strain is plotted in Figure 3.19 and Figure 3.20.

As shown in Figure 3.19, the volumetric strain exhibits a two-stage evolution. First, the volumetric strain linearly decreases with the axial strain. This is because the stress is still located in the elastic regime. So, with the increase of deviatoric stress, the mean effective stress will increase as well. As a result, the elastic volumetric strain will first decrease with the increase of the mean effective stress. However, after the elastic limit is exceeded, the volumetric strain shows an expansive trend. Corresponding to the change in deviatoric stress (see Figure

3.17), the volumetric strain gradually approaches a stable state, and then remains constant for further shearing in the soil sample. Therefore, the MCC model can be used to capture the strain-softening behaviour when the yield stress reaches the wet site of the yield surface.

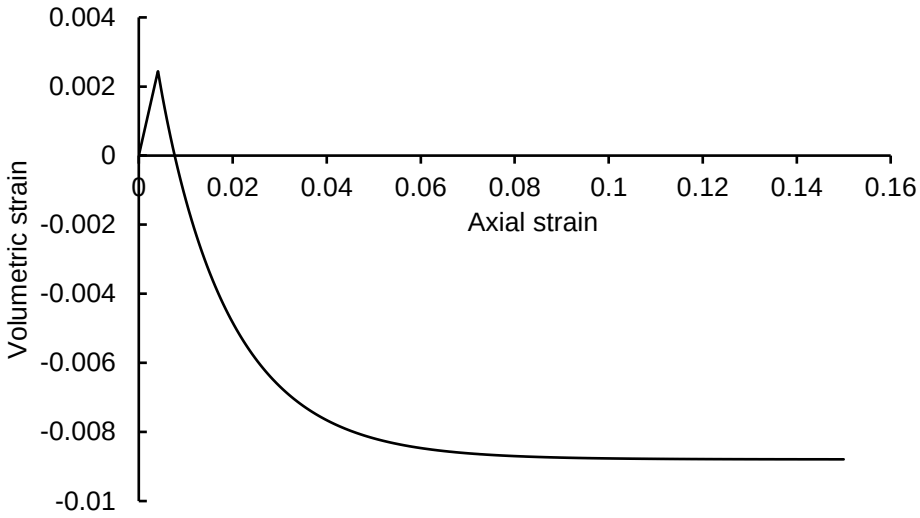

Figure 3.19. Change of volumetric strain corresponding to stress on the wet side of yield surface

The volumetric contraction of soil sample is plotted in Figure 3.20 when the yield stress reaches the dry side of yield surface. As shown in Figure 3.20, the volumetric strain first demonstrates a monotonic decrease during the test, and then gradually approaches a stable state. With the decrease of volumetric strain, the soil strength will increase. As a result, the strain hardening behavior of soil sample appears when the yield stress reaches the dry side of yield surface.

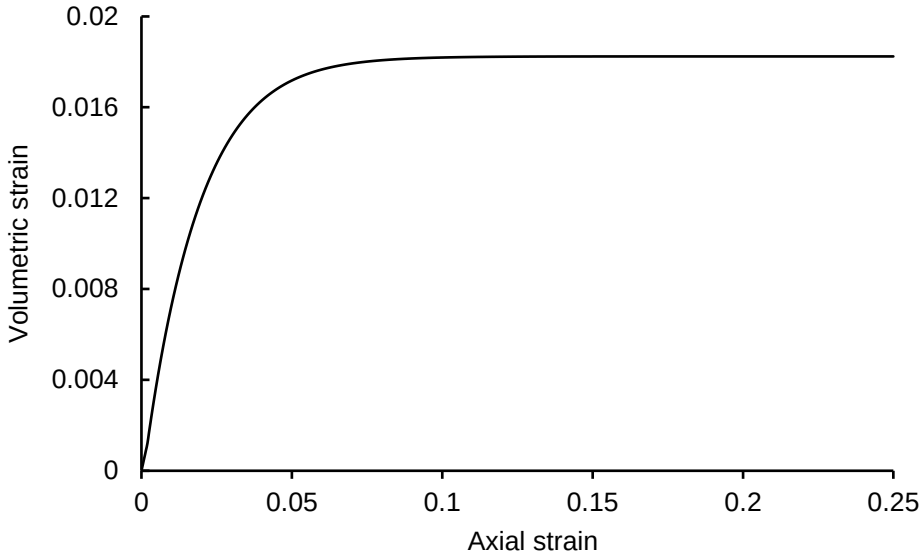

Figure 3.20. Change of volumetric strain corresponding to stress on the dry side of yield surface

3.4 Validation of the coupled elastoplastic-hydraulic model

To simulate the dynamic behaviour of soil under seismic loading conditions, the cyclic triaxial shear tests and shaking table tests have been widely adopted. Through these two types of tests, the nonlinear behaviour (e.g., the development of permanent deformation and excess pore water pressure) can be quantitatively assessed. Therefore, to validate the developed elastoplastic-hydraulic model, the modeling results are compared with the measured data from previous studies.

3.4.1 Case study 1-Cyclic triaxial test

To study the dynamic behaviour of sandy soils, Ural and Gunduz (2014) conducted a series of stress-controlled undrained cyclic triaxial tests. The loose sand soil specimens are mostly composed of quartz. The unit weight of soil is in the range of 17.06 to 19.93 kN/m^3. The size of the cyclic triaxial test samples is 100mm (D)×220mm (H). Soil samples were tested at 1 Hz. All the samples tested

were isotropically consolidated at 100 kPa. The tested samples are considered to be fully saturated. The cyclic triaxial tests were conducted at a stress ratio of 0.25. The stress applied on the soil specimens is presented in Figure 3.21. During the test, the axial strain and excess pore water pressure were measured. To evaluate the predictability of the developed model, experimental data measured by Ural and Gunduz (2014) were adopted.

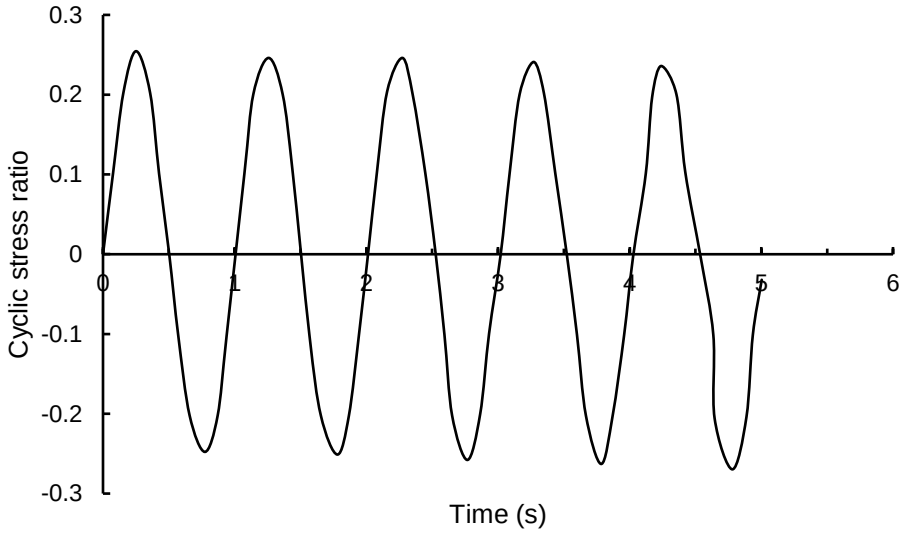

Figure 3.21. The cyclic stress ratio adopted in the triaxial test.

3.4.1.1 Geometry, mesh and boundary conditions

To simulate the cylindrical soil sample, the axisymmetric geometry model is adopted (see Figure 3.25). The values of the model parameters are listed in Table 3.6, and boundary conditions are listed in Table 3.7. The pre-specified cyclic stress (see Figure 3.21) is applied on the top surface of the soil sample.

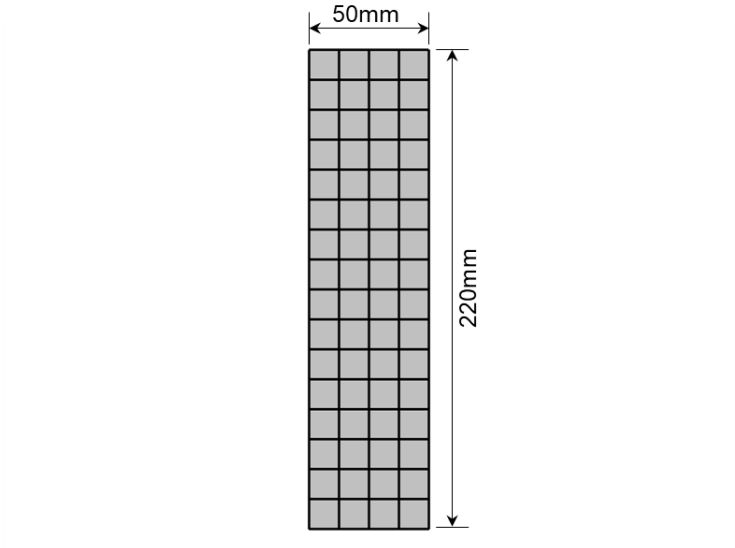

Figure 3.22. Geometry and mesh of simulated soil column

Table 3.6. Value of the input parameters for the simulation of triaxial shear test

Soil Density (kg/m^3)	Poisson's ratio (-)	Porosity (-)	Compressibility (1/Pa)	Initial consolidation pressure (kPa)
1800	0.2	0.36	2.6e-6	100
Swelling Index (-)	Compression Index (-)	Reference pressure/stress (kPa)	Void ratio at reference pressure	Fluidity (1/s)
0.034	0.173	100	0.7	0.09

Table 3.7. Specified boundary conditions of the soil column

Type of B.C[a]	Specified B.C.
Mechanical process	
Top side	Boundary load (100 kPa)
Vertical side	Boundary load (100 kPa)
Bottom side	Roller B.C.
Hydraulic process	
Surrounding sides	No flow
Input motion	
Top layer of soil specimen	Prescribed cyclic stress (The input motion was added to boundary load acting on the top side of soil column)

[a] B.C.: boundary condition.

3.4.1.2 Development of excess pore water pressure

The development of excess pore water pressure (PWP) is shown in Figure 3.23. From this figure, it can be observed that the cyclic stress can significantly affect the excess PWP. Specifically, excess PWP can develop during the loading process and dissipate during the stress releasing process. This is because the triaxial test was conducted under undrained condition. Consequently, the volumetric contraction causes the development of excess PWP, while the volumetric expansion results in the dissipation of excess PWP. Therefore, the effect of volume change on excess pore water pressure can be captured by the developed. Moreover, with the application of cyclic stress on the soil sample, the excess PWP is gradually built-up and cannot be dissipated completely (i.e., the accumulation of excess PWP). This is due to the development of permanent deformation in the soil sample under the cyclic loadings. Since plasticity is incorporated into the assessment of soil deformation, the developed model is able to predict the irreversible deformation in the soil. As a result, the volumetric plastic strain cannot be recovered during the unloading process and thus causes the accumulation of excess pore water. The development of permanent deformation in the soil is clearly shown in Figure 3.24. Through the comparison between predicted results and measured data, it can be found that the developed model is able to adequately capture the development of permanent deformation and associated excess PWP (i.e., the nonlinear behaviour of soil under dynamic loading conditions).

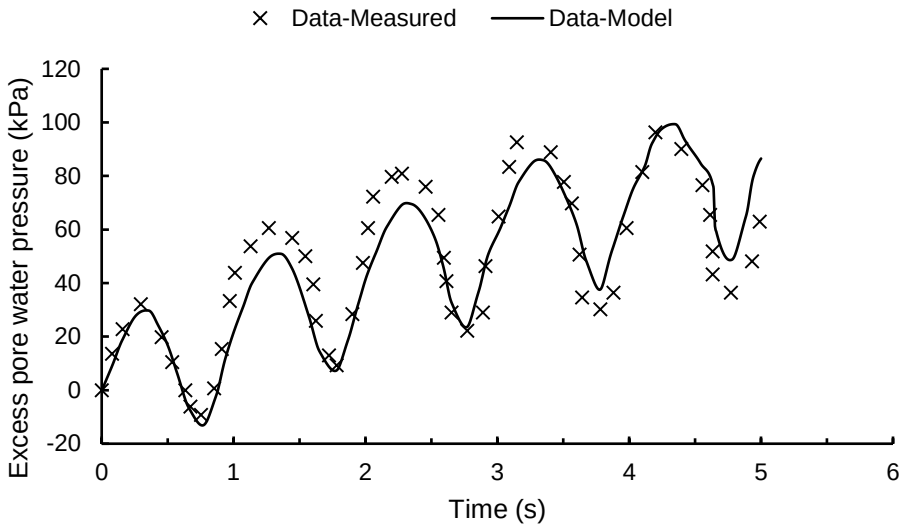

Figure 3.23. Comparison of numerical prediction and experimental data of excess pore water pressure.

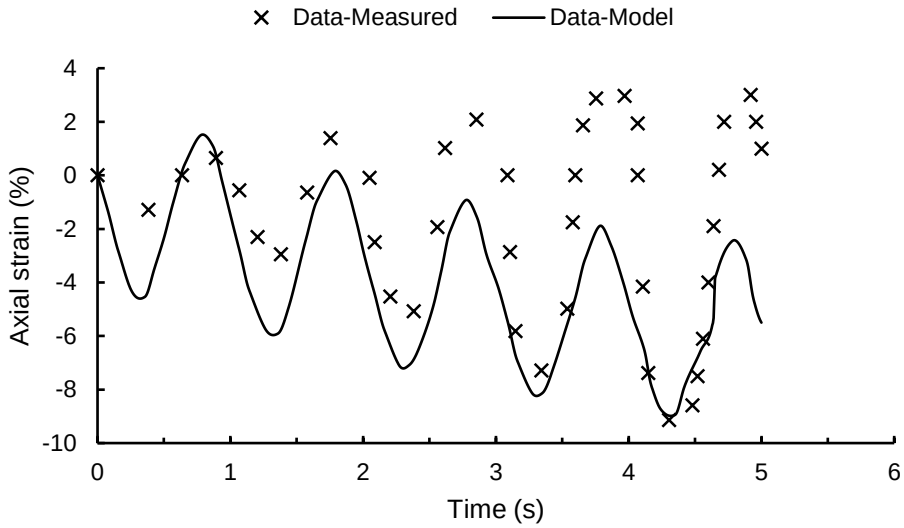

Figure 3.24. Comparison of numerical simulation and experimental data of axial strain.

3.4.2 Case study 2: Shaking table test

To further assess the capability of the coupled elastoplastic-hydraulic model, the shaking table test on sand soil conducted by Taboada and Dobry (1993) is considered in this study. Loose sand at a relative density of 40% was used in the test. The adopted values of model parameters are listed in Table 3.8. The shaking table test is simulated at a centrifugal acceleration of 50g (g is the gravity acceleration). During the test, the soil deposit is subjected to a lateral movement at its base. The input motion is shown in Figure 3.25. As shown in Figure 3.25, the peak value of input acceleration is approximately 0.2g. The adopted geometry and mesh are depicted in Figure 3.26.

In the shaking table test, the laminar box is commonly adopted to contain the soil sample and simulate the response of a semi-infinite loose soil layer during shaking. As a result, the horizontal displacement of mesh nodes located at the two ends of soil at the same elevation is restrained to the have the same value. To model the function of the laminar box, an antisymmetric boundary condition is applied to the left and right end of soil sample. However, horizontal displacement in the front and back directions is not allowed during the shaking table test. Accordingly, a roller boundary condition is adopted on the front surface. In addition, a fixed boundary condition is adopted at the base. Due to the symmetry of geometry and adopted boundary conditions, only half of the model is considered.

To demonstrate the development of excess pore water pressure, three different monitoring points are selected in the soil deposit. The locations of monitoring points are shown in Figure 3.27.

Table 3.8. Model parameters adopted in the shaking table test simulation

Soil Density (kg/m^3)	Poisson's ratio (-)	Initial Porosity (-)	Initial consolidation pressure (kPa)
2132	0.2	0.41	400
Swelling Index (-)	Compression Index (-)	Reference pressure/stress (kPa)	Void ratio at reference pressure
0.013	0.032	100	0.7
Hydraulic conductivity (m/s)	Water density (kg/m^3)	Compressibility of fluid (1/Pa)	Compressibility of soil skeleton (1/Pa)
2.94e-4	1000	4e-10	2.6e-6

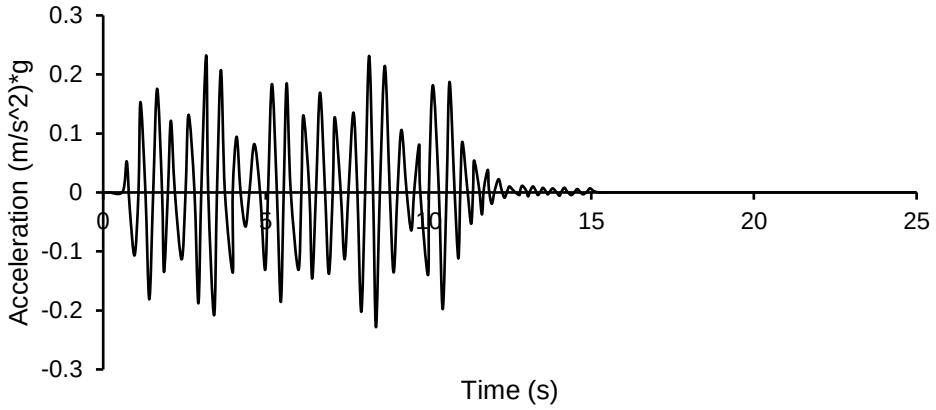

Figure 3.25. Horizontal input motion at bottom.

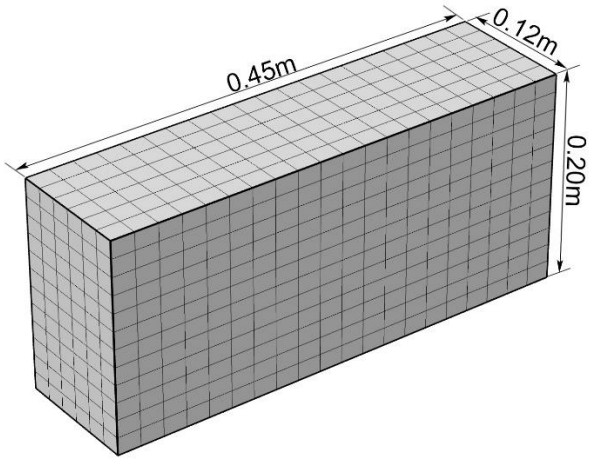

Figure 3.26.Geometry and element mesh adopted in the shaking table test

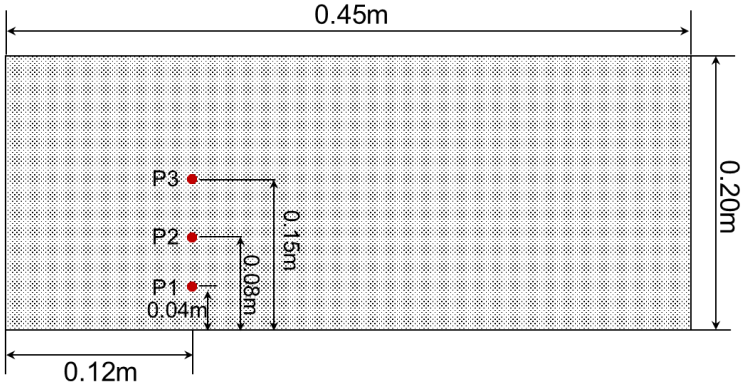

Figure 3.27. Spatial distribution of monitoring points w.r.t. the middle vertical plane of soil deposit.

The variation of pore water pressure at the monitoring points is shown in Figure 3.28. From this figure, it can be observed that (1) the initial hydrostatic pressure increases with the depth of soil deposit (the monitoring point with the elevation of 0.04m has the largest depth w.r.t. the top surface of soil deposit); (2) the development of pore water pressure (i.e., the generation of excess pore water pressure) takes place as the input of base movement. Therefore, the developed model can capture the generation of excess pore water pressure due to the

dynamic loadings; (3) in addition, only a part of the excess of pore water pressure dissipates during test. For example, the maximum pore water pressure at the monitoring point with the elevation of 0.12m is approximately 60 kPa. There are three contributors to the partial dissipation of pore water pressure in the soil. The first contributor is the elastic volumetric strain. With the application of dynamic loadings, the recoverable volumetric strain can be formed and developed in soil. Consequently, the generation of excess of pore water pressure can be observed during the loading processes. However, this portion of excess pore water pressure will completely dissipate during the unloading processes. As a result, the fluctuation of pore water pressure is obtained during the shaking table test. The second contributor to the partial dissipation is attributed to the drainage boundary on the top surface of the soil deposit. Consequently, the dissipation of pore water due to the water drainage can take place. Another important contributor refers to the formation and accumulation of plastic strain in soil deposit. Consequently, the permanent deformation cannot be recovered during the unloading processes, and thus contributes to maintain the excess of pore water pressure. As shown in Figure 3.28, the predicted results are in good agreement with the experimental data at different monitoring points. Therefore, based on the obtained results from this study, it can be confirmed that the developed model can capture the nonlinear behaviour (development of plastic strain, and excess pore water pressure) of soil under dynamic loadings.

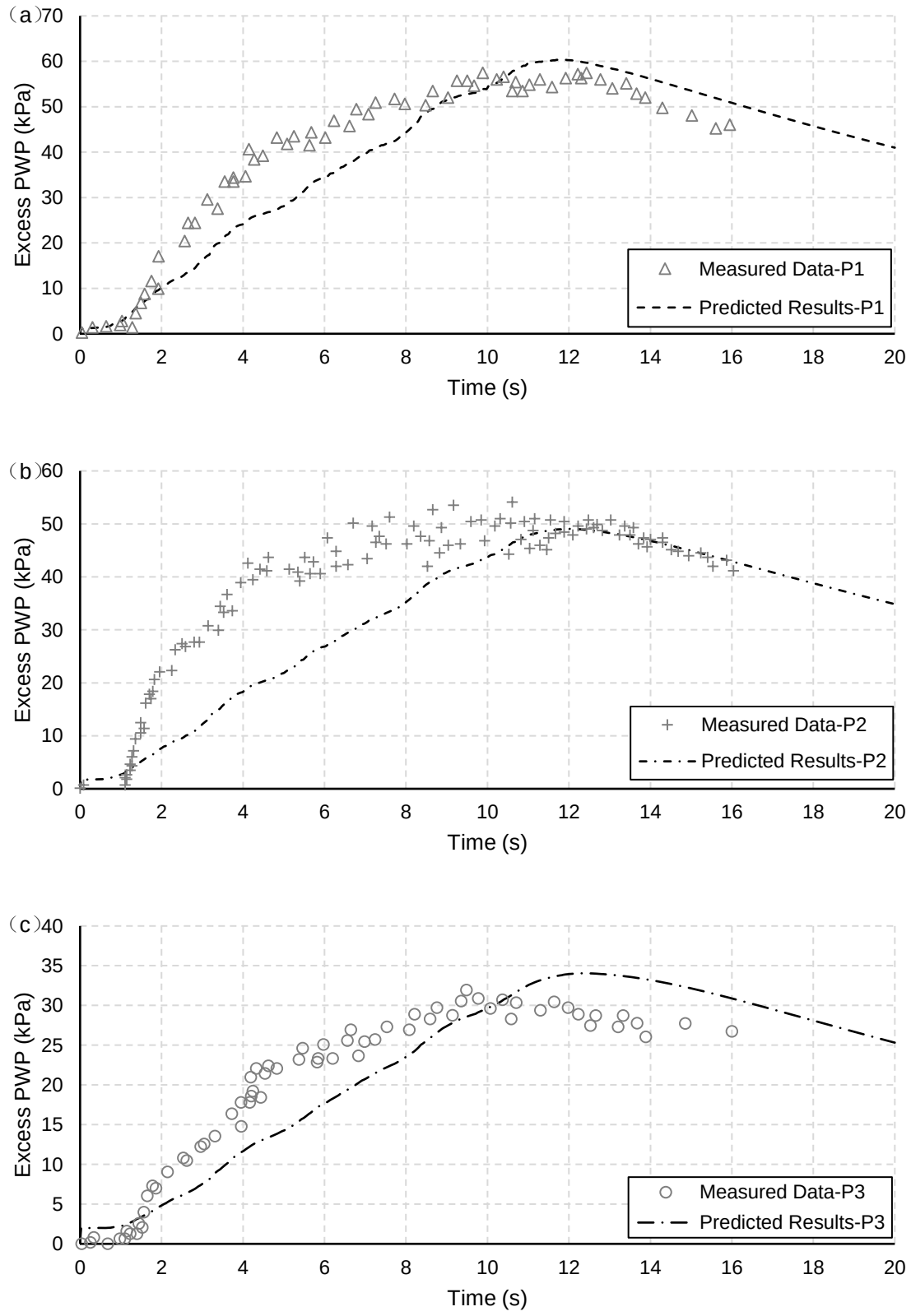

Figure 3.28. Comparison of predicted results and experimental data at (a) point 1 at the elevation of 0.04m; (b) point 2 at the elevation of 0.08m; and (c) point 3 at the elevation of 0.12m.

3.5 Simulation-based Engineering Application

Nuclear power generation was established since the 1950s and provides an alternative in the reduction of greenhouse gases (Carless et al. 2019). Due to the high capital cost of large power reactors generating electricity and the need to service small electricity grids, there is a move to develop small modular reactors (SMRs) with powers smaller than 300 MWe under the direction of the International Atomic Energy Agency (IAEA) (Markou and Genco 2019). SMRs has a number of benefits compared with the larger power reactors. For example, the SMRs could be beneficial in delivering electric power to areas difficult to access or without infrastructure and generating local power for larger population centers. Moreover, the SMRs can effectively reduce the amount of work on-site, which make them simpler and faster to construct (Hidayatullah et al. 2015). In addition, the operation and maintenance costs of SMRs are relatively low. Therefore, SMRs have been attracting considerable attention around the world. SMRs must be seismically qualified in order to prevent release of radionuclides to the environment, following severe earthquakes. The elastoplastic-hydraulic model developed from this study could be a useful tool to verify the sismic qualification and/or optimize the design of SMRs.

In this study, the developed elastoplastic-hydraulic model has been implemented into a commercial finite element analysis program (COMSOL Multiphysics) to perform the seismic analysis of a hypothetical SMR embedded in a loose sand foundation. Table 3.9 shows the material properties used in the finite element analysis.

Table 3.9. Material properties adopted in the finite element analysis

Soil and water properties	Values
Soil Density (kg/m^3)	1800
Poisson's ratio (-)	0.3
Initial porosity (-)	0.41
Initial consolidation pressure (kPa)	200
Swelling Index (-)	0.014
Compression Index (-)	0.54
Reference pressure/stress (kPa)	100
Void ratio at reference pressure (-)	0.7
Hydraulic conductivity (m/s)	2.94e-4
Water density (kg/m^3)	1000
Compressibility of fluid (1/Pa)	4e-10
Compressibility of soil skeleton (1/Pa)	2.6e-6
Rock	
Density(kg/m^3)	2600
Elastic modulus (GPa)	60
Poisson's ratio (-)	0.25
SMR structure	
Density(kg/m^3)	2300
Elastic modulus (GPa)	25
Poisson's ratio (-)	0.2

For the dynamic analysis, a horizontal acceleration (from Saguenay earthquake in 1988, see Figure 3.29) was adopted to simulate the base motion. The Saguenay 1988 is one of the largest recorded earthquakes in eastern Canada and eastern North America during the 20th century, with a moment magnitude of 5.9.

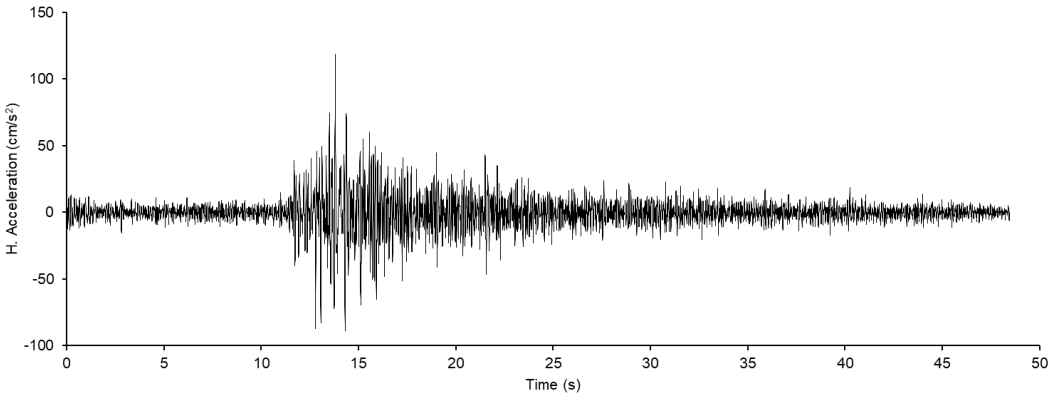

Figure 3.29. Input horizontal acceleration on the bedrock

Figure 3.30 shows the geometry model for each component. To simplify the seismic analysis, it is assumed that the sand soil and bedrock are isotropic and homogenous materials. Moreover, compared with surrounding soils, the SMR and bedrock are relatively rigid and thus are assumed to behaviour elastically under seismic loadings. In addition, only half of the soil and SMR structure were simulated. Detailed information about the mesh discretization is presented in Figure 3.31.

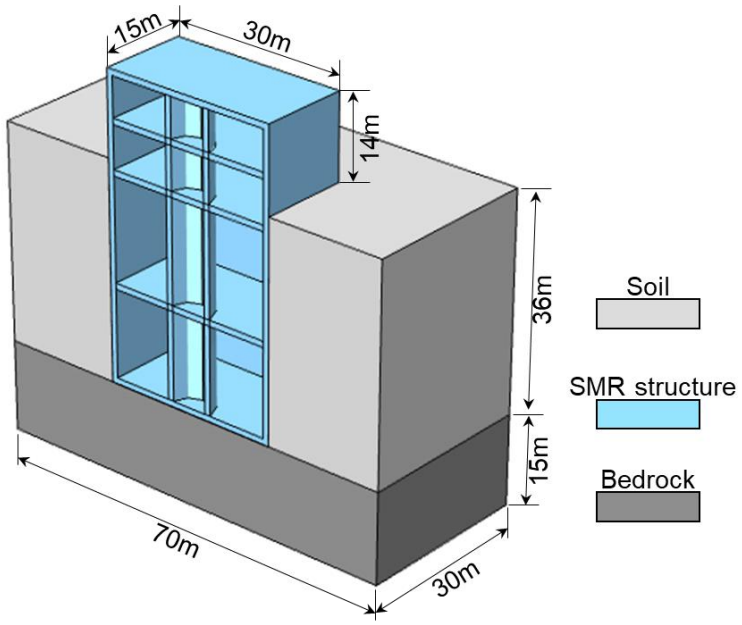

Figure 3.30. Geometry model adopted by the finite element analysis

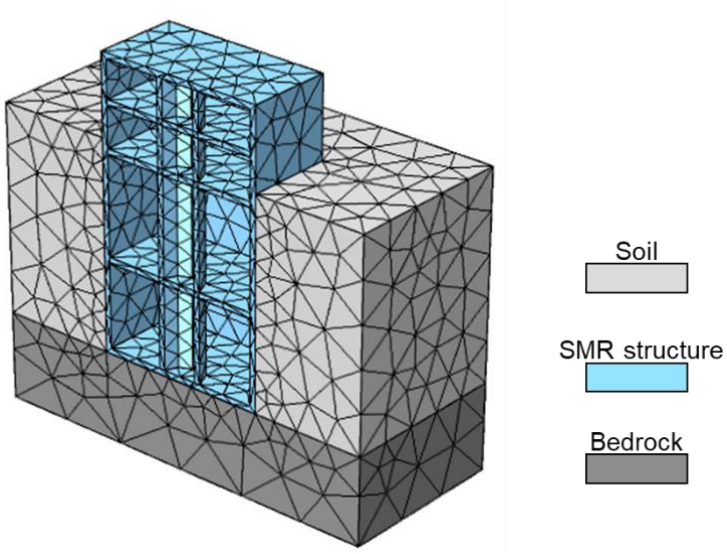

Figure 3.31. Mesh discretization of geometry model

For the applied boundary condition, a low-reflecting boundary was used at the far end (vertical sidewalls) of the soil deposit, and bottom bedrock was set as a roller boundary condition. The ground surface was set as a free boundary. The horizontal acceleration was applied to the bedrock domain. The soil domain is considered in the simulation of hydraulic process. A zero pressure was applied at the top surface of soil and no flow boundary conditions were applied to sidewalls and bottom surface. The bottom bedrock and the SMR structure are assumed to be perfectly connected, for this simulation.

To demonstrate the dynamic behaviour of soil under the SSI effect, three different monitoring points were selected in the soil domain. Point 1 and 2 have same horizontal distance (5m) and different depth (point 1 with a depth of 7.5m and point 2 with a depth of 10m). These two points are used to demonstrate the effect of soil depth on development of excess pore water pressure, which can be further adopted to analyze the occurrence of soil liquefaction. Point 3 is located at

the depth of 7.5m (which is same to point 1) and a horizontal distance of 10 m w.r.t. SMR structure. The comparison of predicted results at point 1 and 3 can be used to demonstrate the effect of SSI on the nonlinear behavior of soil. The detailed information about the spatial positions of monitoring points is presented in Figure 3.32.

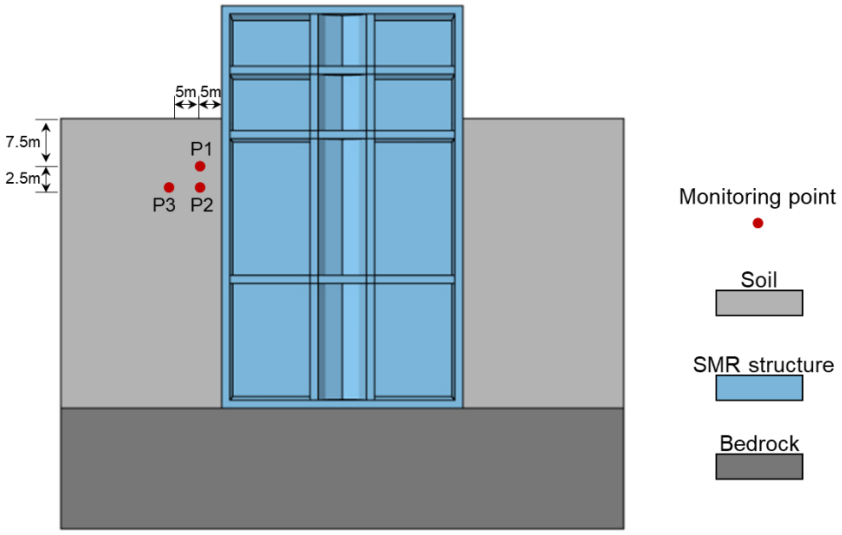

Figure 3.32. Spatial positions of the monitoring points

The development of excess pore water pressure (PWP) at the monitoring points is presented in Figure 3.33. From this figure, it can be observed that the development of pore water pressure (i.e., the generation of excess pore water pressure) takes place as the input of base movement. With the increase of acceleration (see Figure 3.29), the excess pore water accumulates w.r.t. time. The accumulation of excess PWP indicates the development of volumetric plastic strain. Since the horizontal acceleration was applied on the bedrock, the development of excess PWP also confirmed the shearing induced volume change in soil. Therefore, the nonlinear behavior of soil under seismic loading can be captured by

model. Moreover, through comparison of excess PWP between point 1 and 2, it can be found that higher excess PWP develops near the ground surface. This is because the soil shaking can reach a higher extent with the reduction of soil depth. Therefore, the developed model is able to the capture the effect of soil depth on the nonlinear behaviour of soil. In addition, as shown in Figure 3.33, excess PWP shows a discrepancy w.r.t. horizontal positions (excess PWP at point 2 versus point 3). This is due to the soil-structure interaction effect. The response of soil subjected to the impact of structure can further affect the volume change in soil and thus contributes to the development of excess PWP. Therefore, the spatial discrepancy of excess PWP demonstrates that the developed elastoplastic model can capture the effect of SSI on the nonlinear behavior of soil.

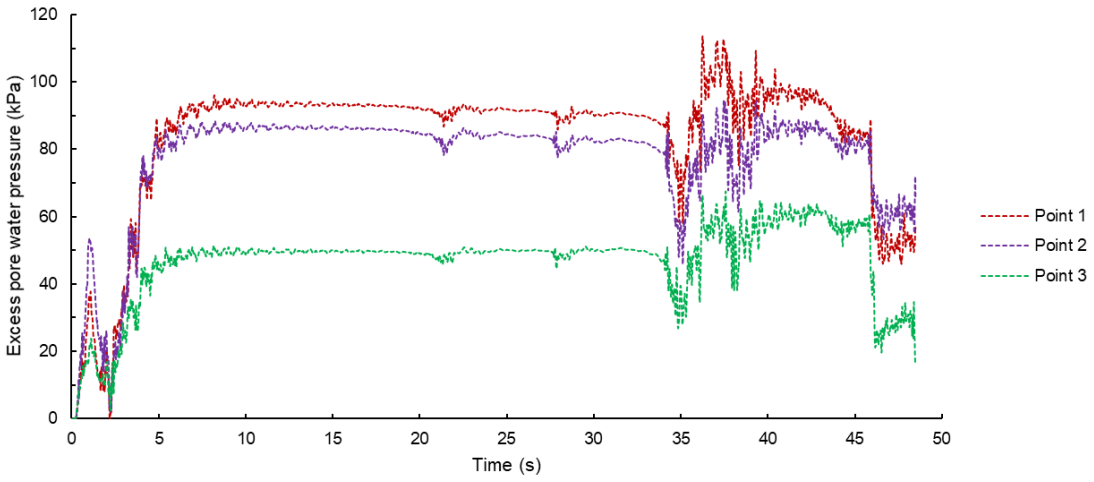

Figure 3.33. Development of excess pore water pressure in soil deposit

To assess the subsurface liquefaction and potential failure in soil, the pore water pressure ratio is calculated and presented in Figure 3.34. The pore water pressure ratio is defined as the ratio between excess pore water pressure and effective

confining pressure. The soil may be liquefied when the pore pressure ratio is in the range of 0.7 to 1.0 (Naesgaard and Byrne 2007; Serafini and Perlea 2010). Based on the obtained data at the monitoring points, it can be observed that the pore pressure ratio gradually increases when the monitoring points approach the SMR structure and ground surface. Consequently, the soil liquefaction may take place near group surface and nuclear structure. Through simulation-based engineering application, it can be found that the developed elastoplastic-hydraulic model is able to capture the SSI effect on the nonlinear behaviours of soil, and thus can be used as a useful tool for the optimal design of SMR structures.

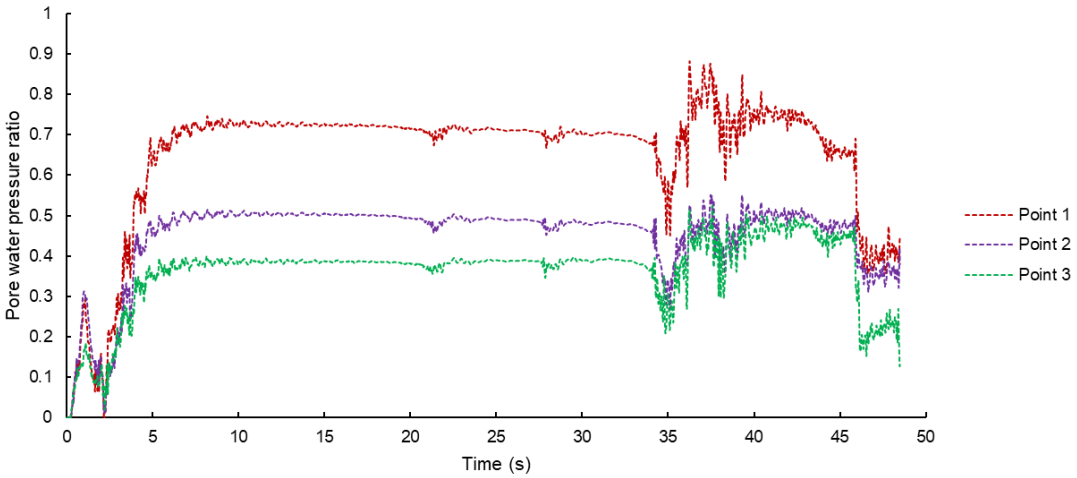

Figure 3.34. Residual pore water pressure ratio under effect of SSI

3.6 Conclusions

The following conclusions are made based on the obtained results in this study.

i. A dynamic coupled visco-elastoplastic-hydraulic model is developed to assess soil behaviors under seismic loadings. It is found that the model can capture the effect of the time rate of the change of volumetric strain on the development of excess pore water pressure. Moreover, effective stress and

viscoplasticity can be used to reliably assess the stress and deformation changes in soil. In addition, all the model parameters have direct physical meaning and can be determined in terms of measurable material properties.

ii. To capture the effect of S-wave propagation on the behaviors of soils, the MCC model was incorporated into a Perzyna-type viscoplasticity model. The obtained results show that the developed model can capture (1) the development of permanent deformation in soil; (2) the shear-induced volume change (including both contraction and expansion); and (3) the generation of excess PWP under the dynamic loadings. The developed model can capture the strain hardening and softening behaviour of soil under complex stress paths, and thus capture the response of soils under the seismic loadings.

iii. To capture the hydraulic process in soil subjected to the dynamic loadings, the time rate of change of volumetric strain was integrated into the momentum equation. Moreover, the compressibility of pore water and soil skeleton is fully considered in the storage term. Consequently, the build-up and dissipation of pore water pressure can be captured by the developed model.

iv. Based on the obtained results from the verification of elastoviscous-hydraulic model and elastoplastic-hydraulic model, it can be stated that the coupled visco-elastoplastic-hydraulic model has the ability to capture nonlinear behaviour of soils (including the development of irrecoverable deformation and associated built-up and dissipation of excess PWP).

Moreover, through numerical analysis of static triaxial shear tests, it can be observed that viscoplasticity is needed to quantitatively assess the rate-dependent behaviour of soil under dynamic loading conditions.

v. The coupled elastoplastic-hydraulic model was validated against the experimental data of cyclic triaxial test and shaking tests on soils. The good agreement between predicted results and measured data clearly demonstrates the good predictability of the developed model.

vi. The validated mathematical model has been used to perform a simulation-based engineering application of a hypothetical SMR structure. Based on the obtained results, it has been found that the developed model can capture the strongly nonlinear behaviorur of soil under SSI effect. Therefore, the developed model can be used as a useful tool for the verification of the seismic qualification and/or the optimization of the design of structures on or embedded in soil foundations, taking into account the effects of groundwater.

3.7 References

Carless, T. S., Talabi, S. M., and Fischbeck, P. S. (2019). "Risk and regulatory considerations for small modular reactor emergency planning zones based on passive decontamination potential." *Energy*, 167, 740-756.

Hidayatullah, H., Susyadi, S., and Subki, M. H. (2015). "Design and technology development for small modular reactors–Safety expectations, prospects and impediments of their deployment." *Prog. Nucl. Energ.*, 79, 127-135.

Lysmer, J., and Kuhlemeyer, R. L. (1969). "Finite dynamic model for infinite media." *Journal of the Engineering Mechanics Division*, 95(4), 859-878.

Markou, G., and Genco, F. (2019). "Seismic assessment of small modular reactors: NuScale case study for the 8.8 Mw earthquake in Chile." *Nucl. Eng. Des.*, 342, 176-204.

Naesgaard, E., and Byrne, P. M. (2007). "Flow liquefaction simulation using a combined effective stress–total stress model." *Proc., 60th Canadian Geotechnical Conference, Ottawa, Ontario*, 21-24.

Santamarina, J. C., and Cho, G. C. (2001). "Determination of critical state parameters in sandy soils—simple procedure."

Serafini, D. C., and Perlea, V. (2010). "Comparison of Liquefaction Triggering Analysis Approaches for an Embankment Dam and Foundation."

Taboada, V. M., and Dobry, R. (1993). "Experimental results and numerical predictions of model." *Proc., International Conference on the Verification of Numerical Procedures for the analysis of soil liquefaction problems*.

Ural, N., and Gunduz, Z. (2014). "Behavior of nonplastic silty soils under cyclic loading." *The Scientific World Journal*, 2014.

Vrakas, A. (2017). "On the computational applicability of the modified Cam-clay model on the ‘dry’side." *Computers and Geotechnics*.

Watanabe, K., Pisanò, F., and Jeremić, B. (2017). "Discretization effects in the finite element simulation of seismic waves in elastic and elastic-plastic media." *Engineering with Computers*, 33(3), 519-545.